Pergamon

0301-9322(94)E0022-B

Int. J. Multiphase Flow Vol. 20, Suppl., pp. 331–386, 1994

0301-9322/94 $26.00 + 0.00

DYNAMIC SIMILARITY IN FLUIDIZATION

L. R. GLICKSMAN, M. R. HYRE and P. A. FARRELL
Mechanical Engineering Department, Massachusetts Institute of Technology, Cambridge, MA 02139, U.S.A.

(Received 28 March 1994)

Abstract—Similitude is a powerful tool which allows a small laboratory experiment at ambient conditions to simulate a much larger commercial fluidized bed. The scaling laws for bed dynamics and heat transfer are systematically developed from the fundamental relationships. Recent results demonstrate the validity of scaling and shed light on the key parameters which must be included in scaling. Simplified forms of the similitude relationships are identified.

Key Words: fluidization, similitude, scaling, heat transfer, models

1. DYNAMIC SIMULATION OF FLUIDIZATION

1.1. Introduction

Fluidized beds are employed in a wide variety of applications such as combustors of dirty fuels, chemical reactors, ore roasters and coating applicators, to name a few. In many commercial applications the fluidized bed has a large diameter and height and operates at elevated temperature and pressure. To properly design a fluidized bed the fluid dynamics must be well understood since it directly influences the bed performance. For example, in a bubbling fluidized bed, the size, frequency and distribution of bubbles are directly linked to particle mixing and gas to solid contacting. A bed of uniformly distributed fine bubbles will yield higher chemical conversion than a bed containing a few large bubbles concentrated at the center. The particle residence time in a circulating fluidized bed combustor has a strong influence on the combustion efficiency and the level of pollutant emission.

The dynamics of a fluidized bed has been found to change as the bed size is increased. Designers are particularly concerned about the relationship between the performance of large commercial beds and results obtained from much smaller pilot plants. There is a critical need to understand and predict the fluid dynamics of large fluidized beds. However, there is a dearth of relevant information available in the field concerning large beds, particularly beds operating at high temperature and pressure. Because of the complexity of the multiphase phenomena, a theoretical solution for the bed behavior based on first principles remains a distant unfulfilled goal. There is a large body of data and approximate analytical models based on results from small experimental beds. It is not obvious how this data can be applied to larger commercial designs.

Detailed fluid dynamic investigations can be carried out more conveniently on small beds at ambient conditions. However, there must be a technique to confidently assure that these experimental results accurately duplicate conditions of larger reactors. Similitude or dimensional analysis represents a powerful tool which will allow a small laboratory experiment at ambient conditions to simulate a much larger commercial bed.

Similitude has been used in many fields to allow small controlled experiments to closely simulate physical phenomena. Wind tunnels are commonly used to determine the aerodynamic properties of aircraft and automobiles. Towing tanks are used to judge the performance of proposed ship designs. Water tables are used to simulate the drainage and flow patterns of large bodies of water. Small scale models are used to determine the performance of building structures in high winds or earthquakes.

Within the last decade investigators have begun applying similitude principles to the study of fluidized bed dynamics. Large commercial fluidized bed combustors have been simulated using

smaller laboratory models to determine proper strategy for part load operation, identify possible causes of erosion of in-bed surfaces and to determine heat transfer performance. The simulations have helped to identify parameters controlling bed dynamics and to investigate fundamental flow phenomena. Of particular note is the initiation of studies to determine the influence of increased bed size on performance: the scale up issue.

Similitude is a powerful experimental tool which can aid the fluidized bed designer and researcher. However, the same maxim holds in this field as in computer programming, a less than careful application can yield useless output or worse, highly misleading design projections. Over its history the field of fluidization has its share of model studies carried out without careful consideration of the similitude relations. Simply building and operating a model with the same geometric shape as the full scale bed will not lead to valid results. In some cases the particles used in the small scale ambient temperature model were identical to those used in the large scale high temperature bed! The results of such studies were less than illuminating.

In this review the application of similitude to fluidized beds will be surveyed. The scaling laws for bed dynamics and heat transfer will be systematically developed from the fundamental relationships. Recent results will be presented which demonstrate the validity of scaling and shed light on the key parameters which must be considered in scaling, as well as those which may be safely put aside.

Similitude principles make it possible to build an experimental model which duplicates the performance of another bed. That bed may be a larger experimental model operated at the same pressure and temperature or it may be a large commercial bed or pilot plant operated at elevated temperature and/or pressure possibly with a different fluid and particle material. We will adopt the nomenclature of commercial bed or target bed being simulated and the term model or experimental model for the bed used to simulate the commercial bed.

1.2. Early Work

The literature is replete with numerous parameters, dimensional and non-dimensional, to characterize the dynamics of a fluidized bed. Wilhelm & Kwauk (1948) correlated the porosity with a modified Reynolds number based on minimum fluidization velocity as the parameter to distinguish between aggregative and particulate fluidization. Romero & Johanson (1962) non-dimensionalized equations proposed by others for bed stability and showed the resulting dimensionless equations contained the dimensionless parameters:

$$\frac{\rho_s - \rho_f}{\rho_f}, \quad \frac{u_{mf}^2}{g d_p}, \quad \frac{d_p u_{mf} \rho_f}{\mu}, \quad \frac{H}{D},$$

where ρ_s is the solid density, ρ_f is the fluid density, u_{mf} is the minimum fluidization velocity, d_p is the particle diameter, μ is the fluid viscosity and H and D are the bed height and diameter, respectively. Wilhelm & Kwauk showed that a single new parameter based on the product of the above parameters did a better job of correlating the transition between aggregative and particulate fluidization than previous criteria which only used the Froude number. Note that, in general, these parameters may influence the bed characteristics in a more complicated form, i.e. as four independent parameters rather than combined in product form. In general, if u_{mf} is given by the Ergun equation, it can be shown that $d_p u_{mf} \rho_f / \mu_f$ is a function of ϵ_{mf}, the voidage at minimum fluidization, ϕ, the particle sphericity and the product $(\rho_s - \rho_f/\rho_f) \cdot g d_p / u_{mf}^2$. That is, aside from the geometric ratios there are only two independent parameters in Romero & Johanson's work.

The Archimedes number has been used to correlate a wide array of phenomena (Zabrodsky 1966).

Richardson & Zaki (1954) used the pi theorem combined with experimental results to obtain a relationship for the ratio of settling velocity at infinite dilution to the superficial velocity as a function of bed voidage, Reynolds number and ratio of particle to bed diameter.

Baeyans & Geldart (1973) established a different set of parameters to characterize the fluidizing characteristics of particles which they demonstrated can be written in terms of dimensionless parameters.

Broadhurst & Becker (1973) developed a list similar to that of Romero & Johanson except Broadhurst used the superficial velocity in place of the minimum fluidization velocity. The

dimensionless parameters were developed from the pi theorem. These parameters were used by Broadhurst & Becker to determine the criteria for minimum fluidization, the onset of bubbling and the onset of slugging. They found the solid to gas density ratio was an important correlating parameter for all three phenomena.

None of these early investigators recognized the power of dimensional analysis to design experimental models which simulate the dynamics of larger units.

2. DIMENSIONAL ANALYSIS AND SIMILARITY

Dimensional analysis is a powerful technique, particularly in situations where the equations governing a physical problem are either unknown or not easily solved. Dimensional analysis reduces the number of independent parameters on which a physical problem depends; the independent parameters are those that affect the value of dependent variables. Each independent parameter can be set regardless of the values of the other independent parameters. Dimensional analysis is also useful for generalizing experimental results and aiding in their correlation. For example, dimensional analysis can be used to show how the friction factor (non-dimensional wall shear stress) in turbulent pipe flow is a function of Reynolds number and dimensionless roughness height, or similarly how the lift coefficient (non-dimensional lift force) for aerodynamic bodies depends on Reynolds number and angle of attack. There are a number of dimensional analysis techniques; Buckingham's pi theorem (Buckingham 1914) and the method of non-dimensionalizing the governing equations and boundary conditions (inspectional analysis) will be discussed.

Experiments on a full-size commercial prototype are often prohibitively expensive and complex. One of the additional benefits of dimensional analysis is that it provides a way of properly scaling between a full-size prototype (target) and a laboratory scale model. By matching the important dimensionless parameters, which result from the dimensional analysis, between the model and the target prototype, dynamically similar behavior (similarity) will be achieved when it is expressed in the proper non-dimensional form. These laws make it possible to obtain useful information regarding the behavior of a full-size prototype using a properly scaled model.

The convention established by Kline (1965) will be adopted here. The term variable is reserved for quantities which vary in space or time for a particular problem [e.g. position, x; time, t; or local velocity $u(x, t)$]. Parameters are quantities which are constant for a particular problem but can vary between two of the same type of problems; examples in fluidized bed systems are: superficial velocity, u_0; particle diameter, d_p; or solid density, ρ_s. Dependent variables such as $u(x, t)$ are functions of independent variables, such as position and time, and the independent parameters.

2.1. Dimensional Homogeneity

The principle of dimensional homogeneity is one of the foundations of dimensional analysis. The principle can be stated as "If an equation truely expresses a proper relationship between variables in a physical process, it will be dimensionally homogeneous; i.e. each of its additive terms will have the same dimensions" (White 1979).

An example of a formula from the fluidization literature which lacks a general functional form due to dimensional difficulties is:

$$f_s^* = 6.5 \times 10^{-3} u_{mf}^{-1.2} \qquad [1]$$

The formula is an expression for the splitting frequency, f_s^* of a single rising bubble. The units of f_s^* are s^{-1} and the units of u_{mf} are m/s, therefore the constant 6.5×10^{-3} has units of $m^{1.2}/s^{2.2}$. Although the expression is dimensionally homogeneous, due to the implicit dimensions of the constant, it cannot be a general relationship for a physical process since a quantity with dimensions of s^{-1} cannot depend solely a parameter with the units of m/s. Based on dimensional considerations, at a minimum a length scale, such as the bubble diameter, is missing from the expression. Equations of this form are only applicable in the range of the data on which they are based; extrapolations outside this range could give spurious results.

2.2. Buckingham Pi Theorem

Buckingham's pi theorem provides a simple method for forming the dimensionless parameters which govern a physical process. The resulting dimensionless parameters are the so-called pi groups.

Buckingham's pi theorem states that if a physical process depends on n independent parameters, it can be simplified to a relationship between $(n-k)$ dimensionless parameters (pi groups). k is the number of dimensionally independent parameters which is less than or equal to the number of dimensions (e.g. M = mass, L = length, T = time) in the original n parameters.

2.2.1. Buckingham pi theorem procedure

The pi theorem is best demonstrated by an example; consider the case where the minimum fluidization velocity (u_{mf}) is the dependent parameter. Buckingham pi reduces the dependence of the minimum fluidization velocity on the relevant independent parameters to its simplest form.

The first step is to identify the complete set of dimensional independent parameters that are pertinent to the physical problem. It should be emphasized that the physics must be correct; if an important independent parameter is left out the dimensional analysis will fail. Similarly, spurious independent parameters unnecessarily complicate the results of the dimensional analysis and reduce its utility. Again, the independent parameters are those that affect the value of a dependent variable but do not affect each other. Typical examples include geometric design or input parameters which can be controlled independently of each other. In this particular example, it can be argued that the minimum fluidization velocity depends on the dominant forces on the particles and the particle geometry. We will assume that the dominant forces on the particles are: the force of buoyancy, proportional to $[(\rho_s - \rho_f)g]$ and d_p^3, viscous forces (μ) and fluid inertia forces (ρ_f). Note that gravity appears combined with the difference in densities in the buoyancy term, not as a separate independent parameter. The particle geometry can be characterized by the mean particle diameter (d_p), the minimum fluidization voidage (ϵ_{mf}) and the particle sphericity (ϕ). Particle inertia, which would require the inclusion of ρ_s in the list of independent parameters, is assumed to be small for conditions near minimum fluidization.

$$u_{mf} = fcn\{(\rho_s - \rho_f)g, \mu, \rho_f d_p, \epsilon_{mf}, \phi\} \quad [2]$$

The next step is to list the dimensions of both the independent and the dependent parameters. The most common dimensions are mass (M), length (L) and time (T). In the case of the minimum fluidization velocity,

$$[u_{mf}] = L/T \qquad [\mu] = M/LT \quad [(\rho_s - \rho_f)_g] = M/L^2T^2$$

$$[\rho_f] = M/L^3 \quad [d_p] = L \qquad [\epsilon_{mf}] = 1$$

$$[\phi] = 1 \quad [3]$$

A dimensionally independent subset of the independent parameters must be specified; the dimensionally independent parameters are used to non-dimensionalize the remaining parameters. In order for the parameters to be dimensionally independent it should not be possible to construct a dimensionless parameter (pi group) from them. Typically, the number of dimensionally independent parameters is equal to the number of dimensions in the problem. Selecting $\rho_f(M/L^3)$, $\mu(M/LT)$ and $d_p(L)$ as the dimensionally independent parameters and non-dimensionalizing the remaining independent parameters and the dependent parameter using these gives:

$$\frac{\rho_f u_{mf} d_p}{\mu} = fcn\left(\frac{(\rho_s - \rho_f)\rho_f g d_p^3}{\mu^2}, \epsilon_{mf}, \phi\right) \quad [4]$$

This can be written more concisely as,

$$Re_{mf} = fcn(Ar, \epsilon_{mf}, \phi) \quad [5]$$

where Re_{mf} is the Reynolds number based on u_{mf} and Ar is the Archimedes number.

A functional form for this relationship is given by the Ergun equation at minimum fluidization conditions

$$\frac{1.75}{\epsilon_{mf}^3\phi}\,Re_{mf}^2+\frac{150(1-\epsilon_{mf})}{\epsilon_{mf}^3\phi^2}\,Re_{mf}=Ar \qquad [6]$$

Wen & Yu (1966a) assumed that ϵ_{mf} is only a function of ϕ and showed that over a wide range of conditions $1/(\phi\epsilon_{mf}^3)$ and $(1-\epsilon_{mf})/(\phi^2\epsilon_{mf}^3)$ are approximately constant. Solving for Re_{mf}, assuming that the coefficients are constant, gives

$$Re_{mf}=\sqrt{C_1^2+C_2\,Ar}-C_1 \qquad [7]$$

where Grace (1982) recommends values of 27.2 and 0.0408 for C_1 and C_2, respectively.

This example illustrates the application of the Buckingham pi approach of dimensional analysis. It also shows how with additional physical insight into the problem simplifications are possible. If ρ_f, ρ_s and g had been listed individually as independent parameters, which would have occurred if no additional physical insight had been used, two additional independent dimensionless parameters would have resulted. The larger the number of independent dimensionless parameters the more complicated the task of correlating experimental data.

2.2.2. Application of Buckingham pi theorem to fluidized bed hydrodynamics

The Buckingham pi procedure, presented in section 2.2.1, can be applied to determine the dimensionless groups which govern the hydrodynamic behavior of fluidized beds. If we take the pressure drop, ΔP, as the dependent parameter of interest we can use Buckingham pi to determine the independent dimensionless parameters on which it depends.

To maintain generality we will resist the temptation to simplify and take the complete list of the independent parameters as:

$$\Delta P=fcn(u_0, g, D, L, d_p, \rho_s, \rho_f, \mu, \phi) \qquad [8]$$

These parameters have the dimensions:

$$\begin{aligned} &[\Delta P]=M/(LT^2) \quad [u_0]=L/T \quad [g]=L/T^2\\ &[D]=L \quad [L]=L \quad [\phi]=1\\ &[\rho_s]=M/L^3 \quad [\rho_f]=M/L^3 \quad [\mu]=M/(LT) \end{aligned} \qquad [9]$$

Choosing u_0, the superficial gas velocity (L/T), D(L) and ρ_f (M/L^3) as the dimensionally independent parameters and non-dimensionalizing the remaining parameters with these gives:

$$\frac{\Delta P}{\rho_f u_0^2}=fcn\left(\frac{gD}{u_0^2},\ \frac{L}{D},\frac{d_p}{D},\frac{\rho_s}{\rho_f},\frac{\mu}{\rho_f u_0 D},\phi\right) \qquad [10]$$

This set of dimensionless parameters is identical to the scaling laws developed by Glicksman (1984), which resulted from the non-dimensionalization of the Jackson (1971) equations of motion for fluidized beds. The number of non-dimensional independent parameters is fixed unless simplifications can be justified, but they can be arbitrarily arranged in different forms. For example the Archimedes number when $\rho_s \gg \rho_f$ (which is common in gas fluidized beds) results from:

$$Ar\approx\left(\frac{\rho_f u_0 d_p}{\mu}\right)^2\cdot\left(\frac{gD}{u_0^2}\right)\cdot\left(\frac{\rho_s}{\rho_f}\right)\cdot\left(\frac{d_p}{D}\right) \qquad [11]$$

It is important to note that Ar cannot be used to replace the three parameters, it can only be substituted for one such that the number of independent parameters remains the same. Simplifications result from physical insight not mathematical manipulation.

2.3. Non-dimensionalization of Governing Equations and Boundary Conditions

The Buckingham pi approach to dimensional analysis quickly and easily produces a set of dimensionless parameters, but it provides no way of determining whether the initial list of independent parameters is complete. The method of non-dimensionalization of the governing equations and boundary conditions does not suffer from this limitation, but the governing

equations and boundary conditions must be able to be completely specified. The governing equations and boundary conditions contain all the pertinent independent parameters. The governing equations can also provide guidance as to when certain parameters dominate others such as when inertial effects dominate viscous effects or vice versa.

The goal of non-dimensionalizing the governing equations is to normalize the equations such that each term is of order unity or less. This makes it possible to look at the order of magnitude of each term for a particular situation to determine when certain terms are negligible relative to others (referred to as order of magnitude or scale analysis). Order of magnitude analysis can also provide information regarding the functional form of the solution to the equation. Order of magnitude arguments are used, for example, to simplify the Navier–Stokes equations in the development of the boundary layer equations. Kline (1965) provides a detailed discussion on non-dimensionalizing the governing equations and boundary conditions.

The first step in non-dimensionalizing the governing equations is to identify the scales of the problem (e.g. length, time and velocity). The scales should be such that dimensionless dependent variables in the equations and boundary conditions are of order unity. Use the scales of the problem to non-dimensionalize each term in the governing equations and boundary conditions. Finally, choose one of the coefficients of a term in each governing equation and boundary condition and divide each term in the equation or boundary condition by it. The resulting dimensionless coefficients of the terms in the normalized equations and boundary conditions are the relevant dimensionless independent parameters. Several examples of this method of dimensional analysis are presented in later sections.

The more complete the governing equations and boundary conditions are the more exact the results of the dimensional analysis will be. It is important to realize the limitations of the governing equations, as for the Buckingham pi method: if all the important independent parameters are not included the dimensional analysis will be incomplete or it will fail.

2.4. Similarity

One of the benefits of dimensional analysis is that it provides the scaling laws between a model and a target prototype such that the two systems will exhibit dynamically similar behavior.

Geometric similarity is a prerequisite to dynamic similarity. A model and a prototype are geometrically similar when all of their linear dimensions are related by a constant scale factor. They also must have the same shape (e.g. all angles must be preserved, etc.). In the fluidization example in section 2.2.2 the non-dimensional groups: L/D and d_p/D are terms which would have to be matched between a model and a prototype to achieve geometric similarity.

A model and a target prototype will exhibit dynamically similar behavior if they are geometrically similar and if all the values of the relevant independent dimensionless parameters are matched between the two. In terms of the Buckingham pi dimensional analysis, by matching all the independent pi groups the non-dimensional variables will be identical. Using the drag on an arbitrary body as an example, if the model and the prototype are geometrically similar and the Reynolds numbers of the flows over the two are identical, the drag, F_D, on the target prototype is related to the drag on the model by

$$F_{D_t} = F_{D_m} \frac{(\rho u^2 L^2)_t}{(\rho u^2 L^2)_m} \qquad [12]$$

where m is for the model and t is for the commercial target prototype. In other words, the non-dimensional drag force of the model and the prototype are identical.

Similarly, if the same dimensionless governing equations and boundary conditions govern both a full-size target prototype and a scale model, the dimensionless solution will be identical. Therefore, if the dimensionless parameters in the non-dimensional governing equations and boundary conditions are matched between the prototype and the model, they will exhibit similar behavior when it is expressed in non-dimensional form.

Scaling of heat transfer in situations where the heat transfer depends on the fluid mechanics requires dynamic similarity in the fluid flows. In addition to hydrodynamic similarity, heat transfer scaling requires matching the relevant energy and property ratios. Buckingham pi and non-dimensionalization of the governing equations are equally applicable to heat transfer problems.

3. DEVELOPMENT OF DIMENSIONLESS SCALING LAWS

The dimensionless parameters which control the modeling of a fluidized bed can either be derived from application of the Buckingham pi theorem or by the non-dimensionalization of the governing equations. Done properly, each method leads to the same result. The use of the governing equations has the merit of tying specific dimensionless parameters to particular physical phenomena (Glicksman 1984, 1988). If the proper equations can be written, even if they cannot be solved, they yield considerable insight into the process.

Two approaches to the governing equations will be undertaken: using the equations of motion for individual particles and the equations of motion for a continuum model of fluids and solids phases. Early derivation of these dimensionless parameters was based on a continuum model (Scharff *et al.* 1978; Glicksman 1984). Inclusion of the individual particle approach extends the results to instances where a continuum model may not be applicable.

The validity of the dimensional analysis depends on using equations which properly describe the physics and include all of the important effects. There are some aspects of the governing physics which are still controversial, in some cases the equations will be simplified when dealing with effects whose proper formulation is unknown or in dispute. Pragmatically, the current success of the scaling experiments using the formulation as presented adds confidence to the use of these simplifications. Also, a limited number of tests have verified the omission of several phenomena.

For simplicity, the fluid will be considered incompressible although the results do not depend on this condition. The continuum equations will be developed similar to those given by Anderson & Jackson (1967). These equations are based on a continuum picture of the suspension of solids in the fluid. The solids and the fluid are considered individual phases and variables for each phase such as velocity of voidage are average values over regions large compared to a single particle but small compared to the scale of the macroscopic bed behavior. The derivation follows that given by Jackson (1971).

For the fluid, conservation of mass is

$$\frac{\partial \epsilon}{\partial t} + \operatorname{div}(\epsilon \bar{u}) = 0 \qquad [12a]$$

and for the solid phase,

$$\frac{\partial}{\partial t}(1-\epsilon) + \operatorname{div}[(1-\epsilon)\bar{v}] = 0 \qquad [13a]$$

where $\bar{u}$ and $\bar{v}$ are the vectorial forms of the fluid and solid phase velocities, respectively.

The equation of motion for the fluid can be written as,

$$\rho_f \epsilon \left[\frac{\partial \bar{u}}{\partial t} + \bar{u} \cdot \nabla \bar{u}\right] + \bar{i}\rho_f g \epsilon - \nabla \cdot E_f + \bar{F} = 0 \qquad [14a]$$

while for the particle phase,

$$\rho_s (1-\epsilon)\left[\frac{\partial \bar{v}}{\partial t} + \bar{v} \cdot \nabla \bar{v}\right] + \bar{i}\rho_s g(1-\epsilon) - \bar{F} - \nabla \cdot E_p = 0 \qquad [15a]$$

where $\bar{i}$ is the unit vector in the vertical direction and the drag force between the fluid and the particle is represented by $\bar{F}$. E_f and E_p are the local average stress tensors associated with the fluid and particle phases, respectively. The proper formulation of the stress tensors is still a subject of controversy. The fluid to particle force term can be represented by a drag term proportional to the relative velocity between the two phases and a virtual mass term (C_A is the added mass coefficient),

$$\bar{F} = \beta(\bar{u} - \bar{v}) + (1-\epsilon)C_A \rho_f \frac{d}{dt}(\bar{u} - \bar{v}) + (1-\epsilon)\nabla \cdot E_f \qquad [16a]$$

Note β is in general not a constant, rather it must be found from a general expression for the drag force.

Given the uncertainty in the form of stress tensors, many authors have adopted a form analogous to single phase Newtonian fluid. For the fluid phase if incompressible,

$$E_{fij} = -P\delta_{ij} + \mu\left(\frac{\partial u_i}{\partial x_j} + \frac{\partial u_j}{\partial x_i}\right) \quad [17a]$$

and for the solid,

$$E_{pij} = -P_p\delta_{ij} + \mu_P\left(\frac{\partial v_i}{\partial x_j} + \frac{\partial v_j}{\partial x_i}\right) \quad [18a]$$

where μ is the fluid viscosity μ_p is the effective viscosity of the particle phase. P is the fluid pressure and P_p is the local average pressure for the particle phase.

The boundary conditions for the bed at the side wall with no net flow of particle across it are at

$$x = 0, D$$

$$v_{\text{normal}} = 0, \quad [19a]$$

where this is the solids velocity normal to the wall.
At the bottom

$$\text{at} \quad y = 0$$

$$v_{\text{normal}} = \frac{G_s}{\rho_s(1-\epsilon)} \quad [20a]$$

where G_s is the average solids feed rate per unit area from outside the bed through the bottom. This form holds when the solids feed is uniformly distributed over the bottom. If solids feed takes place along the side wall an expression similar to [20a] must be used in place of [19a].

For gas velocity,

$$\text{at} \quad x = 0, D \quad \bar{u} = 0 \quad [21a]$$

$$\text{at } y = 0$$

$$\bar{u} = \bar{i}u_0/\Delta \text{ above the distribution holes}$$

$$\bar{u} = 0 \text{ elsewhere} \quad [22a]$$

where Δ is the voidage of the distribution plate assumed to be a perforated plane in this case and u_0 is the superficial gas velocity. For bubble caps or other gas inlet devices, boundary conditions such as [22a] apply over the gas inlet plane of the device. Boundary conditions [19a] and [21a] also apply to the surfaces of any internal elements in the bed. For example heat transfer tubes.

At all x_s, y_s (internal surfaces)

$$\bar{u} = 0, \quad v_N = 0 \quad [23a]$$

Also at the distributor

$$\text{at } y = 0$$

$$P = P_0 \quad [24a]$$

Non-dimensionalizing the variables as,

$$\bar{v}' = \frac{\bar{v}}{u_0}, \quad \bar{u}' = \frac{\bar{U}}{u_0}$$

$$\nabla' = L\nabla,$$

$$t' = \frac{u_0}{L}t$$

$$x' = \frac{x}{L}$$

$$y' = \frac{y}{L} \qquad [25]$$

where L is a typical bed dimension, e.g. the bed height or diameter. Note that u', v', as well as ϵ are dependent variables of x', y' and t' which are determined by the boundary conditions and the independent dimensionless parameters of the governing equations.

Applying these definitions to the governing equations and rearranging them so the parameters form non-dimensional groups, the continuity equations become,

$$\frac{\partial \epsilon}{\partial t'} + \operatorname{div}(\epsilon \bar{u}') \qquad [12b]$$

and

$$\frac{\partial}{\partial t'}(1-\epsilon') + \operatorname{div}[(1-\epsilon)\bar{v}'] = 0 \qquad [13b]$$

The equations of motion in dimensionless form are,

$$\epsilon\left[\frac{\partial \bar{u}'}{\partial t'} + \bar{u}' \cdot \nabla' u'\right] + \bar{i}\frac{gL}{u_0^2}\epsilon - \nabla' \cdot \frac{E_f}{\rho_f u_0^2} + \frac{L\bar{F}}{\rho_f u_0^2} = 0 \qquad [14b]$$

and

$$(1-\epsilon)\left[\frac{\partial \bar{v}'}{\partial t'} + \bar{v}' \cdot \nabla' \bar{v}'\right] + \frac{\bar{i}gL}{u_0^2}(1-\epsilon) - \left(\frac{\rho_f}{\rho_s}\right)\left(\frac{LF}{\rho_f u_0^2}\right) - \left(\frac{\rho_f}{\rho_s}\right)\nabla' \frac{E_p}{\rho_f u_0^2} \qquad [15b]$$

The fluid–particle interaction force becomes,

$$\frac{L\bar{F}}{\rho_f u_0^2} = \frac{\beta L}{\rho_f u_0}(\bar{u}' - \bar{v}') + (1-\epsilon)C_A \frac{d}{dt'}(\bar{u}' - \bar{v}') + (1-\epsilon)\nabla' \cdot \frac{E_f}{\rho_f u_0^2} \qquad [16b]$$

$$\frac{E_{fij}}{\rho_f u_0^2} = \left[\frac{P\delta_{ij}}{\rho_f u_0^2} + \frac{\mu}{L\rho_f u_0}\left(\frac{\partial u_i'}{\partial x_j'} + \frac{\partial u_j'}{\partial x_i'}\right)\right] \qquad [17b]$$

$$\frac{E_{pij}}{\rho_f u_0^2} = \left[\frac{P_p \delta_{ij}}{\rho_f u_0^2} + \frac{\mu_p}{L\rho_f u_0}\left(\frac{\partial v_i'}{\partial x_j'} + \frac{\partial v_j'}{\partial x_i'}\right)\right] \qquad [18b]$$

The dimensionless boundary conditions become,

$$\text{at} \quad x' = 0, D/L$$

$$v'_{\text{normal}} = 0$$

$$\text{at} \quad y' = 0 \qquad [19b]$$

$$v'_{\text{normal}} = \frac{G_s}{\rho_s u_0}\frac{1}{(1-\epsilon)} \qquad [20b]$$

$$\text{at} \quad x = 0, \frac{D}{L}$$

$$\bar{u}' = 0 \qquad [21b]$$

$$\text{at } y = 0 \quad \bar{u}' = i\bar{\mu}/\Delta \text{ above distribution holes}$$

$$\bar{u}' = 0 \quad \text{elsewhere} \qquad [22b]$$

At all internal surfaces x_s', y_s'

$$\bar{u}' = 0, \quad v_N' = 0 \qquad [23b]$$

$$\text{at} \quad y' = 0 \quad P' = \frac{P_0}{\rho_f u_0^2} \qquad [24b]$$

3.1. Fluid–Solid and Interparticle Forces

The drag coefficient β can be expressed in several different limiting forms depending on the flow conditions. At low voidages typical of bubbling beds, the Ergun relationship or similar form can be used. In that case β can be expressed as,

$$\frac{\beta L \varphi_s}{\rho_s u_0} = 150 \frac{\epsilon(1-\epsilon)^2}{\epsilon^3} \frac{\mu L}{\rho_s u_0 \varphi d_p d_p} + 1.75 \frac{(1-\epsilon)|\bar{u}' - \bar{v}'|}{\epsilon^3} \epsilon^2 \frac{L \rho_f}{d_p \rho_s} \quad [26]$$

In the limit of very high voidage, the drag coefficient can be related to the single particle drag coefficient. For the case of spherical particles,

$$\frac{\beta L}{\rho_s U_0} = \frac{3}{4} C_D |\bar{u}' - \bar{v}'| f(\epsilon) \frac{\rho_f}{\rho_s} \frac{L}{d_p} \quad [27]$$

where the drag coefficient, C_D, in turn can be expressed in the form of

$$C_D = f\left[\frac{\rho_f u_0 d_p}{\mu}\right] \quad [28]$$

In the more general case C_D will also be a function of particle shape, sphericity, surface roughness and turbulence intensity of the fluid. The term $P_0/\rho_f u_0^2$ can be ignored when the fluid velocity is small compared to sonic velocity or the absolute pressure does not change enough to influence the thermodynamic properties of the fluid; it will be ignored in this development. Note that the fluid pressure level still influences the fluid density.

From the continuity and momentum equations for the fluid and solid phases along with the boundary conditions the following groups of independent dimensionless parameters are found to control the hydrodynamics,

$$\frac{u_0^2}{gL}, \frac{\rho_s}{\rho_f}, \frac{L\bar{F}}{\rho_f u_0^2}, \frac{E_f}{\rho_f u_0^2}, \frac{E_p}{\rho_f u_0^2}, \frac{G_s}{\rho_s u_0} \quad [29]$$

along with the dimensionless coordinates of the boundaries and internal surfaces. The parameters containing $\bar{F}$, E_f and E_p can be obtained, in principle, from [16b], [17b] and [18b] yielding

$$\frac{u_0^2}{gL}, \frac{\rho_s}{\rho_f}, \frac{\beta L}{\rho_s u_0}, \frac{\mu}{L \rho_f u_0}, \frac{P_p}{\rho_f u_0^2}, \frac{\mu_p}{L \rho_f u_0} \quad [30]$$

as well as bed geometry.

The dimensionless fluid pressure is not included since it is a dependent parameter. The dimensionless drag coefficient $\beta L/\rho_s u_0$ can be expressed in terms of other fluid parameters by the use of [26] or [27] and [28]. For low voidages where the Ergun like expression holds,

$$\frac{\beta L}{\rho_s u_0} = f\left[\frac{\rho_s u_0 d_p^2 \varphi^2}{\mu L}, \frac{L}{d_p \phi} \frac{\rho_f}{\rho_s}\right] \quad [31]$$

while at high voidage, using [26] and [27],

$$\frac{\beta L}{\rho_s U_0} = f\left[\frac{\rho_f u_0 d_p}{\mu}, \quad \varphi \text{ or shape, roughness, fluid turbulence}\right] \quad [32]$$

The physical basis of the particle phase pressure and viscosity still has not been resolved in the fluidization literature. In particular, dealing with stability between minimum fluidization and minimum bubbling, some investigators have considered interparticle forces as purely hydrodynamic, such as Foscolo & Gibilaro (1984) and Batchelor (1988), while others contend that the interparticle forces, are due to phenomena such as electrostatic or van der Waals forces (Rietema & Piepers 1990; Rieetma *et al.* 1993). For very fine particles, particle to particle cohesive forces are recognized as influencing the point of bubbling for gas fluidized beds (Baeyans & Geldart 1973).

For larger particles, the nature of interparticle forces is still unresolved. Well beyond the point of minimum bubbling, a typical operating condition for most commercial gas solid beds, it might be expected that electrostatic or van der Waals forces are not as important as they are near the

point of minimum fluidization. It is likely that particle–particle collisions, dependent on the coefficient of restitution and sliding friction, come into play at much higher u_0/u_{mf}.

Given the lack of concensus concerning the nature and importance of interparticle interactions and the lack of an accepted quantitative form to express the non-hydrodynamic particle–particle interactive forces, such terms will not be considered further in this development. Foscolo *et al.* (1990) have shown that if the interparticle forces are hydrodynamic in nature the dimensionless parameters obtained are identical to those obtained by neglecting interparticle interaction. The success of scaling experiments for bubbling and circulating beds, which to date has been based on parameters omitting the interparticle interactions, suggest that in the range of parameters investigated, such an omission is valid.

3.2. Experimental Investigations of Interparticle Forces

An experimental investigation was carried out by Litka & Glicksman (1985) to determine the influence of particle mechanical properties on the dynamics of a bubbling fluidized bed. They compared the behavior of beds fluidized with two kinds of particles with identical properties save one. In one test, particles of the same density, size, sphericity but different coefficients of restitution were compared. In the second series of tests, smooth and frosted glass particles with two different coefficients of sliding friction were compared. In each series of tests, beds with two different particles were found to have the same bubble frequency and size at a given height and a given $u_0 - u_{mf}$. The beds also exhibited identical vertical particle dispersion, measured by following heated particles within the cold bed. The only exception was the particle with the higher coefficient of friction which exhibited a modest increase in ϵ_{mf} and u_{mf}. Figures 1 and 2 show a comparison of bubble size and verticle particle delay time for one series of tests. Thus, over those tests conditions the two mechanical properties had a negligible influence on the bed dynamics. Since van der Waals forces involve short range interactions, changes in the roughness should produce different contact profiles and noticeable changes in bed behavior of such forces are important. The lack of substantial observable effects suggests the contrary conclusion for modest or large particles.

Chang & Louge (1992) carried out scaling tests in a circulating fluidized bed. They found that coated glass powders with an artificially low surface friction and possibly a different coefficient of restitution gave a substantially different vertical solid density distribution in the column than a bed of common glass powder. The authors conclude that for typical materials with friction coefficients larger than the specially treated powders variations of friction coefficients are expected to have only a minor influence on fluid mechanics. Chang & Louge also report an observation shared by the current authors, circulating beds operated without anti-static treatment in dry air can exhibit substantial variations in flow behavior due to electrostatic charges built up on the particles (and sometimes accompanied by severe electrical discharges which damaged test electronics). The

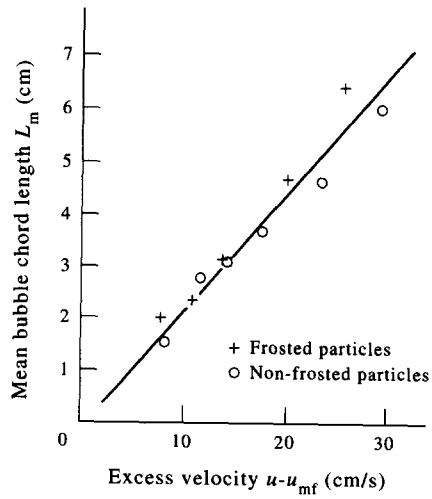

Figure 1. Mean bubble chord length vs excess velocity, frosted and smooth glass particles of the same diameter, density and sphericity, coefficient of sliding friction 0.21 and 0.12, respectively.

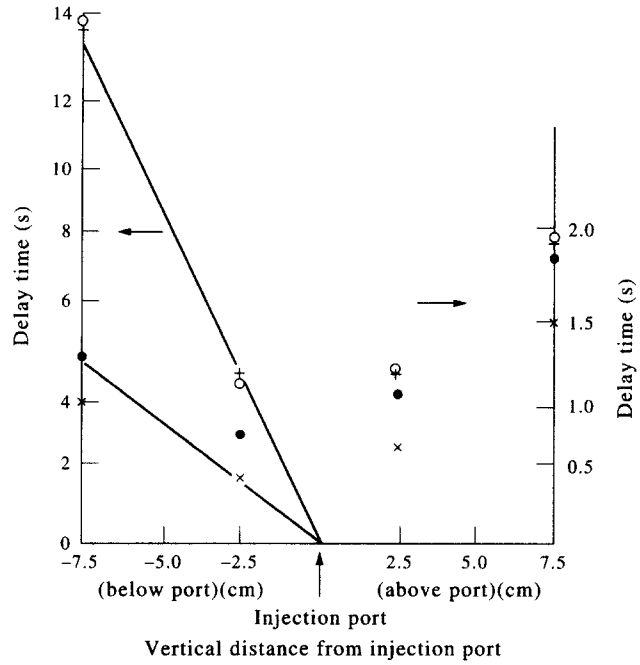

Figure 2. Delay time for 650 μm smooth and frosted glass (note time change above and below injection port). ○, Non-frosted: $u - u_{mf} = 10$ cm/s; +, frosted: $u - u_{mf} = 10$ cm/s; ●, non-frosted: $u - u_{mf} = 20$ cm/s; ×, frosted: $u - u_{mf} = 20$ cm/s.

electrostatic effects are not expected to be present in commercial processes at elevated temperature where the fluidizing gas is more conductive. With proper precautions in ambient temperature beds, this phenomenon has been found to be of negligible influence on the bed dynamics.

Most available evidence suggests that particle mechanical properties related to interparticle collisions and electrostatic forces can be omitted. Although this is far from conclusive over a wide range of conditions, it will be adopted in this treatment. Note that interparticle collisions are not totally omitted from the parameters in this consideration. For collisions governed by relative particle velocity, size and density, but not variations in the mechanical properties, e.g. perfectly elastic or perfectly inelastic collisions, the set of non-dimensional parameters developed below will still give similar behavior.

3.3. Dimensionless Parameters

Simplifying the non-dimensionalization by neglecting interparticle forces which are represented by the particle pressure and effective viscosity in [29] the list of dimensionless parameters becomes,

$$\left[\frac{u_0^2}{gL}, \frac{\rho_s}{\rho_f}, \frac{\beta L}{\rho_s u_0}, \frac{\rho_f u L}{\mu_f}\frac{G_s}{\rho_s u_0}, \text{bed geometry}\right] \quad [33]$$

When the drag coefficient can be described by a Ergun-like expression, then $\beta L/\rho_s u_0$ is, in turn, a function of $\rho_s u_0 (d_p \varphi) d_p \varphi / \mu L$ and $L/\varphi d_p$. In this expression d_p represents the mean diameter when a distribution of different size particles are in the bed.

Traditionally, the mean diameter is defined as the surface area average mean. Although this mean may be appropriate for flow resistance primarily due to surface shear forces, it is not the proper choice for drag which prevails at higher particle Reynolds numbers (nor is it the obvious choice for a mean diameter to use with bed to surface heat or mass transfer). It is more general to include along with the mean particle diameter, the particle size distribution, with the particle size non-dimensionalized with respect to the mean diameter and the particle sphericity. To be more exact, the particle aspect ratio and surface roughness should be included at high particle Reynolds numbers. By use of isotropic material with common

roughness levels these last two parameters can be overlooked. The set of independent dimensionless parameters becomes,

$$\frac{u_0^2}{gL}, \frac{\rho_s}{\rho_f}, \frac{\rho_s u_0 d_p^2 \varphi^2}{\mu L}, \frac{\rho_f u_0 L}{\mu_f}, \frac{G_s}{\rho_s u_0}, \quad \text{bed geometry, } \varphi\text{, particle size distribution (PSD)} \qquad [34]$$

These can be rearranged by combination of parameters, it must be borne in mind that such manipulation by itself does not lead to any decrease in the number of dimensionless parameters. One such modification is,

$$\frac{u_0^2}{gL}, \frac{\rho_s}{\rho_f}, \frac{\rho_s u_0 d_p}{\mu}, \frac{\rho_f u_0 L}{\mu}, \frac{G_s}{\rho_s u_0}, \quad \text{bed geometry, } \varphi\text{, PSD} \qquad [35]$$

In this form u_0^2/gL the Froude number can be viewed as a ratio of inertial to gravity forces; ρ_s/ρ_f is a ratio of particle to fluid inertial forces; $\rho_s u_o d_p/\mu$ is the Reynolds number or ratio of particle inertial to fluid viscous forces; and $\rho_f u_0 L/\mu$ is a Reynolds number based on the bed dimensions and fluid density or ratio of fluid inertial to viscous forces.

Another common form is obtained by combining the Froude and Reynolds numbers to obtain the Archimedes number, which omits u_0,

$$\frac{\rho_f \rho_s d_p^3 g}{\mu^2} = \left(\frac{\rho_f u_0 d_p}{\mu_f}\right)^3 \frac{gL}{u_0^2} \left(\frac{\mu_f}{\rho_f u_0 L}\right) \left(\frac{\rho_s}{\rho_f}\right) \qquad [36]$$

The list of dimensionless parameters can be rewritten as,

$$\frac{\rho_f \rho_s d_p^3 g}{\mu^2}, \frac{\rho_s}{\rho_f}, \frac{u_0^2}{gL}, \frac{\rho_f u_0 L}{\mu}, \frac{G_s}{\rho_s u_0}, \quad \text{bed geometry, } \varphi\text{, PSD} \qquad [37]$$

Note that there is nothing more "fundamental" about one form compared to the others. Each has the same number of dimensionless groups which are made up of independent parameters which can be set by the bed design and operation and the choice of particles. However, when the number of dimensionless groups is simplified by omitting some phenomena, the reduction in number of groups could be influenced by the form chosen.

3.4. Scaling Law Derivation of Horio for Circulating Fluidized Beds (1989)

The most dramatic departure from the above procedure for derivation of scaling laws is that of Horio (1989). Horio has presented a scaling law for CFBs which is based on the clustering annular flow model (CAFM) of Ishii (1989). The CAFM describes the flow in a CFB as particle clusters moving upward in the core and downward in the annulus at the wall. The analysis was similar to that of Nakamura & Capes (1973). Completeness of the model was achieved by assuming minimization of pressure gradient.

Horio's scaling law derivation was based on the requirement that two similar CFBs have equal values of:

(1) voidage distribution;
(2) dimensionless core radius;
(3) gas splitting to core and annulus;
(4) solid splitting to core and annulus;
(5) cluster voidage.

The CAFM equations were then examined to determine how these requirements could be met.

Questions as to the validity of the theory supporting Horio's development are based on deficiencies of the CAFM to fully describe CFB flow and the lack of justification for the premise that the five characteristics listed above comprise all that is of interest in a CFB. In particular, the assumption of pressure drop minimization, although convenient, is not justified physically (Hyre & Glicksman 1994).

The scaling law proposed by Horio for CFBs discussed above can be shown to be equivalent to the simplified set of parameters discussed in section 6. Horio also discussed simplifications to his list of scaling parameters in which the solid/gas density ratio is omitted. He claimed that this simplified scaling law is sufficient for "macroscopic similarity" and sacrifices only cluster size

similarity. This simplified law is identical to the bubbling bed scaling law developed by Horio (1986) and has been shown by Glicksman (1988) to be equivalent to the viscous limit scaling law. Horio's suggestion, that the density ratio can be neglected because sacrificing cluster size does not necessarily alter the macroscopic behavior of a CFB, is somewhat curious since his development is based on the CAFM which assumes clusters are the primary mechanism of particle transport. As will be shown in section 6, density ratio is not a parameter which can be omitted when scaling CFBs.

3.5. An Alternative Evaluation of Fluidized Bed Similarity—Deterministic Chaos and the Kolmogorov Entropy

Recent studies have indicated that fluidized beds may be deterministic chaotic systems (Daw *et al.* 1990; Daw & Harlow 1991; Schouten & van den Bleek 1991; van den Bleek & Schouten 1993). Such systems are characterized by a limited ability to predict their evolution with time. If beds are deterministic chaotic systems, the scaling laws should reflect the restricted predictability associated with such systems.

Van den Bleek & Schouten (1993) have suggested that if two beds are properly scaled, the rate of information change in both systems will be the same. They suggest that two scaled beds will exhibit the same Kolmogorov entropy, or information generation rate, when measured on the same time scale. Hence, they adopt an additional method for verifying dynamic similarity requiring that the information group, Kt, to remain constant (where $t = d_p/u_0$ and K is the Kolmogorov entropy).

If fluidized beds are indeed chaotic, it would be impossible to match values of $K(d_p/u_0)$ exactly by using the scaling parameters described above because chaotic systems are very sensitive to parameter settings. Van den Bleek & Schouten (1993) propose that the dimensionless information group be used as a tool to make the dynamic conditions in two scaled reactors similar by influencing the dependent parameter K through slight changes in one or more independent parameters. For example, the bed superficial velocity could be modified slightly to match $K(d_p/u_0)$.

Further work is needed to determine in which regimes, if any, fluid beds behave as chaotic systems. Moreover, additional testing is required to evaluate the sensitivity of the Kolmogorov entropy to system parameters, and how well the dimensionless information group is matched in beds which exhibit similar behavior as determined by the more common methods of evaluating dynamic similarity.

4. DEVELOPMENT OF THE SCALING LAWS USING THE SINGLE PARTICLE EQUATION OF MOTION

In dilute regions of CFBs and in the freeboard of bubbling beds, gas/solid hydrodynamics may be best represented as individual particles interacting with a turbulent fluid. If this is the case, the assumption of a continuum for the mass of particles in the bed implicit in the Anderson–Jackson equations of motion will not be valid. To investigate the governing hydrodynamic parameters of a particle suspended in homogeneous or wall bounded turbulence, we will write the equation of motion for an individual particle in its entirety. The equation will then be non-dimensionalized to determine the controlling dimensionless parameters.

A particle suspended in a turbulent fluid responds to the random fluid velocity. Calculations presented in the literature relating the turbulence characteristics of particle motion to the turbulence characteristics of the fluid have been based on Tchen's (1947) equation of motion or on Maxey & Riley's (1983) equation. These relations include the effects of the Stokes drag, the body force, the Basset history force and the forces due to added mass and local fluid acceleration. Faxen terms which account for local curvature of the velocity field are also included in Maxey & Riley's equation.

4.1. Core Region of a CFB or Freeboard of a Bubbling Bed

In the core region of a CFB or freeboard of a bubbling bed where particles are far from the wall, the turbulence can be approximated as unbounded and homogeneous. Maxey & Riley gave

the following equation of motion for a sufficiently small spherical particle suspended in unbounded homogeneous turbulence:

$$\frac{1}{6}\pi d_p^3 \rho_s \frac{d\bar{v}}{dt} = \frac{1}{6}\pi d_p^3(\rho_s - \rho_f)\bar{g} - 3\pi\mu d_p\left(\bar{v} - \bar{u}_p - \frac{1}{24}d_p^2\nabla^2\bar{u}_p\right)$$
$$-\frac{3}{2}\pi\mu d_p^2\int_{t_0}^{t}\frac{d}{d\tau}\left[\bar{v} - \bar{u}_p - \frac{1}{24}d_p^2\nabla^2\bar{u}_p\right]\frac{d\tau}{(\pi\nu(t-\tau))^{1/2}}$$
$$-\frac{1}{12}\pi d_p^3\rho_f\frac{d}{dt}\left[\bar{v} - \bar{u}_p - \frac{1}{40}d_p^2\nabla^2\bar{u}_p\right] + \frac{1}{6}\pi d_p^3\rho_f\frac{D\bar{u}_p}{Dt} \qquad [38]$$

The Eulerian fluid velocity at $\bar{x}$ is denoted by $\bar{u}(\bar{x}, t)$ and the Lagrangian position and velocity of the particle are denoted by $\bar{r}(t)$ and $\bar{v}(t)$, respectively. The fluid velocity seen by the particle is $\bar{u}_p = \bar{u}(\bar{r}(t), t)$. It is assumed to have zero mean, or the coordinate system is assumed to be moving with a mean fluid velocity that is uniform in space.

The terms on the right-hand side of [38] are the gravitational force (minus the buoyancy force), the Stokes drag, the Basset history force, the force due to added mass and the force resulting from stress gradients of the fluid flow in the absence of a particle. The added mass term is expressed in terms of the time derivative seen by the particle as it moves through trajectory d/dt. The term defining the influence of fluid stress-gradients on the particle is expressed in terms of the change in fluid velocity along its own trajectory.

The validity of the Maxey–Riley equation of motion is subject to the following limitations:

$$\frac{d_p(\bar{v} - \bar{u}_p)}{\nu} < 1 \qquad [39]$$

$$\left(\frac{d_p^2}{\nu}\right)\left(\frac{u_0}{L}\right) < 1 \qquad [40]$$

$$\left(\frac{d_p}{L}\right) < 1 \qquad [41]$$

For typical velocities, particle sizes and fluid properties found in fluidized beds, inequalities [40] and [41] certainly hold. However, inequality [39] may not be satisfied. For a CFB operating at 800°C with a mean particle diameter of 250 μm the left hand side of the inequality is about 2.5. In other words, the particle Reynolds number based on relative velocity is finite for the particle flows found in fluidized beds. This indicates that the advective terms in the equation of motion cannot be ignored such that the problem reduces to one of unsteady Stokes flow. Based on the work of Odar & Hamilton (1964), Berlemont *et al.* (1990) modified the Maxey–Riley equation to take into account non-small Reynolds numbers. Their equation is

$$\frac{\pi\rho_s d_p^3}{6}\frac{d\bar{v}}{dt} = \frac{\pi(\rho_s - \rho_f)d_p^3\bar{g}}{6} - \frac{\pi\rho_f C_D d_p^2}{8}(\bar{v} - \bar{u}_p - \frac{1}{24}d_p^2\nabla^2\bar{u}_p)\cdot|\bar{v} - \bar{u}_p|$$
$$-\frac{\pi d_p^2\mu C_H}{4}\int_{t_0}^{t}\frac{d}{d\tau}[\bar{v} - \bar{u}_p - \frac{1}{24}d_p^2\nabla^2\bar{u}_p]\frac{d\tau}{\left[\pi\left(\frac{\mu}{\rho_f}\right)(t-\tau)\right]^{1/2}}$$
$$-\frac{\pi d_p^3\rho_f C_A}{6}\frac{d}{dt}(\bar{v} - \bar{u}_p - \frac{1}{40}d_p^2\nabla^2\bar{u}_p) + \frac{\pi d_p^3\rho_f}{6}\frac{D\bar{u}_p}{Dt} \qquad [42]$$

The only difference between the Maxey–Riley equation and the Berlemont equation is the coefficients C_D, C_A and C_H, which take into account non-small particle Reynolds numbers and particle acceleration. $C_A \to 1/2$, $C_D \to 24/\mathrm{Re}_{d_p}$ and $C_H \to 6$ for flows where $\mathrm{Re}_{d_p, u_{sl}}$ and particle convective acceleration approach zero. This limit results in the Maxey–Riley equation.

Some words are appropriate at this point concerning the form of the equation of motion described above. In general, corrections of the form introduced by Odar & Hamilton (1964) and Berlemont *et al.* (1990) are not entirely valid. This is because the entire integration kernel associated with the Basset history term changes due to the non-linearity of a system with velocity oscillations

in the free stream and finite Reynolds numbers. The integration kernel decays at a greater rate than the classical behavior of $(t-\tau)^{1/2}$ for longer timescales (Mei & Adrian 1992; Mei *et al.* 1991b; Lovalenti & Brady 1993a, b, c).

Recent investigations into a more exact form of the hydrodynamic forces in unsteady motion have indicated that the hydrodynamic force will also depend on a Strouhal number. If the characteristic timescale, τ_c, is D/u (where u_* is the shear velocity), the Strouhal number scales as d_p/D. If the characteristic timescale is ν/u_*^2, the Strouhal number scales as Re_{d_p,u_*}.

Neither timescale introduces additional dimensionless parameters. Therefore, while not strictly valid for long timescales, [42] provides a good approximation of particle motion without the loss of any dimensionless groups.

Many effects are neglected in [42]. The sphere is assumed to be isolated and far from any boundary so that particle–particle interactions and particle–boundary interactions can be excluded. This requires that the distance from the nearest particle or boundary is much larger than the particle radius. Effects of particle rotation and lateral forces due to the shear of the undisturbed flow are also not included. In addition, electrostatic forces are ignored.

4.2. Non-dimensionalizing the Equation of Motion for a Particle in Homogeneous Turbulence

For a turbulent flow there is no single set of scales but rather a continuous spectrum of velocity and length scales which must be considered in any application of the particle equation of motion. In the core of a CFB or freeboard of a bubbling bed, the larger, more energetic motions are more characteristic. In this case the length scale is D and the velocity scale is u_* (Hinze 1975). The corresponding time scale is D/u_*.

Non-dimensionalizing [42] using these scales results in

$$\frac{\mathrm{d}\bar{v}'}{\mathrm{d}t'} = \frac{\left(\frac{\rho_s-\rho_f}{\rho_s}\right)\bar{g}D}{u_*^2} - \frac{3}{4}\left(\frac{\rho_f}{\rho_s}\right)\left(\frac{D}{d_p}\right)C_D\left(\bar{v}'-\bar{u}_p'-\frac{1}{24}\frac{d_p^2}{D^2}\nabla'^2\bar{u}_p'\right)|\bar{v}'-\bar{u}_p'|$$
$$-\frac{3}{2\sqrt{\pi}}\left(\frac{\mu^{1/2}}{u_*^{1/2}D^{1/2}\rho_f^{1/2}}\right)\left(\frac{\rho_f}{\rho_s}\right)\left(\frac{D}{d_p}\right)C_H\int\frac{\mathrm{d}}{\mathrm{d}\tau}\left(\bar{v}'-\bar{u}_p'-\frac{1}{24}\frac{d_p^2}{D^2}\nabla'^2\bar{u}_p'\right)\frac{\mathrm{d}\tau}{(t'-\tau)^{1/2}}$$
$$-\left(\frac{\rho_f}{\rho_s}\right)C_A\frac{\mathrm{d}}{\mathrm{d}t'}\left(\bar{v}'-\bar{u}_p'-\frac{1}{40}\frac{d_p^2}{D^2}\nabla'^2\bar{u}_p'\right)+\left(\frac{\rho_f}{\rho_s}\right)\frac{D\bar{u}_p'}{Dt} \qquad [43]$$

The controlling dimensionless parameters which appear in [43] are

$$\left(\frac{\rho_s-\rho_f}{\rho_s}\right)\frac{1}{\mathrm{Fr}_{u_*,D}},\ \left(\frac{\rho_f}{\rho_s}\right)\left(\frac{D}{d_p}\right)C_D,\ \frac{1}{\mathrm{Re}_{u_*,D}^{1/2}}\left(\frac{\rho_f}{\rho_s}\right)\left(\frac{D}{d_p}\right)C_H,\ \left(\frac{\rho_f}{\rho_s}\right)C_A,\ \frac{d_p^2}{D^2},\ \left(\frac{\rho_f}{\rho_s}\right) \qquad [44]$$

The coefficients C_A and C_H are functions of the acceleration number defined as the ratio of convective to local acceleration and Fr is the Froude number. This number was used by Iversen & Balent (1951) and Keim (1956) who derived it by dimensional reasoning alone. If the local length and velocity scales are on the order of the eddy length and fluctuating velocity, and convective length and velocity scales are L and u_*, the acceleration number scales as

$$\mathrm{Ac} \sim \frac{l_e}{L}\frac{u_*^2}{u_{\mathrm{flct.}}^2} \sim 2.73f\left(\frac{D}{L}\right) \qquad [45]$$

using the single phase pipe flow correlations of Hinze to estimate u_*, the eddy length scale (l_e) and the fluctuating velocity ($u_{\mathrm{flct.}}$). For typical fluid bed operating conditions, f (the gas friction factor) is about 0.04. Hence, for moderate to large aspect ratios, the acceleration number will be quite small resulting in the coefficients C_A and C_H tending toward their constant limit of 1/2 and 6, respectively. For conditions where the acceleration number is not small, C_H and C_A will depend on the bed geometry and the bed Reynolds number.

From the first term and the last term in [44] the density ratio and the Froude number based on bed diameter and friction velocity must be constant for similarity. Since C_D is a complex function of Reynolds number based on particle diameter and relative velocity (u_{rel}), $\mathrm{Re}_{u_{\mathrm{rel}},d_p}$ must also be

constant. From the second or the fifth term, the ratio of bed to particle diameter must also be included as a governing dimensionless group. Finally, the third term requires that the Reynolds number based on bed diameter and friction velocity must also be constant. The set of dimensionless parameters can be written as

$$\mathrm{Fr}_{u_*,D}, \left(\frac{\rho_s}{\rho_f}\right), \mathrm{Re}_{u_*,D}, \mathrm{Re}_{u_{rel},d_p}, \left(\frac{D}{d_p}\right) = \frac{\mathrm{Re}_{u_0,D}}{\mathrm{Re}_{u_0,d_p}}, \quad \text{bed geometry} \qquad [46]$$

If relationships of the form for single phase flow are valid, the shear velocity is of the functional form,

$$\frac{u_*}{u_0} \simeq \mathrm{fnc}\left(\frac{1}{\mathrm{Re}_{u_0,D}}\right) \quad \text{(Hinze 1975)} \qquad [47]$$

The list of governing parameters can then be rewritten as:

$$\mathrm{Fr}_{u_0,D}, \left(\frac{\rho_s}{\rho_f}\right), \mathrm{Re}_{u_0,d_p}, \mathrm{Re}_{u_0,D}, \quad \text{bed geometry} \qquad [48]$$

The Reynolds number based on particle diameter and relative velocity does not need to be included in the list because its scales with the Reynolds number based on terminal velocity (u_t) and particle diameter if

$$u_{rel} \sim u_t \qquad [49]$$

The terminal velocity based Reynolds number (Re_t) is a function of only the Archimedes number which can be written as a combination of dimensionless parameters included in [48]

$$\mathrm{Ar} = (\mathrm{Re}_{u_0,d_p})^3 \frac{1}{\mathrm{Fr}_{u_0,D}\,\mathrm{Re}_{u_0,D}} \left(\frac{\rho_s}{\rho_f}\right) \qquad [50]$$

Equation [48] shows that the governing dimensionless parameters of the equation of motion for a single particle are identical to those derived using the Anderson–Jackson equations which treated the mass of particles as a continuum.

For most fluidized beds, the ratio of fluid to solid density is very small. This allows one to ignore the added mass term and the term representing the influence of fluid stress-gradients on the particle. Moreover, the Faxen forces give rise to a relative motion scale of $d_p^2 u_*/D^2$, which is very small in fluid bed applications. This permits one to neglect the Faxen terms in [42]. However, even with these simplifications it can be shown that the governing dimensionless groups do not change. In fact, even when all terms on the right-hand side of [42] except for the drag term and the gravitational term are ignored, the set of dimensionless groups does not change.

4.3. Single Particle Equation of Motion Near a Solid Boundary

Near the wall of a fluidized bed the lift forces associated with shear of the undisturbed flow may become important. In addition, the fluid–particle drag becomes a function of the particle to wall distance. It is important for these forces to be scaled properly when evaluating phenomena very near the wall of the fluid bed. For example, bed-to-wall heat transfer may be a function of this force.

Saffman (1965) showed that a sphere subjected to a uniform shear and rotating with the fluid while translating with a velocity v experiences a side force of relative magnitude

$$1.62 d_p \mu (u_{p_x} - v_x) \left(\frac{d_p^2}{\nu}\right)^{1/2} \left(\frac{\mathrm{d}u_{p_x}}{\mathrm{d}y}\right)^{1/2}.$$

In the core of a fluid bed, this term is negligible due to the low fluid shear rates. However in the viscous sublayer near the wall, the magnitude of the fluid shear can become extremely large resulting in finite effects of shear induced lift.

The presence of a wall will increase the drag coefficient of the particle as compared to that in the case of unbounded flow (Faxen 1923). To account for this effect, modifications to the drag force of the form determined by Faxen (1923), Brenner (1961) and Maude (1961) can be used. Faxen's

expression of the correction to the drag on a small sphere in the direction parallel to the wall, χ_x, is a function of d_p/Y. Y is the particle to wall distance. Brenner (1961) and Maude (1961) independently determined the modification to the drag force for a small particle moving normal to a wall χ_r. It was also found to be a function of d_p/Y.

The equation of motion for a sphere near the wall (neglecting axial velocity gradients) is:

$$\frac{\pi\rho_s d_p^3}{6}\frac{d\bar{v}}{dt} = \frac{\pi(\rho_s-\rho_G)d_p^3 g}{6} - \frac{\pi\rho_f C_D \bar{\chi} d_p^2}{8}(\bar{v}-\bar{u}_p - \frac{1}{24}d_p^2\nabla^2\bar{u}_p)\cdot|\bar{v}-\bar{u}_p| - \frac{\pi d_p^2\mu C_H}{4}\int_{t_0}^{t}\frac{d}{d\tau}[\bar{v}-\bar{u}_p$$
$$-\frac{1}{24}d_p^2\nabla^2\bar{u}_p]\frac{d\tau}{\left[\pi\left(\frac{\mu}{\rho_f}\right)(t-\tau)\right]^{1/2}} - \frac{\pi d_p^3\rho_f C_A}{6}\frac{d}{dt}(\bar{v}-\bar{u}_p-\frac{1}{40}d_p^2\nabla^2\bar{u}_p)$$
$$+\frac{\pi d_p^3\rho_f}{6}\frac{D\bar{u}_p}{Dt} + \frac{1.62\mu d_p^2}{\nu^{1/2}}(v_x-u_{p_x})\left(\frac{du_{p_x}}{dr}\right)^{1/2} \qquad [51]$$

Near the wall neither the bed diameter nor the boundary layer thickness is a suitable length scale. Since the flow there is determined solely by u_* and ν, the proper length scale is ν/u_*. The velocity and time scales are u_* and ν/u_*^2, respectively (Hinze 1975).

Non-dimensionalizing the near-wall equation of motion yields:

$$\frac{d\bar{v}'}{dt'} = \left(\frac{\rho_s-\rho_f}{\rho_s}\right)g\left(\frac{\nu}{u_*^3}\right) - \frac{3}{4}\frac{\left(\frac{\nu}{u_*}\right)}{d_p}\left(\frac{\rho_f}{\rho_s}\right)C_D\bar{\chi}'\left(\bar{v}'-\bar{u}_p'-\frac{1}{24}\frac{d_p^2}{D^2}\nabla'^2\bar{u}_p'\right)|\bar{v}'-\bar{u}_p'|$$
$$-\frac{3}{2\sqrt{\pi}}\left(\frac{\mu}{u_* d_p\rho_f}\right)\left(\frac{\rho_f}{\rho_s}\right)C_H\int_{t_0}^{t'}\frac{d}{d\tau}\left(\bar{v}'-\bar{u}_p'-\frac{1}{24}\frac{d_p^2}{D^2}\nabla'^2\bar{u}_p'\right)\frac{d\tau}{(t'-\tau)^{1/2}}$$
$$-\left(\frac{\rho_f}{\rho_s}\right)C_A\frac{d}{dt'}\left(\bar{v}'-\bar{u}_p'-\frac{1}{40}\frac{d_p^2}{D^2}\nabla'^2\bar{u}_p'\right)+\left(\frac{\rho_f}{\rho_s}\right)\frac{D\bar{u}_p'}{Dt'}+\frac{9.72}{\pi}\frac{\mu}{d_p\rho_s u_*}(v_x'-u_{p_x}')\frac{du_{p_x}'}{dr'}\bar{i}_r \qquad [52]$$

where

$$\bar{\chi}' = fnc(\mathrm{Re}_{d_p,u_*}) \qquad [53]$$

The governing parameters which appear in [52] are:

$$\left(\frac{g\mu}{\rho_f u_*^3}\right), \mathrm{Re}_{u_*,d_p}\left(\frac{\rho_s}{\rho_f}\right)\frac{1}{C_D}, \mathrm{Re}_{u_*,d_p}\left(\frac{\rho_s}{\rho_f}\right)\frac{1}{C_H}, \left(\frac{\rho_f}{\rho_s}\right)C_A, \left(\frac{\rho_f}{\rho_s}\right), \frac{d_p}{D}, \mathrm{Re}_{u_*,d_p}\left(\frac{\rho_s}{\rho_f}\right) \qquad [54]$$

The independent dimensionless parameters are:

$$\mathrm{Re}_{u_0,d_p}, \mathrm{Re}_{u_0,D}, \left(\frac{\rho_f}{\rho_s}\right), \mathrm{Fr}_{u_0,d_p}, C_H \text{ and } C_A \qquad [55]$$

(Note that the first term in [54] can be written as

$$\left(\frac{g\mu}{\rho_f u_*^3}\right) = \frac{1}{\mathrm{Re}_{u_*,d_p}\mathrm{Fr}_{u_*,d_p}}.$$

As discussed earlier, C_H and C_A are nearly constant for conditions found in fluidized beds. For conditions where they are not constant, they only depend on bed geometry and bed Reynolds number. Hence, the set of dimensionless groups which govern particle hydrodynamics in the near-wall region is identical to those governing particle motion in the core, namely

$$\mathrm{Re}_{u_0,d_p}, \mathrm{Re}_{u_0,D}, \left(\frac{\rho_f}{\rho_s}\right), \mathrm{Fr}_{u_0,d_p}, \quad \text{bed geometry} \qquad [56]$$

If the Faxen terms, Basset history term, added mass term, the term representing fluid stress gradients on the particle and the Saffman lift force are ignored, the governing independent parameters do not change.

It should be noted that, in general, the particle fluid drag will also be a function of particle sphericity and bed voidage (Wen & Yu 1966b).

$$F_{\text{drag}} = f(\epsilon)g(\phi)\frac{\pi}{8}d_p^2\rho_g(\bar{v}-\bar{u}_p)|\bar{v}-u_p| \qquad [57]$$

The inclusion of $f(\epsilon)$ and $g(\phi)$ in the drag term extends the analysis to include non-spherical particles. This results in the particle sphericity being added to the list of parameters in [48] and [56].

4.4. Boundary Conditions

A particle with location $y(t)$ in the flow field is required to satisfy the following boundary conditions.

$$\bar{u} = \bar{v} + \bar{\Omega} \times [\bar{x} - \bar{y}(t)] \quad \text{on the particle}$$

$$\bar{u}(\bar{x}, t) = \frac{u_0 \bar{i}}{\epsilon} \quad \text{as} \quad \frac{|\bar{x} - \bar{y}(t)|}{d_p} \to \infty$$

$$\bar{v} = \frac{G_s(t)}{\rho_s(1-\epsilon)}\bar{i} \quad \text{as } \bar{y}(t) \to 0$$

$$\bar{v}(\bar{x}, t) = \frac{u_0}{\epsilon}\bar{i} \quad \text{as } \bar{y}(t) \to L \qquad [58]$$

where Ω is the angular velocity of a particle.

The initial condition is set such that the particle velocity is zero as it enters the flow field, and the disturbance field is zero before $t = 0$.

$$\bar{v}(0) - \bar{u}(\bar{y}(0), 0) - \tfrac{1}{6}d_p^2\nabla^2\bar{u} = 0 \qquad [59]$$

Assuming that particle rotation is negligible, the non-dimensional form of the boundary equation is:

$$\bar{u}' = \bar{v}' \quad \text{on the particle}$$

$$\bar{u}' = \frac{1}{\epsilon} \quad \text{as} \quad \frac{|\bar{x} - \bar{y}(t)|}{d_p} \to \infty$$

$$\bar{v}' = \frac{G_s}{\rho_s U_0(1-t)}\bar{i} \quad \text{as } \bar{y}(t) \to 0$$

$$\bar{v}' = \frac{1}{\epsilon}\bar{i} \quad \text{as } \bar{y}(t) \to L \qquad [60]$$

$$v'(0) - u'(y(0), 0) - \frac{1}{6}\frac{d_p^2}{D^2}\nabla^2 u' = 0 \qquad [61]$$

For fluidized beds, the Faxen force contribution to the initial condition can be dropped resulting in

$$v'(0) - u'(y(0), 0) = 0 \qquad [62]$$

The controlling set of dimensionless groups which result from the single particle equation of motion and the boundary conditions is then

$$\text{Fr}_{u_0,D}, \left(\frac{\rho_s}{\rho_f}\right), \text{Re}_{u_0,d_p}, \text{Re}_{u_0,D}, \frac{G_s}{\rho_s u_0}, \phi, \frac{L}{D} \qquad [63]$$

5. DESIGN OF SCALE MODELS BASED ON FULL SET OF SCALING RELATIONS

5.1. Scale Model Operating Conditions

To construct a model which will give behavior similar to another bed, for example, a commercial bed, all of the dimensionless parameters listed in [35] or [37] must have the same value for the two beds. The requirements of similar bed geometry is met by use of geometrically similar beds; the ratio of all linear bed dimensions to a reference dimension such as the bed diameter must be the same for the model and the commercial bed. This includes the dimensions of the bed internals. The dimensions of elements external to the bed such as the particle return loop do not have to be matched as long as the return loop is designed to provide the proper external solids flow rate and size distribution† (Rhodes & Laussman 1992).

Proper conditions must be chosen to design a scale model to match the dimensionless parameters of the target bed. To model a gas fluidized commercial bed, a scale model using air at standard conditions is most convenient, although several investigators have used other gases (Fitzgerald & Crane 1980; Fitzgerald *et al.* 1984; Chang & Louge 1992) or pressurized scale models (Almstedt & Zakkay 1990; Di Felice *et al.* 1992a, b). The gas choice for the model determines the values of ρ_f and μ. The model particle density is chosen to match the density ratio, so that

$$\left(\frac{\rho_f}{\rho_s}\right)_m = \left(\frac{\rho_f}{\rho_s}\right)_c \qquad [64]$$

where the subscript m is for the model and c is for the commercial bed. For the remaining parameters the form of [35] will be chosen for the dimensionless parameters. Combining the Reynolds number based on bed diameter and the square root of the Froude number,

$$\frac{\rho_f u_0 D}{\mu_f}\frac{\sqrt{gD}}{u_0} = \left(\frac{D^{3/2}\sqrt{g}}{\nu_f}\right)_m = \left(\frac{D^{3/2}\sqrt{g}}{\nu_f}\right)_c \qquad [65]$$

Rearranging,

$$\left(\frac{D_m}{D_c}\right) = \left(\frac{(\nu_f)_m}{(\nu_f)_c}\right)^{2/3} \qquad [66]$$

All of the linear dimensions of the model are scaled to the corresponding dimensions of the commercial bed by the ratio of the kinematic viscosities raised to the two-thirds power. By taking the ratio of Reynolds number based on the particle diameter to Reynolds number based on the bed diameter,

$$\frac{\rho_f u_0 D}{\mu_f}\cdot\frac{\mu_f}{\rho_f u_0 d_p} = \left(\frac{D}{d_p}\right)_m = \left(\frac{D}{d_p}\right)_c \qquad [67]$$

The particle diameters in the model scale by the same factor as the bed diameter, by the ratio of the kinematic viscosities to the two thirds power.

Taking the product of the Reynolds number and the Froude number, using [66] and rearranging,

$$\frac{u_{0_m}}{u_{0_c}} = \left(\frac{\nu_{f_m}}{\nu_{f_c}}\right)^{1/3} = \left(\frac{D_m}{D_c}\right)^{1/2} \qquad [68]$$

By satisfying both [66] and [68], the Reynolds number and the Froude number are kept identical between the model and the commercial bed.

Combining $G_s/\rho_s u_0$ and the product of Reynolds and Froude numbers along with [66] it can be shown that

$$\frac{\left(\frac{G_s}{\rho_s}\right)_m}{\left(\frac{G_s}{\rho_s}\right)_c} = \left(\frac{\nu_{f_m}}{\nu_{f_c}}\right)^{1/3} \qquad [69]$$

†In rare occasions, solid or gas flow fluctuations set up by the return loop design will influence the bed dynamics. In that case the return loop design may be important.

so that the ratio of solids flow to solids density scales as the ratio of the third root of the kinematic viscosity.

To satisfy the full set of dimensionless parameters, once the model fluid pressure and temperature are chosen there is one unique set of parameters for the model which gives similarity. The dependent variables, as non-dimensionalized by [25] will be the same in the respective dimensionless time and spatial coordinates of the model as the commercial bed. The spatial variables are non-dimensionalized by the bed diameter so that the dimensional and spatial coordinates of the model is proportional to two-thirds the power of the kinematic viscosity, as given by [66],

$$\frac{x_m}{x_c} = \left(\frac{\nu_m}{\nu_c}\right)^{2/3} \quad [70]$$

The velocity scales with $\nu_f^{1/3}$, the ratio of time scales can be expressed as

$$\frac{t_m}{t_c} = \left(\frac{\nu_{f_m}}{\nu_{f_c}}\right)^{1/3} \quad [71]$$

Similarly, it can be shown that the frequency scales as

$$\frac{f_m}{f_c} = \left(\frac{\nu_{f_c}}{\nu_{f_m}}\right)^{1/3} \quad [72]$$

Table 1 gives the values of design and operating parameters of a scale model fluidized with air at ambient conditions which simulates the dynamics of a fluidized bed combustor operating at 850°C. Fortunately, the linear dimensions of the model are much smaller, roughly one quarter, than the combustor. The particle density in the model must be much higher than the density in the combustor to maintain a constant value of the gas to solid density ratio. Note that the superficial velocity of the model differs from that of the combustor as well as the spatial and temporal variables.

When modeling a pressurized hot bed (table 2) the ambient temperature model fluidized with air has dimensions very close to those of the pressurized combustor. If another gas is used in the

Table 1. Atmospheric combustor modeled by a bed fluidized at ambient conditions

Given	Commercial bed	Scale model
Temperature (°C)	850	25
Gas viscosity (10^{-5} kg/ms)	4.45	1.81
Density (kg/m^3)	0.314	1.20
Derived from scaling laws		
Solid density	ρ_{sc}	$3.82\rho_{sc}$
Bed diameter, length, etc.	D_c	$0.225D_c$
Particle diameter	d_{pc}	$0.225d_{pc}$
Superficial velocity	u_{oc}	$0.47u_{oc}$
Volumetric solid flux	$(G_s/\rho_s)_c$	$0.47\ (G_s/\rho_s)_c$
Time	t_c	$0.47t_c$
Frequency	f_c	$2.13f_c$

Table 2. Pressurized combustor modeled by a bed fluidized with air at ambient conditions

Given	Commercial bed	Scale model
Temperature (°C)	850	25
Gas viscosity (10^{-5} kg/ms)	4.45	1.81
Density (kg/m^3)	3.14	1.20
Pressure (Pa)	10^6	10^5
Derived from scaling laws		
Solid density	ρ_{sc}	$0.382\rho_{sc}$
Bed diameter, length,	D_c	$1.05D_c$
Particle diameter	d_{pc}	$1.05d_{pc}$
Superficial velocity	u_{oc}	$1.01u_{oc}$
Volumetric solid flux	$(G_s/\rho_s)_c$	$1.01\ (G_s/\rho_s)_c$
Time	t_c	$1.01t_c$
Frequency	f_c	$0.98f_c$

Table 3. Pressurized combustor modeled by a bed *fluidized* with refrigerant vapor 134a at ambient conditions

Given	Commercial bed	Scale model
Temperature (°C)	850	20
Gas viscosity (10^{-5} kg/ms)	4.45	1.19
Density (kg/m^3)	3.14	4.34
Pressure (Pa)	10^6	10^5
Derived from scaling laws		
Solid density	ρ_{sc}	$1.38\rho_{sc}$
Bed diameter, length	D_c	$0.334D_c$
Particle diameter	d_{pc}	$0.334d_{pc}$
Superficial velocity	u_{oc}	$0.58u_{oc}$
Volumetric solid flux	$(G_s/\rho_s)_c$	$0.58\ (G_s/\rho_s)_c$
Time	t_c	$0.58t_c$
Frequency	f_c	$1.7f_c$

model, particularly a gas with a higher density, the model can be made much smaller than the pressurized combustor (see table 3). Care must be taken to select a safe modeling gas and one which yields a solid density for the model which is available.

5.2. *Non-isothermal Conditions*

Since a fluidized bed is characterized by intense solids mixing, most of the bed volume is isothermal. An exception is the immediate vicinity of the distributor or other fluid or solid entrances to the bed. If the fluid entering the bed is at a different temperature than the bed, the entering material undergoes a rapid temperature change. For a gas jet there is a corresponding density and velocity change. For a laboratory model it is difficult to simulate this region exactly.

These thermal effects are confined to the entrance region but they may influence initial bubble formation or particle mixing. An approximate method to compensate for this effect can be used in an isothermal model where the entering fluid temperature is the same as the bed temperature. We will consider the case of a gas jet to allow for density changes due to temperature changes. Generally, the entering velocity is low enough to neglect the influence of the Mach number. The key concern is the size of the orifices of the cold model to properly account for the non-isothermal effect of the commercial bed.

Consider a simple case when the entering jet is heated and expands while entraining solids initially at zero velocity but not entraining fluids from the bed (this does not alter the conclusion, it only simplifies the resulting equations).

For the commercial bed with a temperature change for the entering jet, the mass flow rate at steady state must be the same at the orifice conditions as it is at the bed temperature while the volume flow rate changes. Thus for one dimensional flow of gas

$$\rho_{f_{or}} u_{or} A_{or} = \rho_{f_{Bed}} u_{Bed} A_{Bed} \epsilon \qquad [73]$$

where the left-hand side terms are evaluated at orifice conditions and the right-hand side at bed conditions.

Similarly, if there are no friction losses and there is uniform pressure in the entrance region the momentum balance must yield

$$\rho_{f_{or}} u_{or}^2 A_{or} = \rho_{f_{Bed}} u_{Bed}^2 A_{Bed} \epsilon + \rho_s v_{Bed}^2 A_{Bed} (1 - \epsilon) \qquad [74]$$

where A_{or} is the orifice area.

Dividing [74] by the first term on the right-hand side,

$$\frac{\rho_{f_{or}} u_{or}^2 A_{or}}{\rho_{f_{Bed}} u_{Bed}^2 A_{Bed}} = \epsilon + \frac{\rho_s v_{Bed}^2 A_{Bed}}{\rho_{f_{Bed}} u_{Bed}^2 A_{Bed}} (1 - \epsilon) \qquad [75]$$

To obtain equal solid to bed fluid momentum flux at the same solids void fraction, the ratio of

orifice to bed fluid momentum must be the same in the isothermal model as it is in non-isothermal commercial bed entrance region.

$$\left(\frac{\rho_{f_{or}} u_{or}^2 A_{or}}{\rho_{f_{Bed}} u_{Bed}^2 A_{Bed}}\right)_m = \left(\frac{\rho_{f_{or}} u_{or}^2 A_{or}}{\rho_{f_{Bed}} u_{Bed}^2 A_{Bed}}\right)_c \quad [76]$$

Now multiplying each side by the square of the ratio of fluid mass flow rate at bed condition to model conditions,

$$\left(\frac{\rho_{or_f} u_{or}^2 A_{or}}{\rho_{Bed_f} u_{Bed}^2 A_{Bed}}\right)_m \left(\frac{\rho_{Bed_f} u_{Bed} A_{Bed}}{\rho_{or_f} u_{or} A_{or}}\right)_m^2 \epsilon^2 = \left(\frac{\rho_{Bed_f} A_{Bed}}{\rho_{or_f} A_{or}}\right)_m \epsilon^2 = \left(\frac{\rho_{Bed_f} A_{Bed}}{\rho_{f_{or}} A_{or}}\right)_c \epsilon^2 \quad [77]$$

For the model, the fluid density at the orifice is the same as everywhere else in the model. The voidage in the model and commercial beds should be the same. Thus, [77] becomes

$$\left(\frac{A_{Bed}}{A_{or}}\right)_m = \left(\frac{\rho_{Bed_f} A_{Bed}}{\rho_{or_f} A_{or}}\right)_c \quad [78]$$

The orifice-to-bed area ratio in the model differs from the corresponding area ratio in the commercial bed by the ratio of fluid density leaving the orifice and throughout the bed.

6. SIMPLIFICATION TO THE SCALING LAWS

When constructing a model fluidized with ambient air, matching the full set of scaling parameters results in a unique set of values for the particle density and diameter and for the linear dimensions of the bed. By simplifying the set of scaling relationships, it is possible to relax the constraint on the dimensions of the model relative to the full scale bed.

The full set of scaling relationships were obtained by non-dimensionalizing the equations of motion for the particles and the fluid in a fluidized bed along with their boundary conditions. In most situations, the viscous forces associated with the macroscopic gas and particle velocity gradients are negligible compared to the interphase drag. This is seen in [17b] and [18b] where the terms representing the fluid and particle viscous stresses are multiplied by the inverse of a Reynolds number based on superficial velocity and bed diameter. If it is assumed that these terms can be dropped from the fluid and particle phase stress tensors, non-dimensionalization of the continuum equations yields the following dimensionless parameters:

$$\frac{u_0^2}{gD}, \frac{\rho_s}{\rho_f}, \frac{\beta D}{\rho_s u_0}, \frac{D}{L}, \frac{G_s}{\rho_s u_0} \quad [79]$$

In the general case, $(\beta D)/(\rho_s u_0)$ is related to the viscous and inertial forces of the fluid through the Ergun equation or through the expression for drag on a single sphere. These relationships indicate that $(\beta D)/(\rho_s u_0)$ is dependent on the Reynolds number based on the particle diameter, d_p/D and the dimensionless particle size distribution. Substituting these parameters into [79] yields the full set of scaling parameters described previously above.

6.1. Simplification to the Scaling Laws

Glicksman (1984) showed that the list of controlling dimensionless parameters could be reduced if the fluid–particle drag is primarily viscous or primarily inertial. The standard viscous and inertial limits for the drag coefficient apply. This gives approximately

Viscous: $\mathrm{Re}_{u_{rel}, d_p} |\bar{u}' - \bar{v}'| < 10$

Inertial: $\mathrm{Re}_{u_{rel}, d_p} |\bar{u}' - \bar{v}'| > 1000$ [80]

using the Ergun equation.

The use of a Reynolds number based on relative velocity rather than superficial velocity in setting these limits was suggested by Horio (1990). In setting viscous or inertial limits, it is the interphase

drag which is characterized as being dominated by viscous or inertial forces. The particle inertia is important even if the interphase drag is viscous dominated. This is because of the typically large solid-to-gas density ratio.

6.2. *Viscous Limit*

For viscous dominated flows, it can be assumed that the gas inertia and the gas gravitational forces are negligible. In most situations, the viscous forces in the gas which are associated with macroscopic gas velocity gradients are negligible compared with the interphase drag; the term representing these forces can be removed from the gas momentum equation. The dimensionless gas momentum equation becomes

$$\nabla' p' + \frac{\beta L}{\rho_s u_0}(u' - v') = 0 \qquad [81]$$

From the Ergun equation, the dimensionless drag coefficient can be written as

$$\frac{\beta L \phi}{\rho_s u_0} \simeq 150 \frac{(1-\epsilon)^2}{\epsilon^3}\left(\frac{L}{d_p}\right)\frac{1}{\mathrm{Re}_{u_0, d_p}} \qquad [82]$$

The remaining set of dimensionless equations does not include a density ratio. The ratio between the bed and particle diameters and the Reynolds number based on bed diameter, superficial velocity and solid density appear only in the modified drag expression, in which they are combined. These parameters form a single parameter, as has been discussed by Glicksman (1988) and other investigators. The set of independent parameters controlling viscous dominated flow are then

$$\frac{\rho_s u_0 d_p^2}{\mu D}, \phi, \frac{gD}{u_0^2}, \frac{D}{L}, \frac{G_s}{\rho_s u_0}, \mathrm{PSD} \qquad [83]$$

The first term in the list multiplied by the third term has been shown by Glicksman (1988) to be equivalent to the ratio of superficial and minimum fluidization velocities. The controlling parameters can therefore be written as

$$\frac{u_{mf}}{u_0}, \phi, \frac{gD}{u_0^2}, \frac{D}{L}, \frac{G_s}{\rho_s u_0}, \mathrm{PSD} \qquad [84]$$

For very small particles or small particle-gas relative velocities, the single particle equation of motion at large distances from a boundary approaches the Maxey–Riley equation. If the terms in the equation of motion with a coefficient of (ρ_f/ρ_s) in addition to the Faxen forces are neglected, and it is assumed that the friction velocity is a weak function of bed Reynolds number, the controlling dimensionless parameters are identical to those determined from the continuum flow field analysis. The viscous limit requirement is based on the assumption that the dimensionless interphase drag can be modeled as a linear function of the particle Reynolds number. Because of clustering of particles, this may not be a valid assumption, and the requirements for neglecting gas inertia may be much more stringent. As will be discussed in the experimental verification of simplified scaling laws, a viscous limit for interphase drag may not exist in CFBs.

It must be borne in mind that this set is valid only when fluid inertial effects are negligible, i.e. they are a subset of the general relationships. Glicksman (1984) used the criteria for the viscous limit in a bubbling bed that the ratio of viscous forces to fluid inertial forces in the Ergun equation is ten or larger. From table 1 of that reference, for a bed of glass or sand fluidized with air at standard conditions with u_0/u_{mf} of 3, the viscous limit occurs when particles are less than about 200 μm. In regions where particles behave individually, the viscous limit occurs for particles less than 60 μm (assuming the particle/gas relative velocity is equal to the particle terminal velocity and the single particle viscous limit criterion is $\mathrm{Re}_{u_{rel}, d_p} < 1$).

6.3. Inertial Limit

In the inertial limit, the bulk gas friction is clearly negligible, and this term can be dropped from the gas momentum equation. From the dimensionless equations of motion, it can be shown that the controlling dimensionless parameters are

$$\frac{\beta D}{\rho_s u_0}, \frac{gD}{u_0^2}, \frac{L}{D}, \frac{\rho_f}{\rho_s}, \phi, \text{PSD} \qquad [85]$$

In the high Reynolds number limit, the Ergun equation simplifies to

$$\frac{\beta D}{\rho_s u_0} \simeq 1.75 \frac{(1-\epsilon)}{\epsilon} |\bar{u}' - \bar{v}'| \left(\frac{D}{d_p}\right)\left(\frac{\rho_f}{\rho_s}\right) \qquad [86]$$

The dimensionless interphase drag is only a function of $(\rho_f/\rho_s)(D/d_p)$, ϵ and ϕ; the gas viscosity is unimportant. The governing parameters are then

$$\frac{gD}{u_0^2}, \frac{\rho_f}{\rho_s}, \frac{d_p}{D}, \frac{L}{D}, \phi \quad \text{and} \quad \text{PSD} \qquad [87]$$

At high Reynolds numbers, the viscous drag forces between a single particle and gas are negligible compared to the inertia force. The interphase drag expression can be simplified by setting the drag coefficient equal to 0.44. This coefficient applies for Reynolds numbers based on the relative velocity in the range from 1000 to 100,000. The parameters which result from non-dimensionalizing the resulting equation of motion for a single particle can be shown to be equivalent to those derived from the inertial limit of the continuum analysis.

The minimum size of the particle diameter at the inertial limit in a bubbling bed was approximated by Glicksman (1984) in a manner similar to that for the viscous limit. It was found that one atmosphere $d_{P_{min}}$ is approx. 2.6 and 7.3 mm for bed temperatures of 15 and 800°C, respectively (assuming a particle density of 2.5 g/cm^3). For particles which behave individually, the respective diameters are 1.6 and 4.5 mm (assuming the particle/gas relative velocity is equal to the particle terminal velocity and the inertial limit criterion is $\mathrm{Re}_{u_{rel},d_p} > 1000$).

It is interesting to note that the density ratio enters as a separate parameter in the list developed from the single particle equation of motion, [63], only if the particle motion is accelerating or highly time dependent (virtual mass and Basset history terms become significant). This is a direct result of how the general equation of motion was developed. One of the assumptions used to develop particle equations of motion of the type of Maxey & Riley is that the advective terms in the gas momentum equation can be neglected. This results in the density ratio only entering the list of parameters as a product with the ratio of bed to particle diameters. Similar results are obtained in the inertial limit using the continuum analysis if gas-phase inertial contributions are negligible (Zhang & Yang 1987). If this assumption is not made, the solid to fluid density ratio appears in the list of governing dimensionless groups.

6.4. New Simplified Scaling Laws

The viscous and inertial limits only apply for their respective limits. In order to reduce the number of scaling parameters, Glicksman *et al.* (1993b) explored various forms of the drag relationship to investigate simplifications to the full set of scaling parameters which would be valid over a wide range of Reynolds numbers. The following discussion is a summary of this study.

6.4.1. Low Reynolds number

At low particle Reynolds numbers the Ergun equation can be simplified using only the viscous limit term.

Thus

$$\frac{\beta D}{u_0 \rho_s} \to 150 \frac{\epsilon(1-\epsilon)^2}{\epsilon^3} \frac{\mu D}{\rho_s u_0 (\phi d_p)^2} \quad \text{for} \quad \frac{\rho_f u_0 d_p}{\mu} \to 0 \qquad [88]$$

At the same limit the minimum velocity can be written for gas fluidized beds where $\rho_s - \rho_f$ can be replaced by ρ_s as,

$$u_{mf} = \frac{\rho_s g(1-\epsilon_{mf})}{\left[150\dfrac{1-\epsilon_{mf}^2}{\epsilon_{mf}^3}\dfrac{\mu}{(\phi d_p)^2}\right]} \quad [89]$$

Substituting [89] into [88],

$$\frac{\beta D}{\rho_s u_0} = \frac{g(1-\epsilon)^2}{(1-\epsilon_{mf})\epsilon^2 u_{mf}}\frac{\epsilon_{mf}^3 D}{\rho_s u_0} = \frac{1}{\mathrm{Fr}}\frac{u_0}{u_{mf}}\frac{(1-\epsilon)^2}{\epsilon_{mf}^3(1-\epsilon_{mf})\epsilon^2} \quad [90]$$

Thus, in the low particle Reynolds number limit, maintaining u_0/u_{mf}, ϵ_{mf} and Fr identical between two fluidized bed guarantees that $\beta D/\rho_s u_0$ is also identical. Although ϕ and d_p are eliminated between [88] and [89], in general particle sphericity and dimensionless size distribution should be held constant in the scaling. The use of ϕ and a mean diameter in the Ergun expression only approximates the effects of these parameters. In this limit, the governing parameters given in [79] can be expressed as,

$$\frac{u_0^2}{gD}, \frac{\rho_s}{\rho_f}, \frac{u_0}{u_{mf}}, \frac{D}{L}, \frac{G_s}{\rho_s u_0}, \phi, \mathrm{PSD} \quad [91]$$

where ϵ_{mf} will be a function of particle sphericity and size distribution.

6.4.2. *Large Reynolds number*

Consider the limit of high particle Reynolds numbers where the inertial term in the Ergun equations dominates.

In this limit,

$$\frac{\beta D}{\rho_s u_0} \to 1.75\frac{(1-\epsilon)}{\epsilon}\frac{\rho_f}{\rho_s}\frac{D|\bar{u}' - \bar{v}'|}{\phi d_p} \quad [92]$$

where $u' = u/u_0$ and $u' - v'$ is a dimensionless relative velocity. The minimum fluidization velocity can be expressed as,

$$u_{mf}^2 = \frac{\epsilon_{mf}^3}{1.75}\frac{\phi d_p \rho_s g}{\rho_f} \quad [93]$$

Substituting this into [92] and mutiplying by Fr,

$$\mathrm{Fr}\frac{\beta D}{\rho_s u_0} = \frac{u_0^2}{gD}\frac{\epsilon_{mf}^3 D|\bar{u}' - \bar{v}'|g(1-\epsilon)}{\epsilon u_{mf}^2} = \frac{u_0^2}{u_{mf}^2}\frac{\epsilon_{mf}^3(1-\epsilon)|\bar{u}' - \bar{v}'|}{\epsilon} \quad [94]$$

At large particle Reynolds numbers, just as at the low Reynolds numbers, the dimensionless drag, $\beta D/\rho_s u_0$, is identical when u_0/u_{mf}, ϵ_{mf} and Fr are identical. ϵ, u' and v' are dependent dimensionless variables which are identical for two similar fluidized beds. In this limit the same set of governing dimensionless parameters applies as in the viscous limit, given by [91].

Since the same simplified set of dimensionless parameters holds exactly at both high and low Reynolds numbers, it is reasonable to expect that they will hold, at least approximately, over the entire range of conditions for which the drag coefficient can be determined by the Ergun equation or an equation of similar form. The validity of the simplified parameters can be checked numerically for the intermediate range of values.

6.4.3. *General case*

Of particular concern is the error in the dimensionless drag coefficient when a scale model is designed using the simplified set of scaling rules [91]. The simplified scaling parameters allow smaller models to simulate a given sized target bed. As the length scale is reduced the superficial velocity must be reduced to maintain a constant Froude number. The particle diameter must also be reduced to keep u_0/u_{mf} constant.

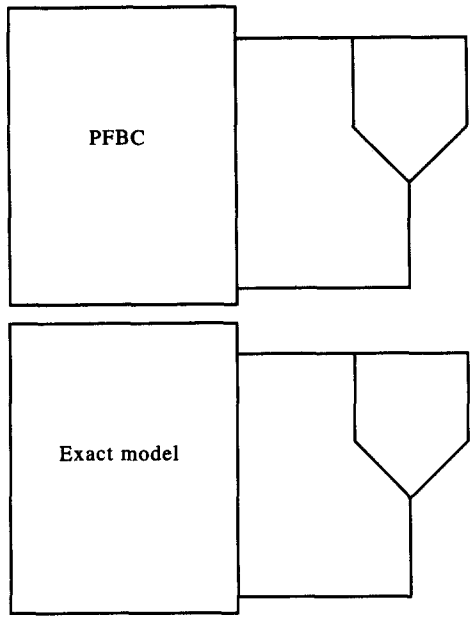

	P	T (°C)	L	u_o
PFBC	101.3 Pa	800	L_o	u_o
Exact model	101.3 Pa	20	L_o	u_o
1/4 Scale simplified model	101.3 Pa	20	$L_o/4$	$u_o/2$
1/16 Scale simplified model	101.3 Pa	20	$L_o/16$	$u_o/4$

Figure 3. Exact and simplified models of a pressurized combustor, shown at the same scale.

To determine the validity of the smaller, simplified models, the dimensionless drag coefficient $\beta D/\rho_s u_0$ can be compared between the models designed using the simplified scaling laws and whose linear dimensions are one quarter and one sixteenth, respectively, of the linear dimensions of a model designed using the full set of scaling laws. Figure 3 shows a comparison of the exact model and the simplified models for a fluidized combustor pressurized to 10^6 Pa. Using the full set of scaling laws the exact model, fluidized by ambient air at one atmosphere, is approximately the same size as the combustor. The models using the simplified scaling laws are reduced in size by their respective assumed length scale. The other parameters of the simplified model are then calculated to match the dimensionless parameters in [91].

The errors in the dimensionless drag coefficient $\beta D/\rho_s u_0$ using the simplified scaling models are shown on figures 4 and 5 for u_0/u_{mf} of 10 and 1000, respectively, plotted as a function of Re_{pE}, the Reynolds number based on parameters for the exact scaled bed. For a particle Reynolds number of 1000 or less, which corresponds to pressurized beds with particles of 1 mm or less, the error in the drag coefficient with the simplified scaling laws is 20% or less for a one-quarter length scale model. The error is 40% or less for a one-sixteenth length scale mode. At u_0/u_{mf} of 1000 and u_{rel}/u_0 of 1/50 the errors for the one-sixteenth scale model are 20% or less for Re_{pE} less than 10^3. For particles of 0.2 mm or less, corresponding to a Reynolds number of 100 or less, the errors in drag coefficient are minimal. When the Ergun equation applies for the drag coefficient, a one-quarter scale model based on the simplified scaling laws should be valid for any conditions. A one-sixteenth scale model should be valid for particle diameters of about 0.2 mm or less for a pressurized bubbling bed with u_0/u_{mf} of 10 and u_{rel}/u_0 of 0.3. At u_0/u_{mf} of 1000 and u_{rel}/u_0 of 1/50, the one-sixteenth scale model should be valid for pressurized beds with particles up to 1 mm in diameter. These conclusions apply when the particle to fluid drag is given by the Ergun equation

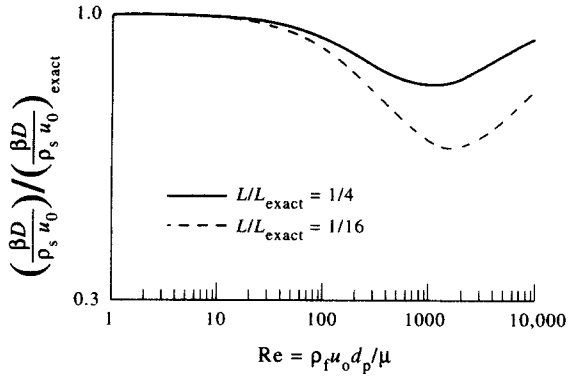

Figure 4. Error in dimensionless drag coefficient, Ergun equation, $u_0/u_{mf} = 10$, $u_{sl}/u_0 = 1/50$.

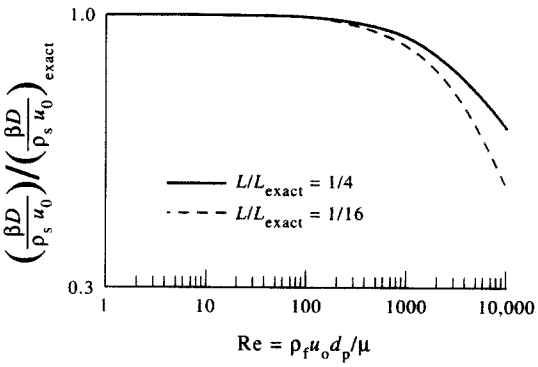

Figure 5. Error in dimensionless drag coefficient, Ergun equation, $u_0/u_{mf} = 1000$, $u_{sl}/u_0 = 0.3$.

or similar relationships and the scaled particles are not so small that interparticle surface forces come into play.

6.4.4. *Clusters*

In the freeboard of a bubbling bed or in the upper portion of a circulating bed where particles generally are considered to act in clusters or groups, a similar examination of scaling of the gas to solid drag can be made. Consider all of the particles grouped into clusters with an effective diameter d_c and the clusters occupying a volume fraction ϵ_c of the bed volume. The cluster to gas drag will be represented by the drag coefficient for a solid sphere of diameter d_c,

$$\beta|\bar{u} - \bar{v}|\frac{\pi d_c^3}{6(1-\epsilon_c)} = \tfrac{1}{2}\rho_f \frac{\pi d_c^2}{4}|\bar{u} - \bar{v}|^2 C_D \qquad [95]$$

This can be rewritten as,

$$\frac{\beta D}{\rho_s u_0} = \frac{3}{4}\left(\frac{\rho_f}{\rho_s}\right)|\bar{u}' - \bar{v}'|C_D \frac{D}{d_c}(1-\epsilon_c) \qquad [96]$$

If the diameter of individual particles does not influence the drag of a cluster of particles, then when the solid-to-gas density ratio is held constant between the combustor and the model, the dimensionless drag $\beta D/\rho_s u_0$ is properly scaled when the fluid to gas density ratio is held constant between the model and the combustor and C_D is invariant.

If the reduced scale models faithfully reproduce the dynamics of the exact case, the cluster dimensions should scale directly with the linear dimensions of the bed. Thus, a one-quarter linear scale model which has a velocity one-half that of the exact case will have a cluster Reynolds number (Re_{d_c}) one-eighth that of the exact bed. From the relationship of C_D with Re the change of C_D with model scale at a given Reynolds number of the exact bed can be determined. Figure 6 shows the shift in C_D using the relationship of White (1974) for length scales of one-quarter, one-eighth and one-sixteenth, respectively, of the exact bed length as a function of the cluster Reynolds number of the exact bed. Also shown on the figure is the typical Reynolds number of an atmospheric combustor with a 0.3 m cluster diameter, approx. 1.5×10^4. In a bubbling bed, the cluster diameter in the freeboard should be at least equal in size to the diameter of bubbles erupting at the bed surface. For beds with horizontal tubes, the bubble diameter will be equal to or larger than the horizontal tube spacing. In a bubbling bed without tubes, the bubbles and clusters can be much larger. In an open circulating bed the cluster diameter is more difficult to determine. It is reasonable to assume its diameter is proportional to the bed diameter, equal in magnitude to the bed diameter or one order of magnitude smaller. From these considerations, the Reynolds number based on the cluster diameter should be 10^4 or larger in an atmospheric combustor with a cluster diameter of 0.2 m. The cluster Reynolds number should be 10^5 or larger in a pressurized combustor. From figure 6 it can be seen that a one-quarter scale or an eighth scale model should have drag coefficients similar to the exact bed. For pressurized beds, the drag coefficients should be very close in magnitude.

6.4.5. Individual particles

If the drag coefficient, β, is influenced by the characteristics of individual particles, the detailed particle dynamics of the simplified scale models must be examined. In this case,

$$\frac{\beta D}{\rho_s u_0} = \frac{3}{4}\left(\frac{\rho_f}{\rho_s}\right)|\bar{u}' - \bar{v}'|C_D \frac{D}{d_p}(1-\epsilon) \qquad [97]$$

where C_D is the drag coefficient of a single particle. This can be rewritten in terms of the single particle terminal velocity which can be found from,

$$\frac{\rho_s \pi d_{pg}^3 g}{6} = \frac{1}{2}\frac{\rho_f \pi d_p^2}{4} C_D u_t^2 \qquad [98]$$

Substituting [98] into [97] to eliminate C_D, one obtains,

$$\frac{\beta D}{\rho_s u_0}\mathrm{Fr} = \frac{u_0^2}{u_t^2}|\bar{u}' - \bar{v}'|(1-\epsilon) \qquad [99]$$

Since u_0/u_{mf} and Fr are held constant in the simplified scaling process, we will examine the ratio u_t/u_{mf} to determine if the drag coefficient $\beta L/\rho_s u_0$ remains constant.

The Ergun equation can be solved to find u_{mf},

$$\rho_f \frac{u_{mf} d_p}{\mu} = \frac{\dfrac{-(150)(1-\epsilon_{mf})^2}{\epsilon_{mf}^3} + \sqrt{\left[\dfrac{-(150)(1-\epsilon_{mf})^2}{\epsilon_{mf}^3}\right]^2 + \dfrac{7(1-\epsilon_{mf})^2}{\epsilon_{mf}^3}\phi^3 \mathrm{Ar}}}{\dfrac{3.5(1-\epsilon_{mf})\phi}{\epsilon_{mf}^3}} \qquad [100]$$

where $\mathrm{Ar} = \rho_s \rho_f d_{pg}^3 g/\mu$ is the Archimedes number.

Using the relationship given by White (1974) for C_D,

$$\mathrm{Re}_t^2 = \frac{\frac{4}{3}\mathrm{Ar}}{\dfrac{24}{\mathrm{Re}_t} + \dfrac{6}{1+\sqrt{\mathrm{Re}_t}+0.4}} \qquad [101]$$

where $\mathrm{Re}_t = \rho_f u_t d_p/\mu$.

At small and large values of Ar, the ratio of u_t/u_{mf} approaches a constant value. In these two limits, the simplified scaling laws will yield exact agreement of u_t/u_{mf} between the combustor and the simplified models. The errors in u_t/u_{mf} are shown in figures 7 and 8 for simplified scale models at two different linear dimensions. Scaling a combustor with comparatively small particles, 0.2 mm or less, gives good agreement for u_t/u_{mf} even at one-sixteenth linear scale, while for large particles a linear scale of one-quarter gives fair agreement for u_t/u_{mf}. Since u_0/u_{mf} is held constant in the simplified scaling laws, close agreement of u_t/u_{mf} also results in close agreement of u_t/u_0.

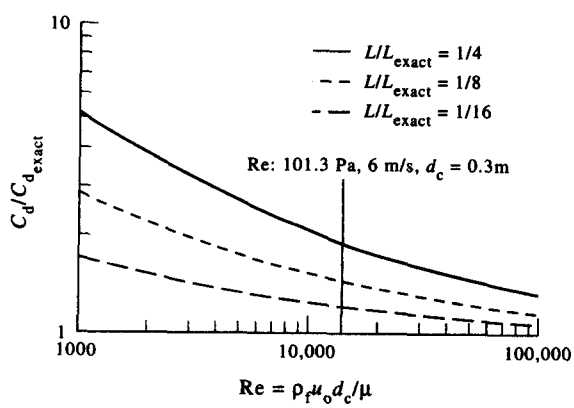

Figure 6. Error in cluster drag coefficient for fixed u_0/u_{mf}, using C_d for a solid sphere.

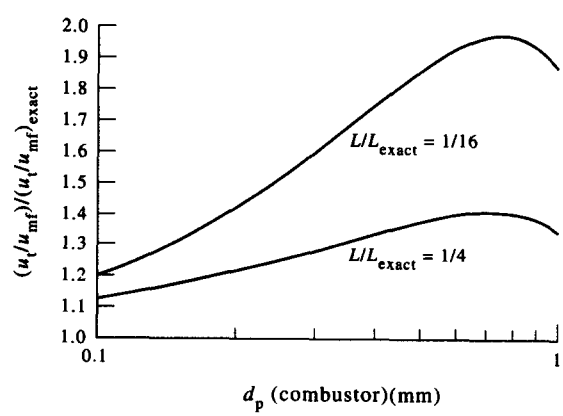

Figure 7. Error in terminal velocity using simplified scaling at 1013 kPa and 800°C.

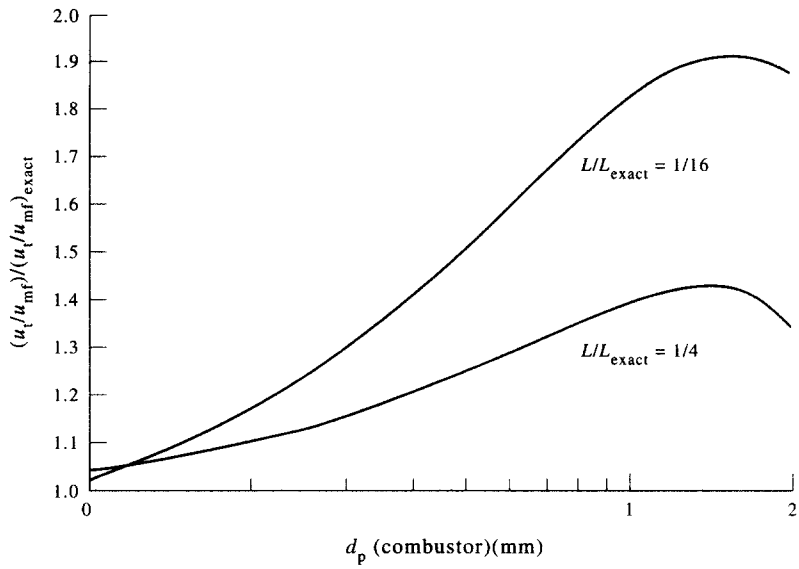

Figure 8. Error in terminal velocity using simplified scaling at 101.3 Pa and 800°C.

7. EXPERIMENTAL VERIFICATION OF DYNAMIC SCALING

Numerous techniques have been used to experimentally verify hydrodynamic scaling in fluidized beds. The overall objective of these techniques is to measure dependent hydrodynamic phenomena that can be used as a basis to compare scaled beds. When two fluidized beds are hydrodynamically similar, their dependent hydrodynamic phenomena, when expressed in dimensionless form, will be identical. In bubbling beds, methods such as video analysis and capacitance probe methods have been used to directly measure bubble properties such as their diameter, growth rate, diameter distribution, frequency and rise velocity. Similarly, optical probes have been used in circulating beds to measure variables such as cluster velocity and length to serve as a basis for scaling comparisons. With these methods the approach is to directly measure local hydrodynamic variables.

A second approach, which is more common due to its ease and accuracy, is the use of time-resolved differential pressure measurements as the dependent hydrodynamic phenomena. In this approach, the pressure measurements are used to characterize the hydrodynamics of the fluidized bed. Lirag & Littman (1971) used statistical analysis of pressure fluctuations to estimate the average size of bubbles leaving a bubbling bed. Fan *et al.* (1981) concluded that bubble motion and coalescence are responsible for pressure fluctuations in fluidized beds. They also found that the amplitude of the pressure fluctuations is related to bubble size. Therefore pressure fluctuation measurements, when properly made, have been shown to reflect bed hydrodynamics. For local bed behavior, the differential pressure measurements should be made over a modest bed level rather than using a single pressure tap in the bed with the other tap in the freeboard. Differential pressure measurements should reflect local conditions. Roy & Davidson (1989) found that the maximum pressure difference between two closely spaced pressure taps is related to the bubble diameter at that level in the bed. Use of a single bed pressure point can make it difficult to interpret results since pressure fluctuations can be due to local effects, bubbles erupting at the bed surface, or even fluctuations in the supply system. Roy & Davidson (1989) found that pressure fluctuations measured using a single pressure point are primarly due to surface bubbles. They also concluded that the dominant frequency and amplitude measured at a single pressure point are independent of position in the bed. A summary of the experimental verifications of hydrodynamic scaling bubbling and circulating fluidized beds is presented below. Three unique sets of scaling laws were used in the experimental studies. To be consistent with the previous scaling laws development they will be referred to as: the full set of scaling laws [35], the simplified set of scaling laws [91] and the viscous limit scaling laws [84]. The CFB scaling law proposed by Horio *et al.* (1989) can be shown to be equivalent to the simplified set of scaling laws. Horio *et al.* (1989) also discussed a

reduced set of scaling laws in which the solid-to-gas density ratio is omitted. This reduced set is equivalent to the bubbling bed scaling laws proposed by Horio *et al.* (1986a) which have been shown by Glicksman (1988) to be equivalent to the viscous limit scaling laws. As will be shown in section 7.2, density ratio is not a parameter which can be omitted when scaling circulating fluidized beds.

Tables 4 and 5 give the values for the full set of scaling parameters for the bubbling bed and the circulating bed studies respectively. The values of other parameters used for scaling are included in the "Other Parameters" column. It was not the objective of all the studies to match each of these parameters, but the tables provide a summary of what groups were matched and how closely they were matched for each of the studies. In some tests additional scaling parameters were unintentionally matched. Figure 9 presents the range of conditions over which scaling comparisons have been made in terms of the Froude and the particle Reynolds numbers.

7.1. Experimental Verification of Scaling for Bubbling Fluidized Beds

Fitzgerald & Crane (1980) were one of the first to evaluate the full set of hydrodynamic scaling parameters. They compared the hydrodynamics of two scaled beds using pressure fluctuation measurements and movies. In one bed cork particles were fluidized with air; the other bed was sand fluidized with pressurized refrigerant 12 vapor. Movies showed qualitative agreement between bubble growth and the solids flow in the beds. The ratio of the bed minimum fluidization velocities was within 20% of the theoretical value; the difference was attributed to the angular shape of the cork particles (ϕ not matched between the beds). The fast Fourier transform of the pressure fluctuations was used to determine the average frequency of the fluctuations. The ratio of average frequencies for the two beds was in fair agreement with the theoretical velocity–time scale factor. The pressure fluctuation data were taken with a single bed pressure tap. This may be responsible for the level of agreement in the frequency ratios. Some additional qualitative slugging comparisons were made using movies of bed behavior; the slugs appeared to have the same scaled lengths and velocities.

Fitzgerald *et al.* (1984) measured pressure fluctuations in an atmospheric fluidized bed combustor and a quarter scale cold model. The full set of scaling parameters was matched between the beds. The autocorrelation function of the pressure fluctuations was similar for the two beds but not within the 95% confidence levels they had anticipated. The amplitude of the autocorrelation function for the hot combustor was significantly lower than that for the cold model. Also, the experimentally determined time-scaling factor differed from the theoretical value by 24%. They suggested that the differences could be due to electrostatic effects. Particle sphericity and size distribution were not discussed; failure to match these could also have influenced the hydrodynamic similarity of the two beds. Bed pressure fluctuations were measured using a single pressure point which, as discussed previously, may not accurately represent the local hydrodynamics within the bed. Similar results were obtained between two two-dimensional beds: a bed of reacted limestone fluidized with helium and a half-scale bed of copper fluidized with air.

Nicastro & Glicksman (1984) experimentally verified the full set of scaling laws for bubbling fluidized beds. They compared the time-resolved differential pressure measurements from a bubbling fluidized bed combustor and a scaled cold model. Good agreement was obtained between the spectral content and the probability density distribution of the differential pressure fluctuations of the hot combustor and the cold model. Figure 10 presents the comparisons. They concluded that hydrodynamic similarity had been achieved between the hot combustor and the cold model. The solid-to-gas density ratio which was not matched exactly in the comparison differed by 23%, but the Reynolds number based on particle diameter (Re_{d_p}) was approx. 5 suggesting the beds were operating in the viscous limit. At low particle Reynolds numbers viscous forces dominate fluid inertial forces making it possible to omit the density ratio from the list of scaling parameters for bubbling beds. When actual hot bed material was used in the cold model, a violation of the scaling laws, the model's behavior was very different from that of the hot bed.

Horio *et al.* (1986a) used three geometrically similar bubbling beds, fluidized with ambient air, to verify their proposed scaling laws. The solid-to-gas density ratio was not varied in the experiments although it was not one of the proposed scaling parameters. By including the density ratio, they, in essence, used the simplified set of scaling parameters. Video analysis of bubble

Table 4. Scaling parameter values for bubbling fluidized bed experimental studies

Reference	Hot/cold	$\rho_f u_0 D/\mu$	u_0^2/gD	ρ_s/ρ_f	L/D	D/d_p	φ	Scaling laws	Other parameters
Fitzgerald & Crane (1980)	cold	8915–11138	0.018–0.027	126	1.0	234	N/A	full	$Re_{d_p} = 381.1–47.6$
	cold	9259–11562	0.018–0.026	110	1.0	235			$Re_{d_p} = 39.4–49.2$
Fitzgerald *et al.* (1984)	hot	28881	0.33	8224	3.0	915	N/A	full	$Re_{d_p} = 31.6$
	cold	32000	0.31	8214	3.0	920			$Re_{d_p} = 34.8$
Nicastro & Glicksman (1984)	hot	4658	0.143	7280	7.21	901	0.80	full	$Re_{d_p} = 5.2$
	cold	4781	0.145	5920	7.21	897	0.80		$Re_{d_p} = 5.3$
Horio *et al.* (1986a)	cold	3514	0.021	2117	Scaled	638	N/A	simplified	$Re_{d_p} = 5.5$ $u_0/u_{mf} = 2.00$
	cold	954	0.022	2117		328			$Re_{d_p} = 2.9$ $u_0/u_{mf} = 1.97$
	cold	247	0.021	2117		174			$Re_{d_p} = 1.4$ $u_0/u_{mf} = 2.00$
Horio *et al.* (1986b)	cold	4448	0.0024	2203	0.325	3297	N/A	simplified	$Re_{d_p} = 1.4$ $u_0/u_{mf} = 4.4$
	cold	1520	0.0023	2203	0.327	2000			$Re_{d_p} = 0.8$ $u_0/u_{mf} = 4.6$
	cold	537	0.0023	2203	0.333	1163			$Re_{d_p} = 0.5$ $u_0/u_{mf} = 5.3$
	cold	105	0.0024	2203	0.340	472			$Re_{d_p} = 0.2$ $u_0/u_{mf} = 4.7$
Newby & Keairns (1986)	cold	1134–2523	0.00068–0.0034	2091	1.67	1800	N/A	full	$Re_{d_p} = 0.63–1.40$ $u_0/u_{mf} = 1.0–2.2$
	cold	1134–2523	0.00068–0.0034	2484	1.67	1800			$Re_{d_p} = 0.63–1.40$ $u_0/u_{mf} = 1.1–2.5$
	cold	1059–2406	0.00062–0.0032	2332	1.67	1800			$Re_{d_p} = 0.59–1.34$ $u_0/u_{mf} = 1.1–2.5$
Zhang & Yang (1987)	cold	65784	0.135	2208	0.462	1137	matched	simplified	$Re_{d_p} = 58$ $u_0/u_{mf} = 1.8$
	cold	12658	0.135	2208	0.422	529			$Re_{d_p} = 24$ $u_0/u_{mf} = 1.8$
	cold	77147	0.185	2208	0.462	1137			$Re_{d_p} = 68$ $u_0/u_{mf} = 2.1$
	cold	14792	0.184	2208	0.422	529			$Re_{d_p} = 28$ $u_0/u_{mf} = 2.1$
	cold	88510	0.244	2208	0.462	1137			$Re_{d_p} = 78$ $u_0/u_{mf} = 2.4$
	cold	16984	0.243	2208	0.422	529			$Re_{d_p} = 32$ $u_0/u_{mf} = 2.4$

Roy & Davidson (1989)	Hot	923	0.462	6667	N/A	225	N/A	full/viscous limit	$Re_{d_p} = 4.1\ u_0/u_{mf} = 5.2$
	cold	1375	0.490	5882		250			$Re_{d_p} = 5.5\ u_0/u_{mf} = 5.0$
	cold	2970	2.100	5882		90			$Re_{d_p} = 33\ u_0/u_{mf} = 1.6$
	cold	5250	5.950	5882		50			$Re_{d_p} = 105\ u_0/u_{mf} = 1.3$
	cold	1388	0.436	2041		188			$Re_{d_p} = 7.4\ u_0/u_{mf} = 6.1$
	cold	5835	0.026	3030		1167			$Re_{d_p} = 5\ u_0/u_{mf} = 13.5$
	cold	6664	0.026	3448		833			$Re_{d_p} = 8\ u_0/u_{mf} = 16.0$
	cold	1250	0.029	2041		833			$Re_{d_p} = 1.5\ u_0/u_{mf} = 8.5$
	cold	4667	0.032	2041		1167			$Re_{d_p} = 4\ u_0/u_{mf} = 4.6$
	cold	11636	0.058	3448		182			$Re_{d_p} = 64\ u_0/u_{mf} = 2.7$
	cold	2184	0.084	2041		182			$Re_{d_p} = 12\ u_0/u_{mf} = 2.1$
Almstedt & Zakkay (1990)	hot	54135	0.21	913	3.13	811	0.82	full	$Re_{d_p} = 66.8$
	cold	53861	0.21	1068	3.12	811	0.75		$Re_{d_p} = 66.4$
	cold	53861	0.21	911	3.12	811	0.82		$Re_{d_p} = 66.4$
	cold	53861	0.21	911	3.12	410	0.82		$Re_{d_p} = 131.4$
Di Felice *et al.* (1992a)	cold	1468–8922	0.009–0.331	1126	N/A	322	1.0	full	$Re_{d_p} = 4.6\text{–}27.7\ u_0/u_{mf} = 1.0\text{–}5.3$
	cold	1351–8025	0.010–0.340	1128		305	1.0		$Re_{d_p} = 4.4\text{–}26.3\ u_0/u_{mf} = 1.0\text{–}5.4$
	cold	1395–8367	0.009–0.333	1136		313	1.0		$Re_{d_p} = 4.6\text{–}26.7\ u_0/u_{mf} = 1.0\text{–}5.0$
	cold	1173–7330	0.007–0.290	1007		304	0.6		$Re_{d_p} = 3.9\text{–}24.1\ u_0/u_{mf} = 0.4\text{–}2.7$
	cold	1468–8809	0.009–0.323	24444		552	1.0		$Re_{d_p} = 2.7\text{–}16.0\ u_0/u_{mf} = 1.1\text{–}6.5$
Di Felice *et al.* (1992b)	cold	31.3–500.4	$(0.21\text{–}53)10^{-5}$	769	5.5	3536	N/A	full	$Re_{d_p} = 0.009\text{–}0.14$
	cold	18.4–402.6	$(0.14\text{–}65)10^{-5}$	794	4.5	2824			$Re_{d_p} = 0.007\text{–}0.14$
	cold	2078–6928	0.0216–0.2405	1100	2.8, 5.6*	305			$Re_{d_p} = 6.8\text{–}22.7$
	cold	2186–7765	0.0192–0.2420	1105	2.6, 5.2*	322			$Re_{d_p} = 6.8\text{–}24.1$
*Slugging cases	cold	15242–35564	0.346–1.89	2000	1.0, 2.0*	112			$Re_{d_p} = 136.1\text{–}317.5$
	cold	24714–37895	0.834–1.96	2036	1.1, 2.1*	115			$Re_{d_p} = 214.9\text{–}329.5$

Table 5. Scaling parameter values for circulating fluidized bed experimental studies

Reference	Hot/cold	$\rho_f u_0 D/\mu$	u_0^2/gD	ρ_s/ρ_f	L/D	D/d_p	$G_s/\rho_s u_0$	φ	Scaling laws	Other parameters
Horio *et al.* (1989)	cold	9885–16063	0.33–0.86	1508	8	2528	0.0028–0.0052	N/A	simplified	$Re_{d_p} = 3.9–6.4$ $u_0/u_{mf} \approx 229–371$
	cold	1236–2008	0.33–0.86	1508	8	816	0.0028–0.0052			$Re_{d_p} = 1.5–2.5$ $u_0/u_{mf} \approx 190–310$
Ishii & Murakami (1991)	cold	9885–14827	0.326–0.734	1508	N/A	3263	0.0056–0.0037	N/A	simplified	$Re_{d_p} = 3.0–4.5$ $u_0/u_{mf} = 381–571$
	cold	1236–1853	0.326–0.734	1508		1078	0.0056–0.0037			$Re_{d_p} = 1.1–1.7$ $u_0/u_{mf} = 333–500$
Tsukada *et al.* (1991)	cold	1518	0.510	1534	8	1078	0.0067	N/A	viscous	$Re_{d_p} = 1.4$ $u_0/u_{mf} = 417$
	cold	2736	0.510	852	8	1078	0.0067		limit	$Re_{d_p} = 2.5$ $u_0/u_{mf} = 417$
	cold	5327	0.510	437	8	1078	0.0067			$Re_{d_p} = 4.9$ $u_0/u_{mf} = 417$
Glicksman *et al.* (1991a)	hot	6984	66.94	8700	48.7	822	0.0017	N/A	full	$Re_{d_p} = 8.5$
	cold	6785	66.54	6000	48.0	646	0.0016	N/A		$Re_{d_p} = 10.5$
Chang & Louge (1992)	cold	15630	13.84	4800	35	855	0.0044	0.69	full	$Fr^* = 131$, $M = 21$
	cold	22977	9.34	4961	35	1835	0.0042	1.0		$Ar^* \approx 45$, $R \approx 4880$
	cold	53454	4.20	4966	35	2985	0.0020	0.73		$Fr^* = 131$, $M = 10$
	cold	22977	9.34	4961	35	1835	0.0020	1.0		$Ar^* \approx 47$, $R \approx 4964$
Glicksman *et al.* (1993a)	hot	29170	5.26	8500	11.43	2917	0.0013	N/A	full	$Re_{d_p} = 10.0$
	cold	30349	5.63	6200	11.25	2759	0.0011			$Re_{d_p} = 11.0$
Glicksman *et al.* (1993b)	cold	3211–5352	7.1–19.7	2117	14.2	412	$(4–7)10^{-3}$	1.0	viscous	$Re_{d_p} = 7.8–13.0$ $u_0/u_{mf} = 106–176$
	cold	3211–5352	7.1–19.7	1167	14.2	326	$(4–7)10^{-3}$	0.6–0.8	limit	$Re_{d_p} = 9.9–16.5$ $u_0/u_{mf} = 176–294$
	cold	25699–45146	7.1–19.6	2117	14.1	1158	$(4–7)10^{-3}$	1.0	simplified	$Re_{d_p} = 22.2–39.0$ $u_0/u_{mf} = 104–174$
	cold	3171–5286	7.2–19.9	2117	14.4	407	$(4–7)10^{-3}$	1.0		$Re_{d_p} = 7.8–13.0$ $u_0/u_{mf} = 106–176$
	cold	24030–43020	7.1–19.6	1167	14.1	900	$(2–3)10^{-3}$	0.6–0.8	simplified	$Re_{d_p} = 26.7–47.8$ $u_0/u_{mf} = 200–333$
	cold	3188–5313	7.2–19.9	1167	14.4	322	$(2–3)10^{-3}$	0.6–0.8		$Re_{d_p} = 9.9–16.5$ $u_0/u_{mf} = 176–294$
	hot	27975–36938	5.6–9.9	8400	12.2	2716	$(0.5–1.8)10^{-3}$	N/A	full/	$Re_{d_p} = 10.3–13.6$
	cold	25008–31993	7.1–12.5	6200	14.1	2253	$(0.5–1.8)10^{-3}$	0.6–0.8	simplified	$Re_{d_p} = 11.1–14.2$ $u_0/u_{mf} = 214–286$
	cold	3891–5075	5.7–10.2	6200	14.4	1538	$(0.5–1.8)10^{-3}$	0.6–0.8		$Re_{d_p} = 2.5–3.3$ $u_0/u_{mf} = 200–267$

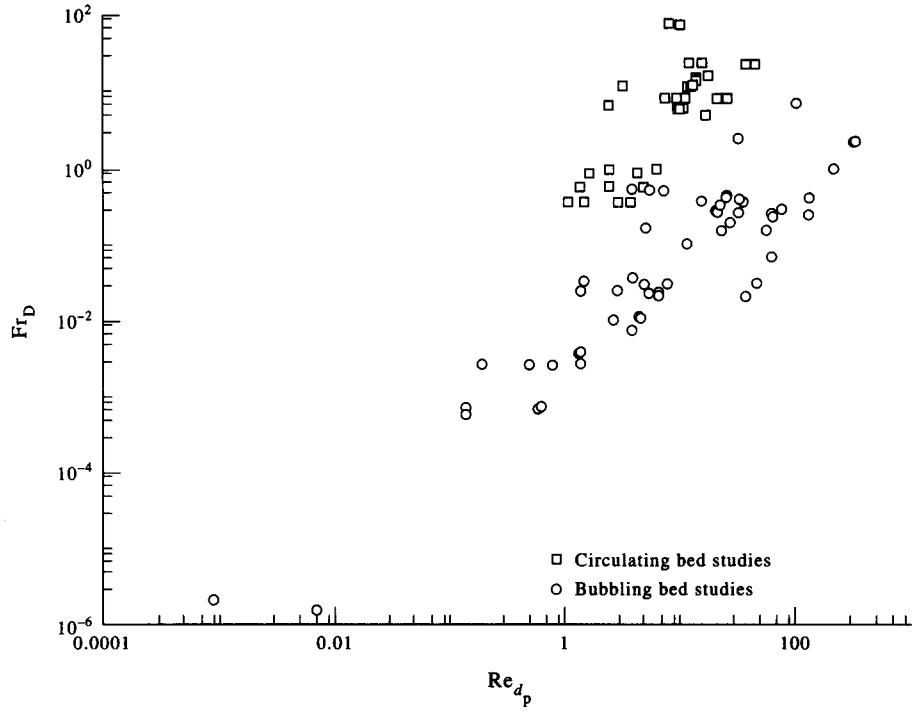

Figure 9. Range of experimental scaling studies.

eruptions at the bed surface were used to determine the cross-sectional average for bubble diameter, bubble diameter distribution and radial distribution of superficial bubble velocity. Similarity was achieved in these hydrodynamic parameters when bed Froude number, density ratio and the ratio of superficial to minimum fluidization velocities were matched.

Horio *et al.* (1986b) verified the bubbling bed scaling laws of Horio *et al.* (1986a) for solid mixing and segregation. Sand was used as a bed material in straight and tapered bed geometries. A bed sectioning technique was used to measure the transient radial dispersion coefficient and the distribution of float tracers. They concluded that bed mixing and the behavior of floating bodies obey the scaling laws in both straight and tapered beds. The solid-to-gas density ratio was held constant in the tests, satisfying the simplified set of scaling laws. The particle Reynolds numbers (Re_{d_p}) were approximately unity or less.

Newby & Keairns (1986) made bubbling bed scaling comparisons between two cold models using the full set of scaling laws. One bed fluidized two different 200 μm glass powders using ambient air. The second bed, which was a half-scale model of the first, used pressurized air to fluidize 100 μm steel powder. High-speed movies showed good agreement between the non-dimensional bubble frequencies in the two beds. Figure 11 is a plot of the non-dimensional bubble frequencies as a function of bed Froude number. They also found reasonably good agreement between the non-dimensional amplitudes of the pressure fluctuations in the beds.

Zhang & Yang (1987) carried out scaling comparisons between two two-dimensional beds with u_0^2/gD and u_0/u_{mf} matched between them. They also inadvertently kept the solid-to-gas density ratio constant; thus they matched the simplified scaling parameters. They found through photographs that the beds appeared qualitatively similar. The beds also had similar dimensionless freeboard entrainment rates and dimensionless bed heights over a range of u_0/u_{mf}.

Roy & Davidson (1989) considered the validity of the full and viscous limit scaling laws at elevated pressures and temperatures. The non-dimensional dominant frequency and amplitude of the pressure drop fluctuations were used as the basis of the comparison. They concluded that when the full set of scaling parameters is matched similarity is achieved. They also suggested that it is not necessary to match the density ratio (ρ_s/ρ_f) and d_p/D—viscous limit scaling—for particle Reynolds numbers (Re_{d_p}) less than 30. Although, the run with Re_{d_p} of 33 had the same density ratio as the low Re_{d_p} runs. These conclusions may be open to different interpretations.

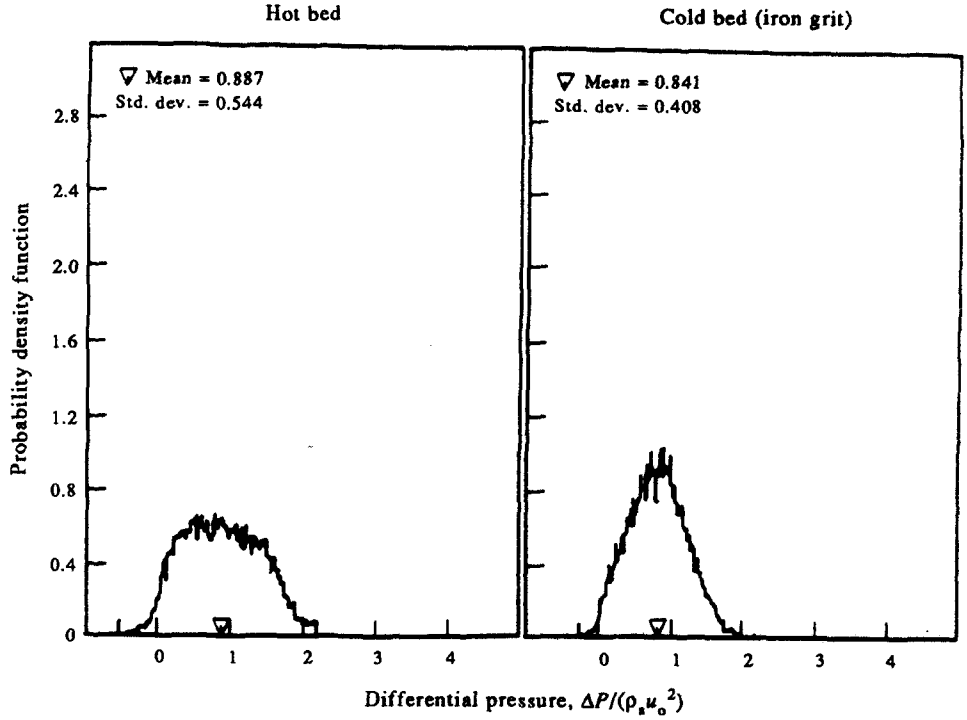

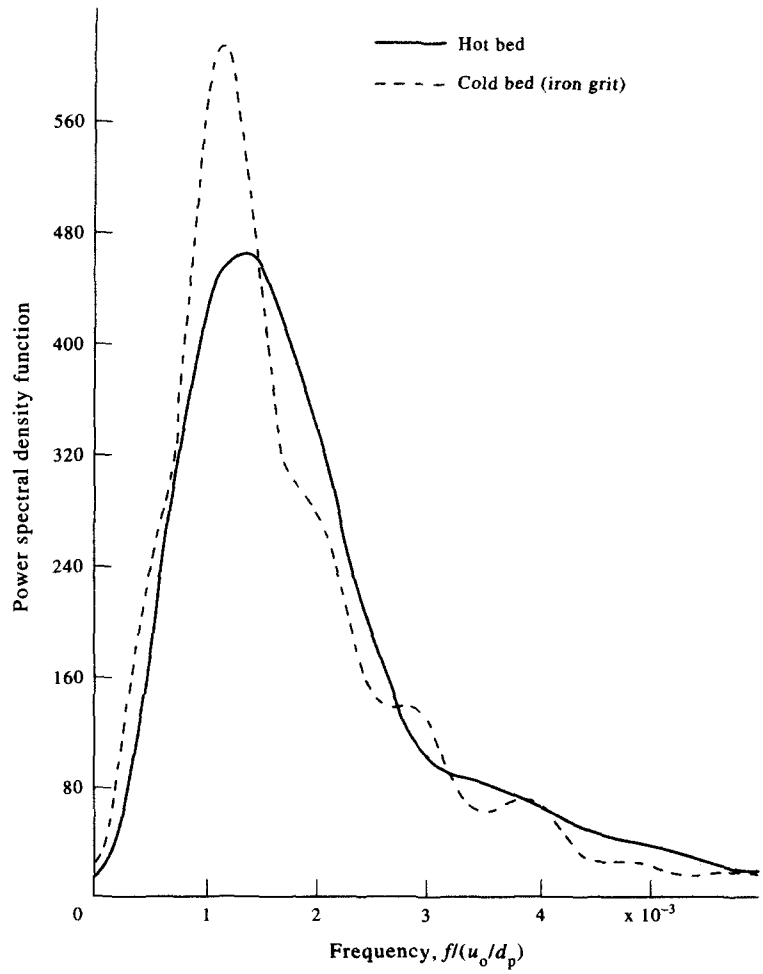

Figure 10. Comparison of hot and cold bed probability density and power spectral density distributions (Nicastro & Glicksman, 1984).

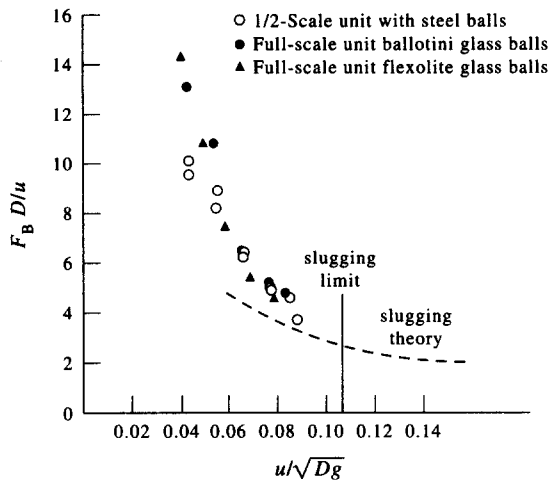

Figure 11. Comparison of non-dimensional bubble frequencies from two cold scaled models (Newby & Kearns, 1986).

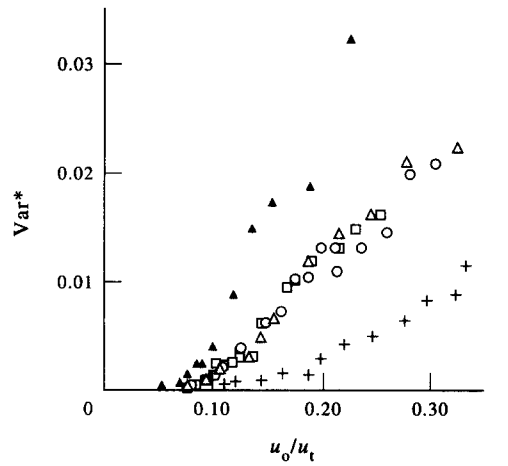

Figure 12. Comparison of dynamic pressure variance for three properly scaled beds and two mis-scaled beds in bubbling regime (Di Felice *et al.* 1992a). Properly scaled: □, laposorb; △, sand; ○, bronze. Intentionally mis-scaled: +, iron; ▲ sand.

As shown in Table 4, the scaling parameters were neither matched closely nor varied in a systematic manner.

Almstedt & Zakkay (1990) made scaling comparisons between a hot PFBC and a pressurized cold scale model using the full set of scaling laws. A capacitance probe was used to measure the mean values of the bubble frequency, pierced length, bubble rise velocity and bubble volume fraction. Scaling comparisons were made using the dimensionless form of these dependent hydrodynamic parameters. Three different bed materials were used in the cold bed: Olivine sand and two different size distributions of the hot-bed material, one properly scaled and one out of scale. The sand had a lower sphericity and higher density than the hot-bed material making it possible to investigate the sensitivity of the scaling to small variations in the density ratio and particle sphericity. The out-of-scale hot-bed material was also used to illustrate the sensitivity of the scaling to the D/d_p parameter. The non-dimensional form of the capacitance probe measurements agreed within 25% for the sand and the properly scaled hot-bed material; the agreement was best in the upper part of the bed. The properly scaled hot-bed material showed only slightly better agreement than that for the sand, but the mismatch in the density ratio and the sphericity for the sand was small. The improperly scaled hot-bed material had a maximum deviation of 38% from the hydrodynamics of the hot-bed combustor. They concluded that behavior which is hydrodynamically similar to that of a pressurized fluidized bed combustor can be achieved using a properly scaled cold model.

Di Felice *et al.* (1992a) investigated the validity of the full set of scaling laws for bubbling and slugging fluidized beds. They used an experimental facility which permitted the pressurization of different diameter test sections to match the scaling parameters. Minimum fluidization measurements, video measurements of bed expansion and pressure fluctuation data were used to compare the similarity of five different bed configurations. Three of the beds were scaled properly, the fourth had a mismatched particle sphericity and the fifth bed was purposefully misscaled relative to the others (see table 4). The voidage at minimum fluidization was found to be the same for all the beds except the one with the different particle sphericity. In the bubbling regime, good agreement in the non-dimensional bed expansion measurements was obtained for all but the bed with the misscaled particle sphericity. The lower particle sphericity increased u_{mf} for the system which effectively shifted the bed expansion curve for this case. The pressure fluctuations for the three properly scaled beds in the bubbling regime showed good agreement while the misscaled beds exhibited poor agreement with the other three. Figure 12 is a plot of the dimensionless dynamic pressure variance for the five beds in the bubbling regime. The two sets of data which deviate from the other three correspond to the misscaled beds.

In the slugging regime Di Felice *et al.* (1992a) found that the bed expansion characteristics were similar to those in the bubbling regime, but the pressure fluctuation characteristics for all five beds were in poor agreement with each other. Figure 13 is the plot of the dimensionless dynamic pressure variance for the five beds in the slugging regime. They attributed this to the importance of particle material properties and particle–particle interactions which are not accounted for in the full set of scaling laws.

Di Felice *et al.* (1992b) evaluated the full set of scaling laws for three different Geldart powder categories (A, B and D) in the bubbling and slugging fluidization regimes. Pressure fluctuations were used as the basis for the scaling comparisons. In the bubbling regime, the RMS and dominant frequencies of the pressure fluctuations showed good agreement for all three powder categories. Only Geldart groups B and D were considered in the slugging regime. They exhibited fair agreement in the RMS of their pressure fluctuations, but their dominant frequencies agreed poorly. They found that the full set of scaling laws are valid for bubbling beds fluidizing powders in Geldart groups A, B and D. They also concluded that the full set of scaling laws should not be used for slugging beds where particle–particle interactions are also thought to be important.

7.2. Experimental Verification of Scaling for Circulating Fluidized Beds

Horio *et al.* (1989) experimentally verified their proposed circulating fluidized bed scaling laws. The solid-to-gas density ratio was not varied in the tests, thus they effectively verified the simplified set of scaling laws. Two cold scaled CFBs, fluidized using ambient air, were used in the verification. Good agreement in the axial solid fraction profiles was obtained for most of the conditions tested. A "choking-like transition" was found to occur for cases with higher solids fluxes and lower gas superficial velocites. A discrepancy in the "choking" transition point for the two beds was attributed to differences in the geometry of the bed exit and the solids recycle lines. The transition point was found to be very sensitive to the particle size ratio. An optical probe was used to verify similarity in the annular flow structures and the cluster velocities.

Ishii & Murakami (1991) evaluated Horio *et al.*'s (1989) CFB scaling relationships using two cold CFB models. Solids flux, pressure drop and optical probe measurements were used to measure a large number of hydrodynamic parameters to serve as the basis for the comparison. Fair to good similarity was obtained between the beds. Dependent hydrodynamic parameters such as the pressure drop and pressure fluctuation characteristics, cluster length and voidage, and the core diameter were compared between the two beds. The gas-to-solid density ratio was not varied between the beds. As seen in table 5, the dimensionless solids flux decreased as the superficial velocity was increased because the solids flux was held constant.

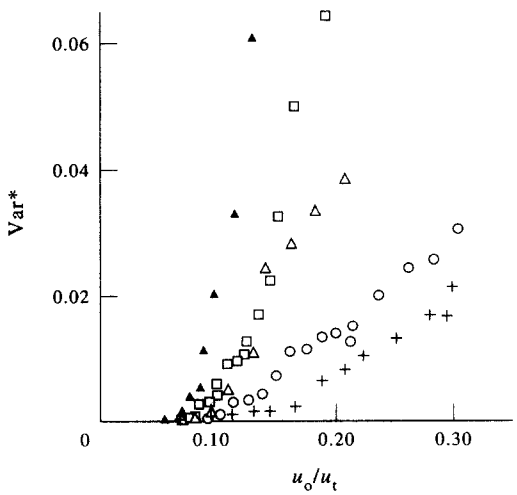

Figure 13. Comparison of dynamic pressure variance for three properly scaled beds and two mis-scaled beds in slugging regime (Di Felice *et al.* 1992a). Properly scaled: □, laposorb; △, sand; ○, bronze. Intentionally mis-scaled: +, iron; ▲ sand.

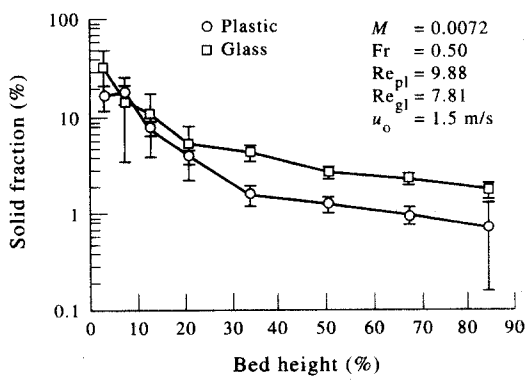

Figure 14. Solid fraction profile comparisons based on viscous limit scaling (Glicksman *et al.*, 1993b).

Tsukada *et al.* (1991) applied Horio *et al.*'s (1989) CFB scaling laws at several different elevated pressures (viscous limit scaling laws). A single bed and bed material were used in the study. A pressure vessel was used to vary the gas pressure. The bed was fluidized with ambient temperature air at three different pressures (0.1, 0.18 and 0.35 MPa). Axial solid fraction profiles and optical probe measurements were used as the basis for their similarity comparison. They found that as the pressure was increased the axial solid fraction profile changed, indicating a change in the hydrodynamics. It was suggested that the effect on the axial solid fraction profile could be due to reaching a Reynolds number limit, e.g. the upper boundary for the viscous limit. They also suggest that it could be due to a change in gas bypassing between the riser and the downcomer. The only parameter which was not matched in this study which had been matched in previous verifications of Horio *et al.*'s (1989) scaling relationships is the gas-to-solid density ratio. It is likely based on the recent results of Glicksman *et al.* (1993b) that this led to the influence of the pressure level on the bed hydrodynamics.

Glicksman *et al.* (1991a) made scaling comparisons between an experimental circulating fluidized bed combustor and a scaled cold model based on the full set of scaling laws. The time-resolved pressure fluctuations and the time-averaged pressure drop were measured. Due to uncertainties in the hot-bed solid circulation measurements, the cold-bed solids flux was adjusted until the average bed solid fraction matched that of the hot bed. The vertical solid fraction profiles, the probability density function and the Fourier transform of the pressure fluctuations were compared between the hot and cold bed. Good agreement was obtained between the vertical solid fraction profiles except near the top of the beds. It was suggested that the differences in the solid fraction profiles at the top of the bed could be due to protrusions or wall roughness in the hot bed which were not modeled in the cold bed. Good agreement was also obtained in the comparison of the probability density distribution and the Fourier transform of the pressure fluctuations.

Chang & Louge (1992) carried out tests on a circulating bed in which they could vary the gas composition. By combining this with particles of different density and size they were able to scale a series of different size hot commercial beds with diameters up to five times larger than the cold bed. Comparisons between glass and plastic particles show identical mean vertical solids fraction profiles. The corresponding pressure fluctuations for plastic and glass are found to scale with $\rho_s g\phi d_p$; one would expect the pressure fluctuations to scale with $\rho_s u_0^2$. This is probably an artifice of the experimental design since $\mathrm{Fr}^2 = u_0^2/g\phi d_p$ was matched in the comparisons where as Froude number based on bed diameter could not be matched since the experimental bed diameter was fixed in the tests. The inability to alter the bed diameter also made it impossible to match the D/d_p scaling parameter. Chang & Louge matched a modified form of the full set of scaling laws. Particle sphericity is not explicitly included as an independent parameter, rather it is included with the particle diameter based on a combination of the gas to particle drag coefficient. Their modified parameters are:

$$\mathrm{Fr}^* = \frac{u_0}{g\phi d_p}, \quad L^* = \frac{D}{d_p\phi}, \quad M = \frac{G_s}{\rho_s u_0}, \quad R = \frac{\rho_s}{\rho_f} \quad \text{and} \quad \mathrm{Ar}^* = \frac{\rho_s\rho_g(d_p\phi)^3 g}{\mu^2}.$$

The values of the parameters matched for scaling are presented in the "Other Parameters" column of table 5. Steel and glass particles were also compared. The similarity using steel and glass was poor because the bed using the steel particles was choked while the bed with glass particles was not. Yang's (1983) correlation indicates that choking is a strong function of the Froude number based on bed diameter (Fr_D). Fr_D could not be matched between the beds which caused them to choke under different conditions.

Glicksman *et al.* (1993a) evaluated the full set of scaling laws for circulating fluidized beds. Solid fraction data were obtained from the 2.5 $\mathrm{MW_{th}}$ Studsvik CFB prototype. The full set of scaling laws were evaluated through solid fraction profile comparisons between Studsvik and a one-quarter scale cold model. Fairly good agreement was obtained; the profiles most closely matched in the top of the beds. Differences between the profiles were attributed to uncertainty in the hot-bed solid flux measurements and to the mismatch in the solid-to-gas density ratio.

The viscous limit scaling laws were also evaluated by Glicksman *et al.* (1993b) in a series of two tests using circulating beds. Scaling was attempted between glass/steel and glass/plastic (i.e.

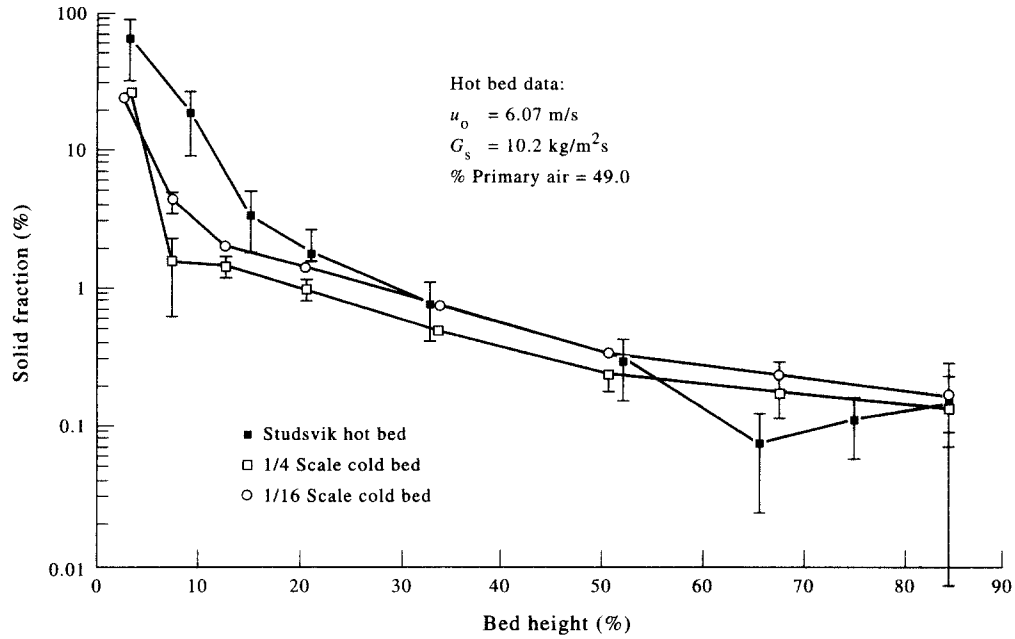

Figure 15. Solid fraction profile comparisons based on the simplified and the full set of scaling laws (Glicksman *et al.*, 1993b).

different density ratios) in the same bed. The average solid fraction profiles, probability density functions, and power spectral densities were all in poor agreement. Figure 14 is a sample solid fraction profile comparison based on viscous limit scaling. It is believed the beds were operating near the point of incipient choking condition as predicted by the Yang (1983) correlation. Because this correlation indicates that choking is a strong function of the solid-to-gas density ratio, it was concluded that the viscous limit scaling parameters are unable to model bed hydrodynamics near the boundary between different flow regimes. They concluded that since low u_0 is required for the viscous limit scaling to be valid while sufficiently high u_0 is required to prevent choking, the applicability of the viscous limit scaling parameters for CFBs is limited. It was suggested that these scaling parameters may have a wider range of validity in bubbling beds.

The simplified scaling laws were used by Glicksman *et al.* (1993b) to compare two geometrically similar beds one having linear dimensions four times larger than the other. In one series of tests properly sized plastic particles were used in both beds, in another test series glass particles were

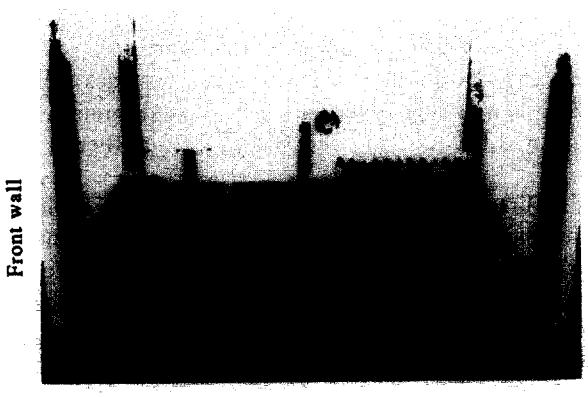

Figure 16. Model of 20 MW bubbling fluidized bed combustor showing tube arrangement.

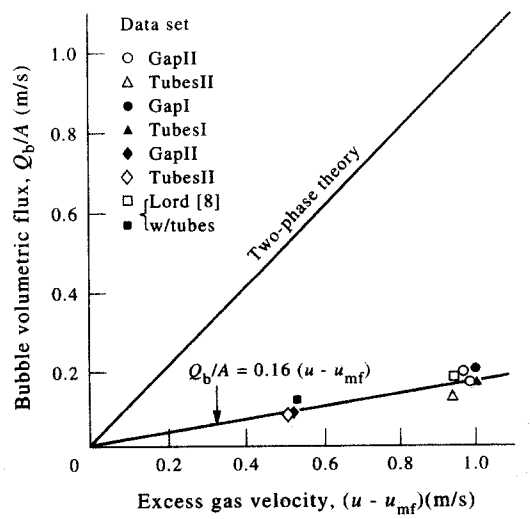

Figure 17. Bubble volumetric flux versus excess gas velocity for optical probe data of bubbling bed.

used in the two beds. The average solid fraction profiles showed excellent agreement. The probability density functions and power spectral densities also agreed well. In contrast to the viscous limit scaling results, the simplified scaling laws gave good agreement even for conditions where Yang's (1983) correlation predicted the bed was choked.

Glicksman *et al.* (1993b) verified the simplified scaling laws for hot beds by comparing the solid fraction profiles for the Studsvik bed, the one-quarter scale cold model, and a one-sixteenth scale cold model. The average solid fraction profiles were in good agreement for most of the conditions tested. The agreement was excellent between the one-quarter scale cold model, which utilized the full set of scaling laws, and the one-sixteenth scale model which utilized the simplified set of scaling laws. Thus, any disagreement between the Studsvik bed and the one-sixteenth scale model is not due to the simplifications of the full set of scaling laws. The density ratio was not matched exactly between the hot bed and the two cold beds which may have affected the agreement. Figure 15 provides a typical comparison of the solid fraction profiles in the three beds. The authors concluded that the simplified set of scaling laws, which includes the solid-to-gas density ratio, gives acceptable results over a wide range of particle densities and bed sizes, even when the length ratio is as small as one-sixteenth.

8. APPLICATIONS OF SCALING TO COMMERCIAL FLUIDIZED BED UNITS

A substantial number of experimental investigations have demonstrated the validity of scaling. This has increased awareness of the concept and confidence in its application. Although applications to commercial designs have been undertaken, unfortunately only a modest number have been documented in the open literature.

Scaling has many useful applications. The dynamic characteristics of different bed designs can be quickly compared. The influence of bed diameter on hydrodynamic behavior can be studied by the use of several different models. The models allow easy experimental examination of existing operating characteristics. The beds also can be used to quickly confirm the influence of proposed modifications. Since the models operate at ambient conditions, it is possible to instrument them to observe detailed behavior. This allows a better understanding of the

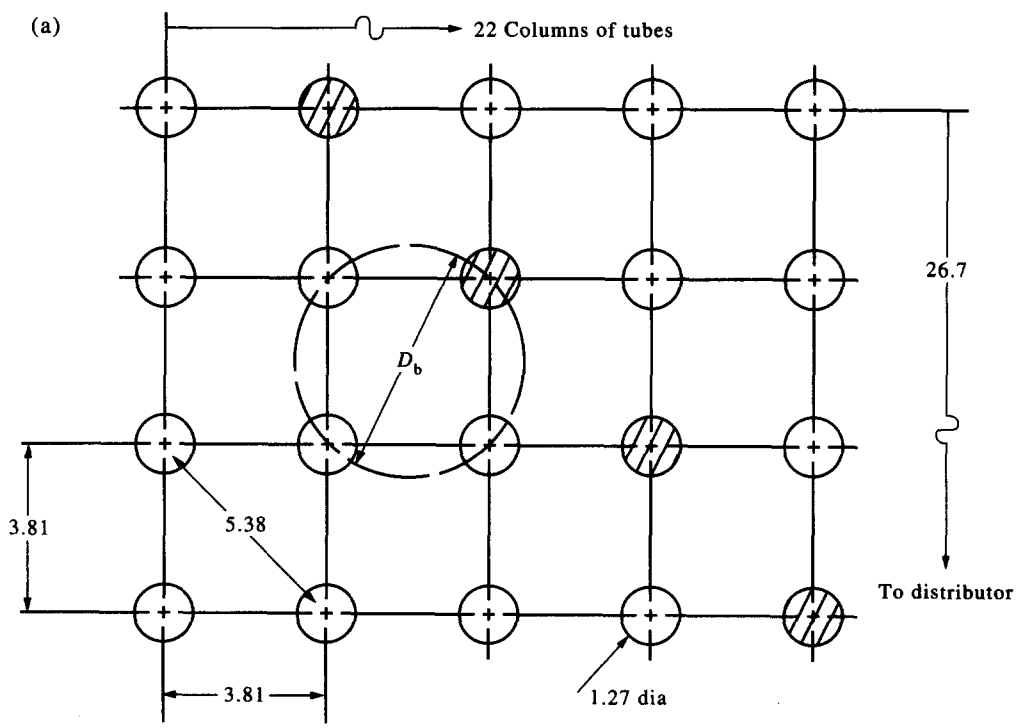

Figure 18(a). *Caption overleaf.*

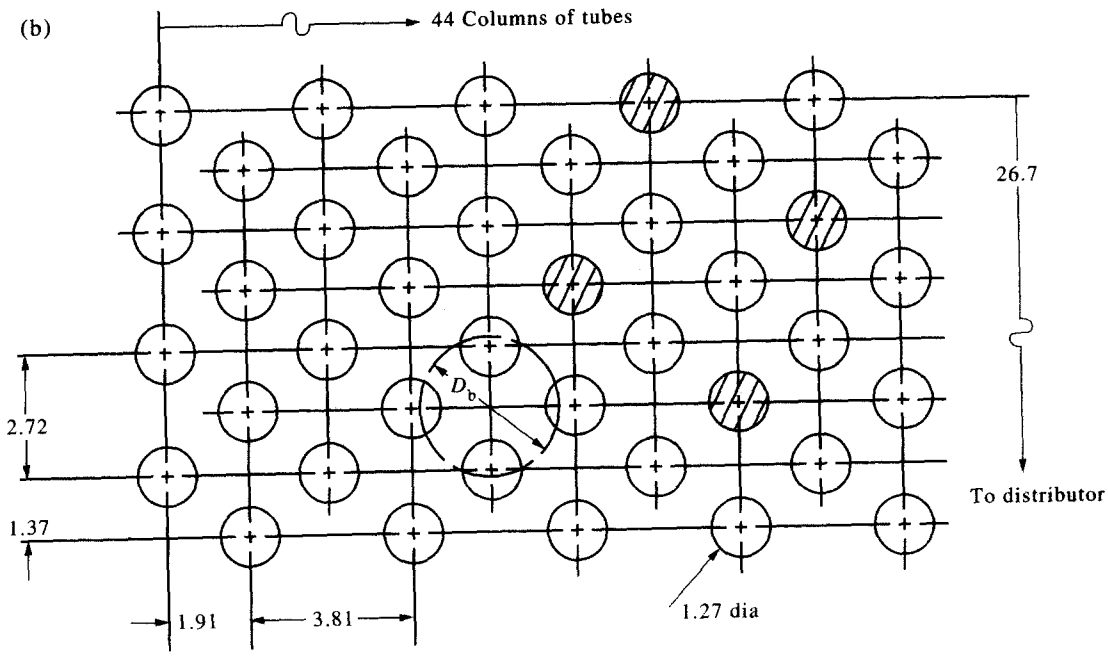

Figure 18(b)

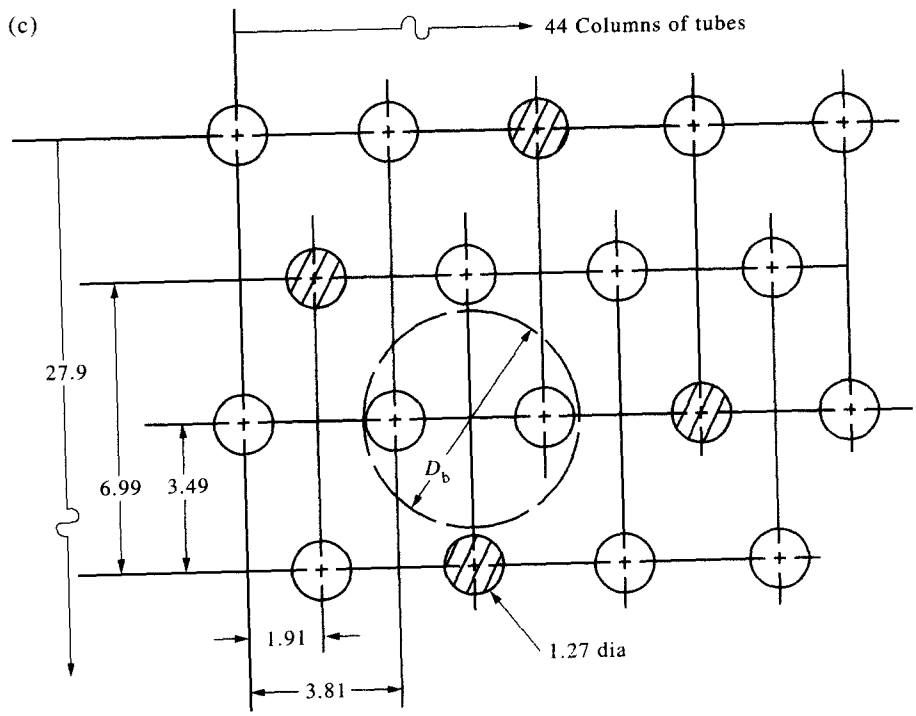

Figure 18(c)

Figure 18. Tube configurations used for bed expansion studies. Note: all dimensions in cm scaled to equivalent sizes in the combustor.

fundamental physics as well as the identification of hydrodynamic factors needed for proper correlation of performance.

8.1. Bubbling Beds

The earliest scaling studies were directed at atmospheric bubbling bed combustors. To date, a rich variety of questions have been addressed.

Jones & Glicksman (1986) constructed a model of the 20 MW bubbling bed pilot plant jointly sponsored by the Tennessee Valley Authority and the Electric Power Research Institute (EPRI) at Paducah, Kentucky. Figure 16 shows a photograph of the model of the in-bed tubes installed in the scale model. The model which is roughly 100 × 120 cm in cross section simulates two-thirds of the entire 20 MW pilot plant. Care was taken to carefully match the pilot plant tube bundle geometry and distributor design. Steel grit particles with the same dimensionless size distribution and sphericity as the hot bed material were used. The full set of scaling parameters was matched in the model and the combustor. The largest discrepancy was in the solid to gas density ratio which was 18% smaller in the model than the pilot plant.

Optical probes were used to measure the bubble size, frequency and velocity within the dense bed. The bubble velocity for an actively bubbling bed was found to closely agree with the drift flux form proposed by Davidson & Harrison (1963). In contrast, the volumetric flow rate of the bubbles was found to be far less than that predicted by the two-phase hypothesis (figure 17).

Later observations of this model showed that when bubbles erupt at the surface the accompanying gas flow has a velocity much higher than the bubble rise velocity (Glicksman & Piper 1987). This led to a mechanistic model for gas throughflow aided by the low resistance of the bubble cavity (Yule & Glicksman 1988) and an accurate prediction of bubble volume flow rate and bed expansion (Glicksman *et al.* 1991b).

A major question in the design of a commercial sized bubbling bed is the need to identify part load operating techniques. While reducing the total combustion rate, it is desirable to keep bed operating temperature constant while reducing the heat transfer to the water filled tubes within the bed. One technique utilized the contraction of the bed which accompanies a decrease in superficial velocity. As the bed contracts, some of the tube rows are uncovered reducing the net heat transfer. The scale model allowed many different tube arrangements to be tested, figure 18 shows three of the six different tube bank configurations which were tested. The validity of the scaling technique was confirmed by a comparison of the bed expansion measured for the pilot plant and that found in the model equipped with the same tube bank geometry (figure 19).

A second method to reduce load while maintaining constant bed temperature is to reduce the superficial velocity of a portion of the bed cross section to a value below u_{mf}. In this design the bed does not contain vertical partitions above the distributor. The scale model was used to determine the rate of growth of the fixed bed in the defluidized zone along with the heat transfer to tubes in that region. Figure 20 shows a typical pattern of particle accumulation in a slumped zone adjacent to an actively fluidized zone. Heat transfer coefficients are also shown.

In a bubbling bed operating at high ratio of u_0/u_{mf} there is a considerable amount of solids present in the freeboard, particularly near the bed surface in the so-called splash zone. The high density

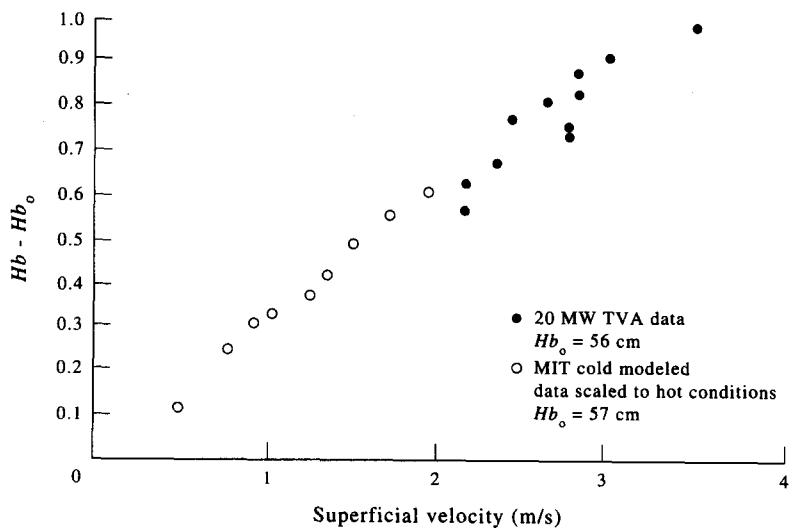

Figure 19. Comparison of bubbling combustor bed expansion with MIT scale model (Glicksman *et al.* 1989).

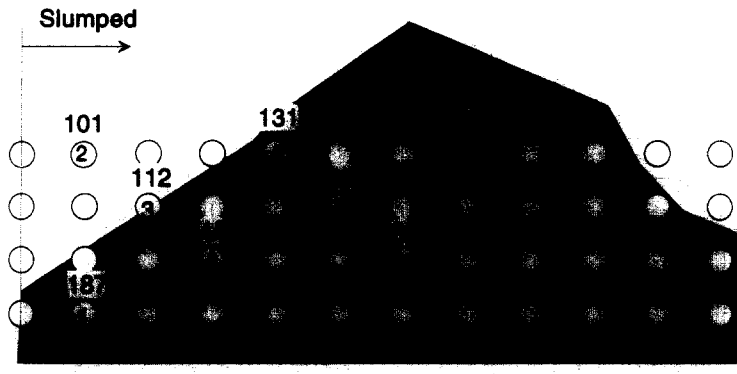

Figure 20. Particle accumulation in slumped zone adjacent to active bed: air velocity through active region = 151 cm/s; air velocity through slumped region = 7.3 cm/s; numbers above heater are heat transfer coefficients in W/m^2°C after 15–30 min.

of particles in the freeboard can cause substantial combustion and emission release in that zone as well as freeboard overheating if tubes are not present. The average density of solids was measured in the freeboard of the scale model of the 20 MW pilot plant (Glicksman & Piper 1987). As shown in figure 21, the average density in the freeboard decreases exponentially with distance above the dense bed. Also shown on the figure is the predicted behavior based on a bubble eruption model (Glicksman & Yule 1991).

The heat transfer from tubes in the freeboard was also measured for the 20 MW model. Figure 22 shows a comparison of the measured overall heat transfer coefficient in the 20 MW pilot plant versus that predicted from the scale model test.

Ackeskog *et al.* (1993) made the first heat transfer measurements in a scale model of a pressurized bubbling bed combustor. These results shed light on the influence of particle sizes, density and pressure levels on the fundamental mechanism of heat transfer, e.g. the increased importance of the gas convective component with increased pressure.

A multisolids bed contains a mixture of large solids which are contained in a dense region at the bottom of the bed and finer particles which recirculate through the bed and external cyclone. Ake & Glicksman (1989) used a cold scale model of a multisolids combustor to determine the dense bed expansion (see figure 23). The measured expansion in a properly scaled quarter-scale model using steel pellets to simulate the coarse particles and to satisfy solid to gas density ratio gave good

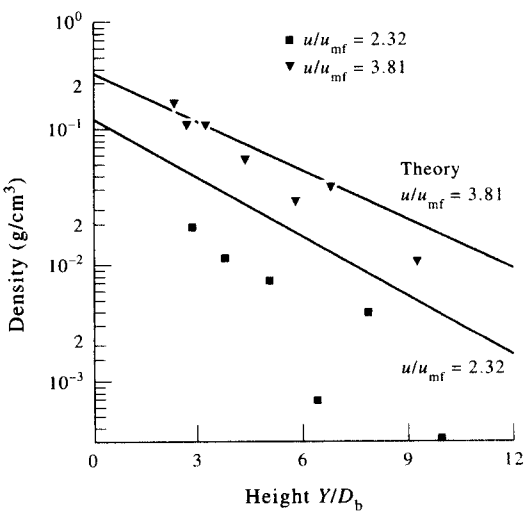

Figure 21. Density in freeboard of bubbling bed, present theory with D_b equal to horizontal tube pitch, 3.9 cm [data of Glicksman & Piper (1987), theory Glicksman & Yule (1991)].

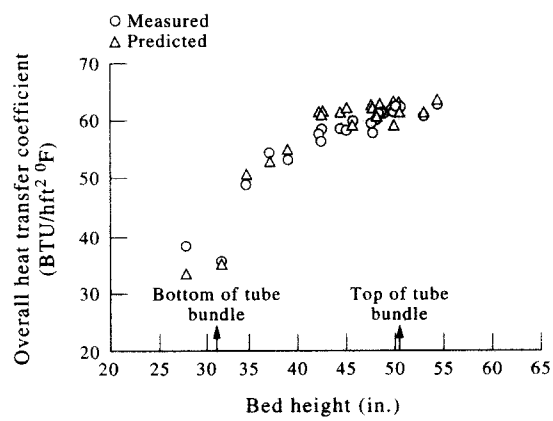

Figure 22. Comparison of heat transfer coefficient measured in 20 MW bubbling bed combuster vs prediction from MIT cold test.

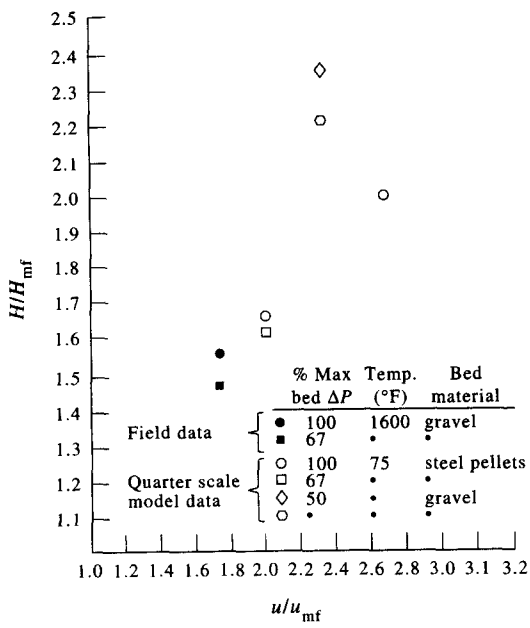

Figure 23. Expanded bed height model data compared to field data for multi-solids fluidized bed for properly scaled steel pellets and mis-scaled gravel particles.

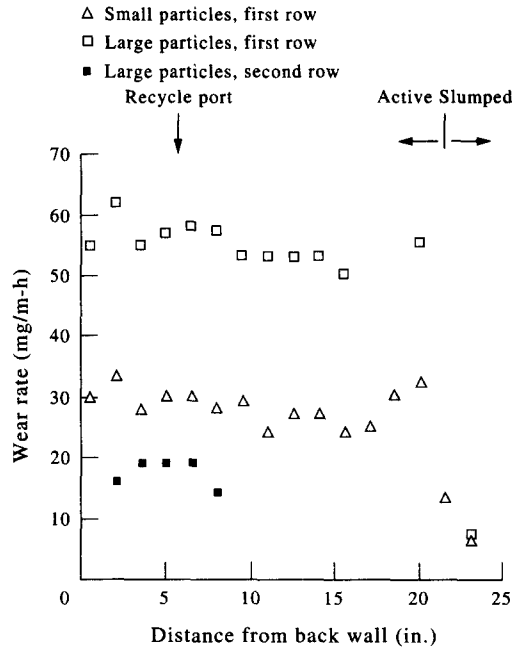

Figure 24. Wear rates for in-line tubes, simulation of 20 MW bubbling bed combustor.

agreement with field data. It was also demonstrated that an improperly scaled cold model, using the same coarse material as the hot bed which gave incorrect gas to particle density ratio substantially overpredicted the bed expansion.

Tube erosion has been observed in both atmospheric and pressurized bed combustors. The scaling analysis presented earlier can be used to construct an accurate hydrodynamic simulation of the commercial bed. This can be used to qualitatively investigate factors related to tube wear such as the location of highest wear around the circumference of an individual tube and the location within the bed of highest wear. Quantitative wear rates cannot be obtained from model tests unless the parameters governing both the hydrodynamics and the wear phenomena are matched between the model and the commercial bed. Figure 24 shows relative tube wear for the model of the TVA-EPRI 20 MW bubbling bed pilot plant.

8.2. Circulating Fluidized Bed Applications

As mentioned previously, Horio and co-workers have used scale models of circulating beds to assist in the formulation of fundamental understanding and quantitative relationships of hydrodynamics in circulating bed combustors. Models have been based on a clustering annular flow characterization. Experimental studies have included the use of fiber optic probes to determine vertical and lateral density profiles. In addition, innovative photographic techniques have been used to visualize the behavior of clusters in illuminated two-dimensional planes in the dilute region of a circulating bed (Horio *et al.* 1993).

Chang & Louge (1992) carried out scaling experiments for circulating beds using the full set of scaling parameters. By use of dense gas, their experimental bed can simulate rather large pressurized beds. In his studies Louge has shown that in extreme cases, the coefficient of friction and possibly the coefficient of restitution of specially prepared particles can alter the bed hydrodynamics.

Westphalen & Glicksman (1993) demonstrated close agreement between a scale model based on the full set of scaling relationships and a 2.5 MW_{th} circulating fluidized bed combustor operating at atmospheric pressure. Bed exit geometry and wall inserts and steps are shown to substantially alter the vertical density distribution in the bed.

9. HEAT TRANSFER

9.1. Introduction

Heat transfer is an important rate process in many fluidized bed systems. In bubbling beds, internal heat transfer tubes are used to control the bed temperature and serve as a source of steam generation in fluidized bed combustors. In circulating beds heat transfer is primarily to the walls of the bed. As is the case for bed hydrodynamics, designers need means to project heat transfer results from laboratory models to larger commercial units. Moreover, the models must produce heat transfer conditions which are similar to the commercial conditions to insure the applicability of the model results.

The heat transfer behavior is closely tied to the bed hydrodynamics. However, similarity of hydrodynamics does not guarantee similarity of heat transfer as well. This requires consideration of additional factors which will result in additional dimensionless parameters to be matched between the experimental model and the commercial bed. The addition of thermal parameters may preclude full similarity of all hydrodynamics and heat transfer parameters. We will approach the issue by first setting out the full set of governing parameters and then examining circumstances where this set can be relaxed.

9.2. Governing Equations for Heat Transfer

We will take a phenomenological view to the different heat transfer mechanisms and develop the set of governing dimensionless parameters by non-dimensionalizing the governing energy equations. We will not repeat the corresponding equations of motion which also bear on the problem since they have been developed in previous sections. Viewing the system as a continuum or as a collection of individual particles will yield similar forms for the parameters analogous to the results for hydrodynamics. Our attention will focus on heat transfer between a fluidized bed and an immersed heat transfer surface or a bounding wall. Typically, the heat transfer has been characterized as that due to particle convection, gas convection and thermal radiation. Particle convection is heat transfer due to the exchange of particles near the surface and the bed interior with their corresponding heat capacity. Gas convection is the heat transfer from the surface due to gas motion and its corresponding heat capacity. Operationally, gas convection is the balance of the convective heat transfer not ascribable to particle convection. For some cases the distinction between the two mechanisms is not precise. Radiation is a separate physical mechanism of heat transfer but it may interact with the other forms of heat transfer, particularly particle convection.

The overall phenomenological model of heat transfer for either bubbling, slugging or circulating beds is generally agreed to consist of the intermittent contact of a rather dense group of particles in the form of an emulsion, packet or cluster, interspersed with periods of contact with a high voidage fluid phase, e.g. a bubble. The time averaged heat transfer coefficient can be represented as,

$$h = fh_{pc} + (1-f)h_{gc} \qquad [102]$$

where h is the overall average heat transfer coefficient, h_{pc} represents the average heat transfer coefficient when the dense phase is in contact with the surface, h_{gc} is the heat transfer under the dilute phase and f is the temporal or spatial average fraction of the surface area occupied by the dense phase. For high temperatures, radiation effects must be included in both the dense and dilute phases.

The dense phase heat transfer is generally represented by a thermal resistance described by a renewal model for the emulsion (Mickley & Fairbanks 1955) which for short times is considered in series with a thermal resistance at the fluid interface between the dense phase and the wall (Baskakov 1964).

$$(h_{pc})^{-1} = h_w^{-1} + h_e^{-1} \qquad [103]$$

where h_w and h_e are the wall and dense phase coefficients, respectively.

With the boundary conditions on temperature $T = T_w$ at the bed wall and $T = T_b$ far from the wall. In dimensionless form†

$$\left(\frac{h_{pc}d_p}{k_f}\right)^{-1} = \left(\frac{h_w d_p}{k_f}\right)^{-1} + \left(\frac{h_e d_p}{k_f}\right)^{-1} \quad [104]$$

where k_f is the fluid thermal conductivity.

For a uniform emulsion or cluster with mean properties,

$$\frac{h_e d_p}{k_f} \sim \frac{d_p}{k_f}\frac{k_e}{\sqrt{\alpha_e t}} \sim \sqrt{\left[\frac{d_p^2 k_e^2}{k_f^2}\right]\left[\frac{(1-\epsilon_e)\rho_s c_{p_s}}{k_e}\right]\frac{u}{Lt}} \quad [105]$$

where α_e, the effective thermal diffusivity of the cluster or emulsion, is expressed in terms of the emulsion properties, the effective emulsion conductivity, k_e and solid specific heat c_p. The time of contact is non-dimensionalized as ut/L or t'. Rewriting [105],

$$\frac{h_e d_p}{k_f} \sim \frac{1}{\sqrt{t'}}\sqrt{\frac{(1-\epsilon_e)\rho_s c_{p_s} u d_p^2}{Lk_f}\left(\frac{k_e}{k_f}\right)} \quad [106]$$

where ϵ_e and t' are set by the hydrodynamics.

$(\rho_s c_{p_s} u d_p^2)/(Lk_f)$ is a dimensionless parameter which is the ratio of the thermal time constant of a particle to the time of contact set by the hydrodynamics. Note u is a characteristic velocity of particle clusters or bubbles in contact with the heat transfer surface. For bubbling beds the characteristic velocity is dependent on u_0, for circulating beds it should be the cluster falling velocity at the wall. The ratio k_e/k_f for a uniform mixture of particles and fluid is found to be a function of the true particle conductivity, k_s, the fluid conductivity and the void fraction, see for example, Gelperin & Einstein (1971)

$$\frac{k_e}{k_f} = f\left[\frac{k_s}{k_f}, \epsilon_e\right] \quad [107]$$

where it is shown that k_e/k_f is a weak function of k_s/k_f.

If the bed is at high temperature and the fluid is a gas there will be radiant transfer between particles making up the media. For particles large compared to the wavelength of infrared radiation the radiant transfer within the media can be approximated by an effective conductivity, k_r (Chen & Churchill 1963; Glicksman & Decker 1982) as

$$k_r \approx \tfrac{8}{9} d_p \sigma T^3 \quad [108]$$

which should be added to k_e in [106]. This leads to an additional dimensionless parameter $d_p((\sigma T^3)/(k_f)$ where σ is the Stefan Boltzmann constant and T is the absolute temperature. If the particle diameter approaches the wavelength of the radiation additional parameters enter, primarily the complex index of refraction of the particles and the fluid and the particle shape. These will be omitted in this treatment.

From the foregoing [106], [107] and [108] we can establish the functional relationship,

$$\frac{h_e d_p}{k_f} = f\left[t', \epsilon_e, \frac{\rho_s c_{p_s} u d_p^2}{Lk_f}, \frac{k_s}{k_f}, \frac{d_p \sigma T^3}{k_f}\right] \quad [109]$$

The additional resistance at the wall, at low temperature and moderate particle size, can be approximated by a conduction resistance through a gas layer which is some fraction of a particle diameter. Such a gas layer may represent the actual situation at the wall of a circulating bed (Lints & Glicksman 1993a) whereas in a bubbling bed it is a simple approximation for contact resistance (Gloski *et al.* 1984). For larger particles and high slip velocities near the wall, the gas conduction term may be augmented by a convection term, given as a function of particle Reynolds number (see Glicksman & Decker 1982) for bubbling beds or a function of Archimedes number (Baskakov

†To non-dimensionalize this a mean value of d_p is used, it is not clear if this should be averaged in the same way as the mean value used for the hydrodynamics. This point is moot if the same dimensionless size distribution is used for the model and the full size bed.

& Suprun 1972) which can be related to the Reynolds number at u_{mf}. The overall equation for the wall coefficient of heat transfer with radiation included becomes

$$\frac{h_w d_p}{k_f} = \delta^{-1} + \mathrm{Co}\,\mathrm{Re}_{d_p}\,\mathrm{Pr}_f + \frac{d_p}{k_f}\frac{\sigma T_w^3\left(1+\dfrac{T_w}{T_e}\right)}{\left(\dfrac{1}{\epsilon_w}+\dfrac{1}{\epsilon_B}-1\right)}\left(1+\frac{T_w^2}{T_e^2}\right) \qquad [110]$$

where Pr is the Prandtl number and ϵ_w and ϵ_B are the emissivity of the wall and the effective emissivity of the medium, respectively. The latter is determined by the surface properties of the particles and the geometry of the dense medium. δ, the dimensionless particle to wall spacing, and Co are constants which should be hydrodynamic functions. Radiation enters through the dimensionless radiation conduction term, which also appeared in [109], along with the ratio of absolute temperatures. If the wall and bed are close in absolute temperatures this factor can be omitted and the radiation conduction term can be expressed using the mean temperature between the bed and the heat transfer surface. Note that T_e is an intermediate temperature between T_w and T_B which can be found once h_w and h_e are determined. Thus T_w/T_e should be a function of the factors controlling h_w and h_e along with T_w/T_B.

Thus, we can write

$$\frac{h_w d_p}{k_f} = f\left[\mathrm{Re}_{d_p}\,\mathrm{Pr}_f, \frac{d_p\sigma T_w^3}{k_f}, \frac{T_w}{T_B}, \epsilon_w, \epsilon_B, \epsilon_e\right] \qquad [111]$$

Combining these developments, the overall particle convection heat transfer coefficient can be expressed as,

$$\frac{h_{pc} d_p}{k_f} = f\left[\frac{\rho_s c_{p_s} u d_p^2}{L k_f}, \frac{k_s}{k_f}, \mathrm{Re}_{d_p}\,\mathrm{Pr}_f, \frac{d_p\sigma T_w^3}{k_f}, \frac{T_w}{T_B}, \epsilon_w, \epsilon_p, \text{bed hydrodynamics}\right] \qquad [112]$$

For low temperatures, where radiation is unimportant the last four dimensionless terms can be omitted. For moderate particle Reynolds numbers, below approx. 10–30, the product of Reynolds number and Prandtl number is unimportant for bubbling beds. The ratio of particle to gas conductivity has a modest influence on the ratio of effective emulsion to gas conductivity. For a gas fluidized bed with non-metallic particles, the emulsion to gas conductivity ratio at a fixed emulsion void fraction can be taken as approximately constant. For very large particles and short contact times at the heat transfer surface, e.g. 1 mm particles with a contact time of a second or less, the first term in [112] is unimportant since the particles remain close to T_B during their contact time. For smaller particles or longer contact time, this term is a key parameter influencing h_{pc}. For all cases it is necessary to properly simulate the bed hydrodynamics.

9.3. Gas Convection Component

For dense bubbling or circulating beds, particle convection with radiation included dominates the heat overall transfer. Van Heerden *et al.* (1953) and Baskakov & Suprun (1972) carried out parallel mass and heat transfer experiments for gas fluidized bubbling beds, Ebert *et al.* (1990) did a similar experiment for air fluidized circulating beds to establish that particle convective effects dominate over gas convection. Here gas convection includes both gas convective effects at the surface in the vicinity of clusters as well as gas convection for surfaces covered by a dilute mixture of particles and fluid. For liquid fluidized beds and for circulating beds or freeboard regions of a bubbling bed where the particle concentration is very low, fluid convective heat transfer becomes important.

Lints & Glicksman (1993b) analyzed extensive data for a circulating bed which indicated that the gas convection can be approximated by the single phase heat transfer. This would suggest that

$$\frac{h_{gc} D}{k_f} = f\left[\frac{\rho_f u D}{\mu_f}, \mathrm{Pr}_f, \text{void geometry}\right] \qquad [113]$$

where D is a typical system dimension, e.g. the bed diameter or heat transfer surface length. For bubbling beds, the bubble length along the heat transfer surface might be a more logical dimension,

but the bubble length as well as any other void geometry should be related to D through the hydrodynamic parameters. Another possible factor is the gas turbulence level near the surface. If there are particles mixed within the void then an effective specific heat and gas conductivity should be used in the Prandtl number based on the mass fraction of solids and fluid.

9.4. Heat Transfer Surface Geometry

For particular heat transfer surface designs the surface geometry may influence the heat transfer and possibly the bed hydrodynamics. For tube bundles within a bubbling fluidized bed the inter-tube spacing may be important as well as the bundle orientation and location relative to the distributor, the bed wall or the free surface. Thus, the geometric ratios of tube spacing to tube diameter and tube vertical location to bed height must be scaled.

For finned surfaces the usual fin efficiency parameter, $h_w \text{perimeter}/k_{fin} A_{\text{cross section}}$, holds as well as the ratio of fin spacing to particle diameter for tightly spaced fins (Glicksman & Modlin 1986). For non-circular horizontal tubes, the tube profile can influence heat transfer. Recent results suggest that the shape of a circulating bed wall (Wu *et al.* 1989) and its roughness (Glicksman *et al.* 1993c) can influence the bed to wall heat transfer. This would require a dimensionless wall roughness in the scaled model which matched the target bed.

9.5. Heat Transfer Scaling Procedures

Ideally, heat transfer measurements should be carried out in a scaled bed which simultaneously matches all of the hydrodynamic scaling parameters as well as all of the heat transfer parameters with the target bed. With proper hydrodynamic scaling the wall coverage fraction, average distance between the cluster or emulsion and the wall, the emulsion void fraction and the average time of emulsion contact with the heat transfer surface will be properly simulated. All of the above factors enter into the heat transfer mechanism. However, the heat transfer is also dependent on the thermal parameters to establish full similarity. In most instances, it is usually not possible to simultaneously match all of the hydrodynamic and thermal parameters. For example, the ratio of thermal to hydrodynamic time constants, the first term in [112], involves both hydrodynamic and thermal parameters. The hydrodynamic parameters ρ_p, U, L and d_p are used to satisfy flow similarity while k_f is set by the choice of fluid. Thus, c_p of the solid is the only free parameter and it is limited by the choice of solids which satisfy hydrodynamic similarity.

To facilitate thermal scaling, the order of magnitudes in which each of the parameters can be neglected is given in table 6. These considerations are based on the mechanistic model for heat transfer presented earlier.

When τ_T/τ_H is large the thermal time constant of particles is larger than the contact time at the heat transfer surface. The particle temperature remains approximately at the bulk bed temperature during the contact period and exact match of τ_T/τ_H is unnecessary, although it is important that the model also has τ_T/τ_H large. Particular limiting values for this parameter depend on the specific flow regime. For horizontal tubes in bubbling beds the hydrodynamic time constant should be the average period between bubble passage at a given location. For heat transfer to the wall of a

Table 6. Range where dimensionless thermal parameters can be neglected

Parameter	Modest influence in these ranges
$\frac{\tau_T}{\tau_H} = \frac{\rho_p c_p u d_p^2}{L K_f}$	$\gg 1$
k_s/k_f	~ 1, weak effect in other ranges
$\text{Re}_{d_p} \text{Pr}$	$\text{Re}_{d_p} \text{Pr} < 10$ for bubbling beds
$\frac{d_p \sigma T_W^3}{k_f}$	$\ll 1$
T_W/T_B	~ 1 and $\frac{d_p \sigma T_W^3}{k_f} \ll 1$
$\epsilon_{w1}, \epsilon_p$	$\frac{d_p \sigma T_W^3}{K_f} \ll 1$

circulating bed τ_H is the particle or cluster contact time at the wall which can be approximated by taking the particle velocity at the wall as 1–2 m/s and the length of vertical travel generally believed to be between 10 and 100 cm.

As mentioned above the effective conductivity of the emulsion is a weak function of k_p/k_f; when this ratio is near unity the effective conductivity is approximately equal to the fluid conductivity. Re_{d_p} Pr enters in the gas convection which augments particle to wall heat transfer. It is only important at elevated pressure and large particle size.

At low temperatures or for high conductivity fluids where the radiation–conduction ratio is small, radiation is unimportant eliminating the need to match any of the radiation parameters.

Note, when one or more parameters can be neglected in the target bed to be scaled it is important to construct the experimental model so that the corresponding dimensionless parameters are in the range where they can also be neglected.

9.6. Experimental Results

9.6.1. Incomplete thermal scaling

Unfortunately, even when some of the thermal parameters can be neglected, it may be unlikely that proper scaling of all of the remaining parameters can be achieved. In that case, the experimental scaling results must be combined with modeling to achieve results which apply to the commercial bed.

At one extreme, only the hydrodynamic parameters are matched between model and full sized bed, while none of the thermal parameters are matched. Ackeskog *et al.* (1993) compared heat transfer measurements in a hot pressurized combustor and those in a cold pressurized model scaled using the full set of hydrodynamic scaling parameters. They made thermal measurements for a tube bundle and for heat transfer probes inserted in the bed. No attempt was made to match dimensionless heat transfer parameters. Rather, the authors used a model in the literature for the particle convective component and they assumed the hot bed and cold model had the same bed voidage. This allowed a prediction of the particle convection based on the cold bed results. The heat transfer model combined with the heat transfer results from the scaled bed were used to derive the hydrodynamic factors used in the model. These factors were used in applying the model to the hot bed. This technique depends on the validity of the heat transfer model. The comparison of the hot to cold results also requires an estimate of the radiative transfer. The authors obtained reasonable agreements betweeen the hot and cold results with a maximum deviation of 19%. However some of the spatial variations of heat transfer differed between hot data and prediction based on the cold bed results.

9.6.2. Comparison between cold beds

Glicksman *et al.* (1993c) carried out heat transfer experiments on two geometrically similar beds whose linear dimensions differed by a factor of four. Three separate heat transfer panels were installed on one wall of the bed. The beds were both cold and were hydrodynamically scaled to match all of the simplified scaling parameters. By using the same particle material and gas at the same temperature in both beds the ratio of thermal to hydrodynamic time constants are also held constant. For small particles, u_{mf} can be approximated using only the viscous term of the Ergun equation, thus the ratio of the thermal, τ_T, to hydrodynamic times, τ_H, can be given as,

$$\frac{\tau_T}{\tau_H} = \frac{\rho_s c_{p_s} u d_p^2}{L k_f} = \left(\frac{c_{p_s}}{k_f}\right)\frac{\rho_s u d_p^2}{L} = \frac{c_{p_s}}{k_f}\frac{\mathrm{Fr}\,\rho_s g d_p^2}{u} \sim \frac{c_{p_s}}{k_f}\frac{\mu(\mathrm{Fr})u_{mf}}{u} \qquad [114]$$

In the simplified hydrodynamic scaling, u/u_{mf}, Fr and ρ_s/ρ_r are held constant. Thus, in the work of Glicksman *et al.* (1993c), by using the same solid between the two beds, τ_T/τ_H and k_p/k_f were held constant between the two beds. Both beds were at room temperature so that radiation is negligible. The convection augmentation $Re_p Pr_f$ is also small. Figure 25 shows a comparison of the Nusselt thermal scaling relationships when all important parameters are matched between the two beds.

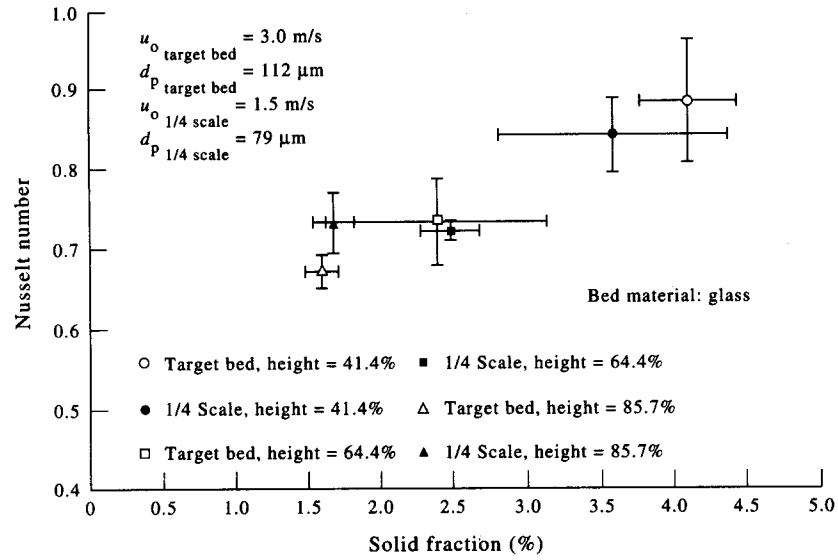

Figure 25. Comparison of Nusselt numbers between properly scaled circulating fluidized beds at several bed heights.

In general cases where the simplified scaling relationships are used and u_{mf}/u, ρ_f/ρ_s and Fr are held constant then for small particles,

$$\frac{\tau_T}{\tau_H} \sim \frac{c_{p_s}}{c_{p_f}}\left(\frac{c_p \mu}{k}\right)_f \mathrm{Fr}\frac{u_{mf}}{u_0} = \frac{c_{p_s}}{c_{p_f}} \mathrm{Pr}_f \mathrm{Fr}\frac{u_{mf}}{u_0} \qquad [115]$$

and constancy of τ_T/τ_H requires the use of fluids and solids with identical values of the product $c_{p_s}/c_{p_f}\mathrm{Pr}_f$. The Prandtl number remains constant at a value near 0.7 for most gases over a wide range of temperatures. To maintain τ_T/τ_H constant between the model and target bed, the ratio of particle to fluid specific heat must be equal when the particles are small enough for u_{mf} to be governed by the viscous term in the Ergun equation. Note, at the other limit of large particles τ_T/τ_H will become larger than unity and will not remain an important factor in the heat transfer.

When using a low temperature model to obtain heat transfer data to be applied to a bed fluidized with hot gas, it is unlikely that the radiation conduction parameter can be matched. If hydrodynamic similarity holds, the dimensionless wall coverage, wall to particle spacing and emulsion void fraction should be matched. At this point it is necessary to introduce a heat transfer model. Using a renewal model as described in the previous section one must determine the most important thermal parameters. For large heat transfer surfaces and small particle diameters typical of the walls of circulating beds, the emulsion resistance, [106], should predominate over the wall resistance. This becomes, with radiation, [108], included in the effective conductivity,

$$\frac{h_c d_p}{k_f} = \frac{1}{\sqrt{t'}}\sqrt{\frac{(1-\epsilon_e)\rho_s c_{p_s} u d_p^2}{L k_f}\left(\frac{k_e}{k_f}\right)} \sim \frac{1}{\sqrt{t'}}\sqrt{(1-\epsilon_e)\frac{c_{p_s}}{c_{p_f}}\mathrm{Pr}_f \frac{u_{mf}}{u}\mathrm{Fr}\left(1-\frac{\rho_s}{\rho_f}\right)\left(\frac{k_e}{k_f}+\frac{8}{9}\frac{d_p \sigma T^3}{k_f}\right)} \qquad [116]$$

Thus in the case of the simplified scaling laws, which results in equal values of t', heat transfer similarity requires an equality between the terms,

$$\left[\mathrm{Pr}_f\left(\frac{c_{p_s}}{c_{p_f}}\right)\left(\frac{k_e}{k_f}+\frac{8}{9}\frac{d_p \sigma T^3}{k_f}\right)\right]_{\text{hot target}} = \left[\mathrm{Pr}_f \frac{c_{p_s}}{D_{p_f}}\frac{k_e}{k_f}\right]_{\text{cold model}} \qquad [117]$$

Note, in this case it is unnecessary to also hold an additional term k_p/k_f constant. If the cold bed parameter given by the right-hand side of [117] is not equal to the hot bed parameter, then the measured Nusselt number in the cold bed must be adjusted by the square root of the ratio of the left hand side term to the right-hand side term in [117].

At the other extreme, for large particles with short residence time, e.g. a large particle bubbling bed with rapid particle exchange at the heat transfer surface, the surface resistance, [110], should

predominate. Results for Nusselt number in a low temperature model should be adjusted by the ratio of $h_w d_p/k_f$ between the hot and cold bed, given by [110] to obtain a prediction of the hot bed Nusselt number.

Results for Nusselt number in a low temperature model should be adjusted by the ratio of $((Nu)_w$ hot bed)/$((Nu)_w$ cold model) to obtain a prediction of the hot bed Nusselt number.

In both the case of the large particle and small particle limits a measurement or estimate of the percent of surface covered by dilute phase must be made. For the cold bed the dilute phase heat transfer will be small unless f becomes very small. For the hot bed the heat transfer coefficient under the dilute phase is given by radiation between the heat transfer surface and the bulk bed. This correction is approximate only if f is not well known.

10. CONCLUSIONS

Similitude allows a fluidized bed at ambient conditions to model the behavior of a commercial bed at elevated temperature and pressure. Numerous experimental investigations have confirmed the validity of the dynamic modeling for atmospheric and pressurized bubbling beds. Results for circulating beds indicate that the scaling laws also apply for that flow regime. It is important to match the dimensionless hydrodynamic parameters as well as maintaining geometric similarity. There are some questions that additional dimensional parameters may be needed for slugging beds and to characterize the stability limits between minimum fluidization and minimum bubbling limits. Verification of the scaling laws for pressurized circulating beds has not been attempted nor has the application to liquid fluidized or three-phased beds been made.

The use of small, properly scaled laboratory models should facilitate the design of larger commercial beds based on results of smaller pilot plants. The models can be used to shed light on particle and gas dynamics, mixing processes, wear of in-bed components and heat transfer within the bed, among others. Substantial design modifications can be quickly tested to resolve performance anomalies of existing commercial beds.

If atmospheric air is used as the fluidizing gas, models of hot atmospheric beds are substantially smaller than the commercial beds. Models of pressurized beds approach the commercial beds in size if the full set of scaling parameters are retained. Models based on a simplified set of scaling parameters have shown in preliminary tests to yield models with characteristics equivalent to models based on the full set. The simplified set allows the models to be significantly smaller than the commercial beds even for hot pressurized beds. This offers the hope of modest laboratory models which can simulate very large commercial units. Further confirmation of the simplified scaling models is required.

As an alternative, cold models can be fluidized with gases denser than air or the models can be pressurized; either technique will result in smaller models.

The scaling laws can be extended to model bed to wall heat transfer. These require one or more additional scaling parameter and/or a data analysis technique based on a mechanistic heat transfer model. Particle convection can be most easily modeled. Gas convection and radiation become more challenging.

Similitude analysis not only allows the use of experimental models to simulate the dynamics of larger beds, it aids in the identification of governing dimensional parameters which should help shape the analysis and correlation of bed behavior.

Modeling can also be extended to other phenomena such as wear or erosion of in-bed surfaces. Presently, modeling provides qualitative indications; proper formulation and modeling of wear phenomena should allow quantitative assessments to be made.

10.1. Future Work

The full set of scaling laws must be checked for cold scale models of hot circulating bed combustors to determine if use of the proper density ratio gives close agreement.

The simplified scaling laws need to be verified for use with pressurized bubbling and circulating beds. Work in this direction is currently underway in the authors' laboratory.

The use of scaling to study size effects can resolve the effect of bed diameter on dynamical and heat transfer parameters.

Acknowledgements—One of the authors (L.R.G.) would like to acknowledge the contributions of the many former MIT students who carried out scaling studies of fluidized beds. Much of this research has been sponsored by the Electric Power Research Institute, the National Science Foundation, the U.S. Department of Energy and the Tennessee Valley Authority.

REFERENCES

ACKESKOG, H. B. R., ALMSTEDT, A. E. & ZAKKAY, V. 1993 An investigation of fluidized-bed scaling: heat transfer measurements in a pressurized fluidized-bed combustor and a cold model bed. *Chem. Engng Sci.* **48,** 1459–1473.

AKE, T. R. & GLICKSMAN, L. R. 1989 Scale model and full scale test results of a circulating fluidized bed combustor. *Proc: 1988 Seminar on Fluidized Bed Combustion Technology for Utility Applications*, EPRI, 1-24-1.

ALMSTEDT, A. E. & ZAKKAY, V. 1990 An investigation of fluidized-bed scaling—capacitance probe measurements in a pressurized fluidized-bed combustor and a cold model bed. *Chem. Engng Sci.* **45,** 1071–1078.

ANDERSON, T. B. & JACKSON, R. 1967 A fluid mechanical description of fluidized bed. *I & EC Fundamentals* **6,** 527–539.

BAEYANS, J. & GELDART, D. 1973 Predictive calculations of flow parameters in gas fluidized bed and fluidization behavior of various powders. *Proc. Int. Symp. on Fluidization and its Applications*, Toulouse, pp. 263–273, 681–690.

BASKAKOV, A. P. 1964 The mechanism of heat transfer between a fluidized bed and a surface. *Int. Chem. Engng* **4,** 320–324.

BASKAKOV, A. P. & SUPRUN, V. M. 1972 Determination of the convective component of the heat-transfer coefficient to a gas in a fluidized bed. *Int. Chem. Engng* **12,** 324–326.

BATCHELOR, G. K. 1988 A new theory for the instability of a fluidized bed. *J. Fluid Mech.* **31,** 657–668.

BERLEMONT, A., DESJONQUERES, P. & GOUESBET, G. 1990 Particle Lagrangian simulation in turbulent flows. *Int. J. Multiphase Flow* **16,** 19–34.

BRENNER, H. 1961 The slow motion of a sphere through a viscous fluid towards a plane surface. *Chem. Engng Sci.* **16,** 242–251.

BROADHURST, T. E. & BECKER, H. A. 1973 The application of the theory of dimensions to fluidized beds. *Proc. Int. Symp. Ste. Chimie Indust.*, Toulouse, pp. 10–27.

BUCKINGHAM, E. 1914 On physically similar systems; illustrations of the use of dimensional analysis. *Phys. Rev.* **4,** 345–376.

CHANG, H. & LOUGE, M. 1992 Fluid dynamic similarity of circulating fluidized beds. *Powder Technol.* **70,** 259–270.

CHEN, J. C. & CHURCHILL, S. W. 1963 Radiant heat transfer in packed bed. *AIChE Jl* **9,** 35–41.

DAVIDSON, J. F. & HARRISON, D. 1963 *Fluidized Particles*. Cambridge University Press, Cambridge, U.K.

DAW, C. S. & HARLOW, J. S. 1991 Characteristics of voidage and pressure signals from fluidized beds using deterministic chaos theory. *Proc. 11th Int. Conf. Fluidized Bed Combustion* **2,** 777–786.

DAW, C. S., LAWKINS, W. F., DOWNING, D. J. & CLAPP, N. E. 1990 Chaotic characteristics of a complex gas–solids flow. *Phys. Rev. A* **41,** 1179–1181.

DI FELICE, R., RAPAGNA, S. & FOSCOLO, P. U. 1992a Dynamic similarity rules: validity check for bubbling and slugging fluidized beds. *Powder Technol.* **71,** 281–287.

DI FELICE, R., RAPAGNA, S., FOSCOLO, P. U. & GIBILARO, L. G. 1992b Cold modelling studies of fluidised bed reactors. *Chem. Engng Sci.* **47,** 2233–2238.

EBERT, T. A., GLICKSMAN, L. R. & LINTS, M. 1990 Heat transfer in circulating fluidized beds: determination of particle convective and gas convective components. *Proc. AIChE A. Mtng* Chicago, II, 11–16 Nov.

FAN, L. T., HO, T. C., HIRAOKA, S. & WALAWENDER, W. P. 1981 Pressure fluctuations in a fluidized bed. *AIChE Jl* **27,** 388–396.

FAXEN, H. 1992 Die Bewegun einer Starren Kugel Langs der Achse eines mit zaher Flussigkeit gefullten Rohres. *Arkiv. Mat. Astron. Fys.* **17,** 1–28.

FITZGERALD, T. J. & CRANE, S. D. 1980 Cold fluidized bed modeling. *Proc. 6th Int. Conf. Fluidized Bed Combustion* **III,** 815–820.

FITZGERALD, T., BUSHNELL, D., CRANE, S. & SHIEH, Y. 1984 Testing of cold scaled bed modeling for fluidized-bed combustors. *Powder Technol.* **38,** 107–120.

FOSCOLO, P. U. & GIBILARO, L. G. 1984 A fully predictive criterion for the transition between particulate and aggregate fluidization. *Chem. Engng Sci.* **39,** 1667–1675.

FOSCOLO, P. U., DI FELICE, R., GIBILARO, L. G., PISTONE, L. & PICCOLO, V. 1990 Scaling relationships for fluidisation: the generalized particle bed model. *Chem. Engng Sci.* **45,** 1647–1651.

GELPERIN, N. I. & EINSTEIN, V. G. 1971 Heat transfer in fluidized beds. In *Fluidization* (Edited by DAVIDSON, J. F. & HARRISON, D.). Academic Press, New York.

GLICKSMAN, L. R. 1984 Scaling relationships for fluidized beds. *Chem. Engng Sci.* **39,** 1373–1379.

GLICKSMAN, L. R. 1988 Scaling relationships for fluidized beds. *Chem. Engng Sci.* **43,** 1419–1421.

GLICKSMAN, L. R. & DECKER, N. A. 1982 Heat transfer from an immersed surface to adjacent particles in fluidized beds. *Proc. 7th Int. Conf. on Fluidized Beds*, Philadelphia, pp. 45–50.

GLICKSMAN, L. R. & MODLIN, J. 1986 Heat transfer with low density particles in a fluidized bed. *Proceedings of the Eighth International Heat Transfer Conference*, San Francisco, pp. 2605–2609.

GLICKSMAN, L. R. & PIPER III, G. A. 1987 Particle density distribution in the freeboard of a fluidized bed. *Powder Technol.* **53,** 179–186.

GLICKSMAN, L. R. & YULE, T. 1991 Prediction of the particle flow conditions in the freeboard of a freely bubbling fluidized bed. *Proc. AIChE Annual Meeting: Fluidization and Fluid–Particle Systems*, Los Angeles, 17–22 Nov.

GLICKSMAN, L. R., HYRE, M. R. & WESTPHALEN, D. 1993a Verification of scaling relations for circulating fluidized beds. *Proc. 12th Int. Conf. on Fluidized Bed Combustion*, pp. 69–80.

GLICKSMAN, L. R., HYRE, M. R. & WOLOSHUN, K. 1993b Simplified scaling relationships for fluidized beds. *Powder Technol.* **77,** 177–199.

GLICKSMAN, L. R., HYRE, M. R. & WOLOSHUN, K. 1993c Scale models of circulating fluidized bed combustors: simplification of the scaling laws and the scaling of convective heat transfer. Report # DOE/MC/25049-3372, USDOE, Washington, D.C.

GLICKSMAN, L. R., YULE, T. & DYRNESS, A. 1991b Prediction of the expansion of fluidized beds containing tubes. *Chem. Engng Sci.* **46,** 1561–1571.

GLICKSMAN, L. R., WESTPHALEN, D., BRERETON, C. & GRACE, J. 1991a Verification of the scaling laws for circulating fluidized beds. In *Circulating Fluidized Bed Technology III* (Edited by BASU, P., HORIO, M. & HASATANI, M.). Pergamon Press, Oxford.

GLICKSMAN, L. R., YULE, T., CARSON, R. & VINCENT, R. 1989 Comparison of results from TVA 20 MW fluidized bed combustor with MIT cold scale model. *Proc. 1988 Seminar on Fluidized Bed Combustion Technology for Utility Applications*, EPRI GS-6118, 1-20-1.

GLOSKI, D., GLICKSMAN, L. & DECKER, N. 1984 Thermal resistance at a surface in contact with fluidized bed particles. *J. Heat Mass Transfer* **27,** 599–610.

GRACE, J. R. 1982 Fluidized-bed hydrodynamics. In *Handbook of Multiphase Systems* (Edited by HESTRONI, G.). Hemisphere, Washington, D.C.

HINZE, J. O. 1975 *Turbulence*. McGraw–Hill, New York.

HORIO, M. 1990 Scaling laws of circulating fluidized beds. Workshop on Materials Issues in Circulating Fluidized-Bed Combustors, EPRI Report 65-6747.

HORIO, M., KUROKI, H. & OGASAWARA, M. 1993 The flow structure of a three-dimensional circulating fluidized bed observed by the laser sheet technique. *Proc. 4th Int. Circulating Fluidized Bed Conf.*, Somerset.

HORIO, M., ISHII, H., KOBUKAI, Y. & YAMANISHI, N. 1989 A scaling law for circulating fluidized beds. *J. Chem. Engng Jap.* **22,** 587–592.

HORIO, M., NONAKA, A., SAWA, Y. & MUCHI, I. 1986a A new similarity rule for fluidized bed scale-up. *AIChE Jl* **32,** 1466–1482.

HORIO, M., TAKADA, M., ISHIDA, M. & TANAKA, N. 1986b The similarity rule of fluidization and its application to solid mixing and circulating control. In *Fluidization V* (Edited by OSTERGAARD, K. & SORENSEN, A.). Engineering Foundation, New York.

HYRE, M. & GLICKSMAN, L. R. 1994 On the assumption of minimum energy dissipation in circulatory fluidized beds. Submitted for publication.

ISHII, H. & MURAKAMI, I. 1991 Evaluation of the scaling law of circulating fluidized beds in regard to cluster behaviors. In *Circulating Fluidized Bed Technology III* (Edited by BASU, P., HORIO, M. & HASATANI, M.). Pergamon Press, Oxford.

IVERSON, H. W. & BALENT, R. 1951 A correlating modulus for fluid resistance in accelerated motion. *J. Appl. Phys.* **22,** 324–328.

JACKSON, R. 1971 Fluid mechanical theory. In *Fluidization* (Edited by DAVIDSON, J. F. & HARRISON, D.). Academic Press, New York.

JONES, L. & GLICKSMAN, L. R. 1986 An experimental investigation of gas flow in a scale model of a fluidized-bed combustor. *Powder Technol.* **45,** 201–213.

KIEM, S. R. 1956 Fluid resistance to cylinders in accelerated motion. *Proc. ASCE, J. Hydraul. Div.* **82,**

KLINE, S. J. 1965 *Similitude and Approximation Theory.* McGraw–Hill, New York.

LIRAG, R. C. & LITTMAN, H. 1971 Statistical study of the pressure fluctuations in a fluidized bed. *AIChE Symp. Ser., No. 166* **67,** 11–22.

LINTS, M. & GLICKSMAN, L. R. 1993a The structure of particle clusters near the wall of a circulating fluidized bed. *AIChE Symp. Ser. 296, Fluid–Particle Processes; Fundamentals and Applications* **89,** 35–47.

LINTS, M. & GLICKSMAN, L. R. 1993b Parameters governing particle to wall heat transfer in a circulating fluidized bed. *Proc. 4th Int. Conf. on Circulating Fluidized Bed Combustors*, Somerset.

LITKA, T. & GLICKSMAN, L. R. 1985 The influence of particle mechanical properties on bubble characteristics and solid mixing in fluidized beds. *Powder Technol.* **42,** 231–239.

LOVALENTI, P. M. & BRADY, J. F. 1993a The hydrodynamic force on a rigid particle undergoing arbitrary time-dependent motion at small Reynolds number. *J. Fluid Mech.* **256,** 561–605.

LOVALENTI, P. M. & BRADY, J. F. 1993b The force on a sphere in a uniform flow with small-amplitude oscillations at finite Reynolds number. *J. Fluid Mech.* **256,** 607–614.

LOVALENTI, P. M. & BRADY, J. F. 1993c The force on a bubble, drop or particle in arbitrary time-dependent motion at small Reynolds number. *Phys. Fluids A* **5,** 2104–2116.

MAUDE, A. D. 1961 The end effects in a falling-sphere viscometer. *Br. J. Appl. Phys.* **12,** 242–251.

MAXEY, M. M. & RILEY, J. J. 1983 Equation of motion for a small rigid sphere in a nonuniform flow. *Phys. Fluids* **26,** 883–889.

MEI, R. & ADRIAN, R. J. 1992 Flow past a sphere with an oscillation in the free-stream velocity and unsteady drag at finite Reynolds number. *J. Fluid Mech.* **237,** 323–341.

MEI, R., ADRIAN, R. J. & HANRATTY, T. J. 1991a Particle dispersion in isotropic turbulence under Stokes drag and Basset force with gravitational settling. *J. Fluid Mech.* **225,** 481–495.

MEI, R., LAWRENCE, C. J. & ADRIAN, R. J. 1991b Unsteady drag on a sphere at finite Reynolds number with small fluctuations in the free-stream velocity. *J. Fluid Mech.* **233,** 613–633.

MICKLEY, H. S. & FAIRBANKS, D. F. 1955 Mechanics of heat transfer to fluidized beds. *AIChE Jl* **1,** 374–384.

NEWBY, R. A. & KEAIRNS, D. L. 1986 Test of the scaling relationships for fluid-bed dynamics. In *Fluidization V* (Edited by OSTERGAARD, K. & SORENSEN, A.), pp. 31–38. Engineering Foundation, New York.

NICASTRO, M. T. & GLICKSMAN, L. R. 1984b Experimental verification of scaling relationships for fluidized bed. *Chem. Engng Sci.* **39,** 1381–1391.

ODAR, F. 1966 Verification of the proposed equation for calculation of the forces on a sphere accelerating in a viscous fluid. *J. Fluid Mech.* **25,** 591–592.

ODAR, F. & HAMILTON, W. S. 1964 Forces on a sphere accelerating in a viscous fluid. *J. Fluid Mech.* **18,** 302–314.

RHODES, M. J. & LAUSSMAN, P. 1992 A study of the pressure balance around the loop of a circulating fluidized bed. *Can. J. Chem. Engng* **70,** 625–630.

RICHARDSON, J. F. & ZAKI, W. N. 1954 Sedimentation and fluidization, part 1. *Trans. Inst. Chem. Engr* **32,** 35–53.

RIETEMA, K. & PIEPERS, H. W. 1990 The effect of interparticle forces on the stability of gas-fluidized beds—I. Experimental evidence. *Chem. Engng Sci.* **45,** 1627–1639.

RIETEMA, K., COTTAAR, E. J. A. & PIEPERS, H. W. 1993 The effect of interparticle forces on the stability of gas-fluidized beds—II. Theoretical derivation of bed elasticity on the basis of Van der Waals forces between powder particles. *Chem. Engng Sci.* **48,** 1687–1697.

ROMERO, J. B. & JOHANSON, L. N. 1962 Factors affecting fluidized bed quality. *Chem. Engng Prog.* **44,** 28–37.

ROY, R. & DAVIDSON, J. F. 1989 Similarity between gas-fluidized beds at elevated temperature and pressure. In *Fluidization VI*, pp. 293–300. Engineering Foundation, New York.

SAFFMAN, P. G. 1968 The lift on a small sphere in a slow shear flow. *J. Fluid Mech.* **22,** 385–400. (Corrigendum: *J. Fluid Med.* **31,** 624.)

SCHARFF, M. F., GOLDMAN, S. R., FLANAGAN, T. M., GREGORY, T. K. & SMOOT, L. D. 1978 Project to provide an experimental plan for the Merc 6′ × 6′ fluidized bed cold test model. Final Report J77-2042-FR, U.S. Department of Energy, Contract EY-77-C-21-8156.

SCHOUTEN, J. C. & VAN DEN BLEEK, C. M. 1991 Chaotic behavior in a hydrodynamic model of a fluidized bed reactor. *Proc. 11th Int. Conf. on Fluidized Bed Combustion* **1,** 459–466.

TCHEN, C. M. 1947 Mean value and correlation problems connected with the motion of small particles suspended in a turbulent fluid. Ph.D. thesis, Delft, Nijhoff, The Hague.

TIEN, C. L. 1988 Thermal radiation in packed and fluidized beds. *ASME J. Heat Transfer* **110,** 1230–1240.

TSUKADA, M., NAKANISHI, D., TAKEI, Y., ISHII, H. & HORIO, M. 1991 Hydrodynamic similarity of circulating fluidized bed under different pressure conditions. *Proc. 11th Int. Conf. Fluidized Bed Combustion*, pp. 829–834.

VAN DEN BLEEK, C. M. & SCHOUTEN, J. C. 1993 Can deterministic chaos create order in fluidized bed scale-up? *Chem. Engng Sci.* **48,** 2367–2373.

VAN HEERDEN, C., NOBEL, A. P. P. & VAN KREUELEN, D. W. 1953 Mechanism of heat transfer in fluidized beds. *Ind. Engng Chem.* **48,** 1237–1242.

WEN, C. Y. & YU, Y. H. 1966a A generalized method for predicting the minimum fluidization velocity. *AIChE Jl* **12,** 610–612.

WEN, C. Y. & YU, Y. H. 1966b Mechanics of fluidization. *Chem. Engng Prog. Symp.* **62,** 100–111.

WESTPHALEN, D. & GLICKSMAN, L. R. 1993 Experimental verification of scaling for a commercial-size CFB combustor. *Proc. 4th Int. Conf. on CFB*, Hidden Valley, Pa, 1–5 Aug.

WHITE, F. M. 1974 *Viscous Fluid Flow*. McGraw–Hill, New York.

WHITE, F. M. 1979 *Fluid Mechanics*. McGraw–Hill, New York.

WILHELM, R. H. & KWAUK, M. 1948 Fluidization of solid particles. *Chem. Engng Proc.* **44,** 201–218.

WU, R. L., GRACE, J. R., LIM, C. J. & BRERETON, C. M. H. 1989 Suspension—surface heat transfer in a circulating fluidized-bed combustor. *AIChE Jl* 1685–1691.

YANG, W. C. 1983 Criteria for choking in vertical pneumatic conveying lines. *Powder Technol.* **35,** 143–150.

YULE, T. & GLICKSMAN, L. R. 1988 Gas flow through erupting bubbles in fluidized beds. *AIChE Symp. Ser. Fluidization Engineering: Fundamentals and Applications 262* **84,** 1–9.

ZABRODSKY, S. S. 1966 *Hydrodynamics and Heat Transfer in Fluidized Beds*. MIT Press, Cambridge, Mass.

ZHANG, M. C. & YANG, R. Y. K. 1987 On the scaling laws for bubbling gas-fluidized bed dynamics. *Powder Technol.* **51,** 159–165.